OFFICE

OF

RESEARCH

# LEHIGH UNIVERSITY

THE FATIGUE STRENGTH
OF FILLET WELDED CONNECTIONS

by

Karl H. Frank

October 1971

Fritz Engineering Laboratory Report No. 358.37

## DOCUMENT CONTROL DATA - R & D

*Security classification of title, body of abstract and indexing annotation must be entered when the overall report is classified)*

| 1. ORIGINATING ACTIVITY (Corporate author) | 2a. REPORT SECURITY CLASSIFICATION |
|---|---|
| Lehigh University | Unclassified |
| | 2b. GROUP |

**3. REPORT TITLE**

THE FATIGUE STRENGTH OF FILLET WELDED CONNECTIONS

**4. DESCRIPTIVE NOTES (Type of report and inclusive dates)**

**5. AUTHOR(S) (First name, middle initial, last name)**

Karl H. Frank

| 6. REPORT DATE | 7a. TOTAL NO. OF PAGES | 7b. NO. OF REFS |
|---|---|---|
| October 1971 | 162 | 54 |
| 8a. CONTRACT OR GRANT NO. | 9a. ORIGINATOR'S REPORT NUMBER(S) |
| N 00014-68-A-0514 | Fritz Eng. Lab. Rep. No. 358.37 |
| b. PROJECT NO. | |
| 358 | |
| c. | 9b. OTHER REPORT NO(S) (Any other numbers that may be assigned this report) |
| d. | |

**10. DISTRIBUTION STATEMENT**

"Approved for public release; Distribution unlimited".

| 11. SUPPLEMENTARY NOTES | 12. SPONSORING MILITARY ACTIVITY |
|---|---|
| | Office of Naval Research |

**13. ABSTRACT**

This report describes a study of the fatigue behavior of fillet welded joints stressed perpendicular to the weld line. The study included an experimental phase in which the stress-life and cracking behavior of load and non-load carrying fillet weld joints was determined. This experimental study concentrated on the fatigue behavior in the transition region between high and low cycle fatigue ($10^3$ cycles to $10^5$ cycles of load application).

The second phase of the study was the determination of the fracture mechanics stress intensity factor for cracks at the weld toe or root of fillet welded joints. The finite element technique was used to determine the compliance of typical fillet welded joints. The results of this analysis showed taht the stress intensity factor was a function of weld size, weld angle, plate thickness and weld penetration. Relationships to estimate the stress intensity factor were developed.

The third phase of the study was the correlation of the experimental fatigue stress-life behavior of fillet welded joints with the predicted behavior using the concepts of the fracture mechanics of stable crack growth. The study showed that the fatigue behavior of various joint geometries could be correlated using the stress intensity factors developed in phase two. The correlation included failures from cracking at the root and toe of the fillet weld. The analysis provided a good estimate of the observed fatigue behavior for fatigue lives from $10^3$ to $2 \times 10^7$ cycles of load application.

**DD FORM 1473** (PAGE 1)

| 14                KEY WORDS | LINK A | | LINK B | | LINK C | |
|---|---|---|---|---|---|---|
| | ROLE | WT | ROLE | WT | ROLE | WT |
| | | | | | | |

THE FATIGUE STRENGTH OF FILLET WELDED CONNECTIONS

by

Karl Heinz Frank

October 1971

- i

## ACKNOWLEDGEMENTS

## TABLE OF CONTENTS

# LIST OF TABLES

# LIST OF FIGURES

# ABSTRACT

This report describes a study of the fatigue behavior of fillet welded joints stressed perpendicular to the weld line. The study included an experimental phase in which the stress-life and cracking behavior of load and non-load carrying fillet weld joints was determined. This experimental study concentrated on the fatigue behavior in the transition region between high and low cycle fatigue $(10^3$ cycles to $10^5$ cycles of load application).

The second phase of the study was the determination of the fracture mechanics stress intensity factor for cracks at the weld toe or root of fillet welded joints. The finite element technique was used to determine the compliance of typical fillet welded joints. The results of this analysis showed that the stress intensity factor was a function of weld size, weld angle, plate thickness and weld penetration. Relationships to estimate the stress intensity factor were developed.

The third phase of the study was the correlation of the experimental fatigue stress-life behavior of fillet welded joints with the predicted behavior using the concepts

ABSTRACT

This report describes a study of the fatigue
behavior of fillet welded joints stressed perpendicular to
the weld line. The study included an experimental phase in
which the stress-life and cracking behavior of load and non-
load carrying fillet weld joints was determined. This
experimental study concentrated on the fatigue behavior in
the transition region between high and low cycle fatigue
($10^3$ cycles to $10^5$ cycles of load application).

The second phase of the study was the determination
of the fracture mechanics stress intensity factor for cracks
at the weld toe or root of fillet welded joints. The finite
element technique was used to determine the compliance of
typical fillet welded joints. The results of this analysis
showed that the stress intensity factor was a function of
weld size, weld angle, plate thickness and weld penetration.
Relationships to estimate the stress intensity factor were
developed.

The third phase of the study was the correlation
of the experimental fatigue stress-life behavior of fillet
welded joints with the predicted behavior using the concepts

of the fracture mechanics of stable crack growth. The study showed that the fatigue behavior of various joint geometries could be correlated using the stress intensity factors developed in phase two. The correlation included failures from cracking at the root and toe of the fillet weld. The analysis provided a good estimate of the observed fatigue behavior for fatigue lives from $10^3$ to $2 \times 10^7$ cycles of load application.

## 1.   INTRODUCTION

This dissertation is concerned with the study of the fatigue behavior of fillet welded joints.  Historically this subject has held the interest of many investigators. Interest was generated by the general use of fillet welded joints in welded construction.  Fillet welds are usually more economical than other types of welds and are extensively used.  However, experimental studies showed that fillet welded joints had low fatigue strengths when they were stressed in a direction perpendicular to the weld line.  This led to further studies in attempts to determine why these reductions were observed.

Early studies of the fatigue behavior of fillet welded joints showed that their fatigue lives were a function of weld size and joint geometry.[1-7]  Photoelastic studies were used to evaluate the influence of the joint geometry upon the state of stress in the joint.[8,9]  These studies provided insight into the stress distribution within the joints and provided an indication of the stress concentrations which exist at the toe and root of the weld. Nearly all of these stress studies were concerned with the static behavior of the joint.  They did not provide a

relationship between joint geometry and applied stress and
their relationship to fatigue life.

The increased use of welded construction during
the late 1950's focused attention on the fatigue behavior
of fillet welded joints. Numerous investigations were
undertaken on different joint geometries, steels and
welding processes.[10-25] A review of these studies is
given in Ref. 26. This work showed that the principle
variables influencing the fatigue life of a fillet welded
joint were the geometry of the joint and the applied stress
range. The static strength of the base metal was observed
to have little influence on the fatigue strength for the
range of steels used in bridge and building construc-
tion.[25,26] In addition, the type of welding process
employed in the manufacturing of the joint as well as the
strength of the deposited weld had little influence. They
wei  observed to only influence the fatigue behavior if they
chai  ed the weld profile significantly and/or provided a
weld with different sized defects.[15,27]

Recently fracture mechanics has been employed to
analyze the fatigue behavior of fillet welded
joints.[25,28,29,30] These studies yielded qualitative
information about the influence of joint geometry upon the

observed fatigue behavior. However, adequate estimates of the fracture mechanics stress intensity factor for cracks in fillet welded joints were not available. Quantitative estimates of fatigue life behavior require more accurate estimates of the stress intensity relationship.

The results of these previous studies have not provided a means to quantitatively estimate the fatigue life of fillet welded joints. Each set of test results must be treated separately since no means exists to correlate the behavior of joints with different geometries. The influence of weld size and penetration, plate thickness and initial flaw size has not been studied analytically. This dissertation describes the results of an analytic and experimental study of the fatigue behavior of two simple fillet welded joints stressed perpendicularly to the weld line. A method of quantitatively estimating the influence of joint geometry upon the fatigue life behavior of fillet welded cruciform joints is developed. The study consisted of three major phases.

The first phase was an experimental investigation to determine the low cycle fatigue behavior of two fillet welded joints. Previous studies examined the high cycle life-low stress region. This study examined the transition region between low cycle life (less than 1000 cycles) and

high cycle life (greater than 100,000 cycles) of high strength steel fillet welded joints. The purpose of this phase of the study was to determine the stress-life behavior and the mode of failure.

The second phase of the study involved a stress analysis of the test joints using the finite element technique. The purpose was to examine the effect of joint geometry upon the stress distribution in the joint and provide fracture mechanics stress intensity factors for the cracking behavior.

The third phase of this study correlated the fatigue behavior of the test joints with their geometry. This was accomplished by relating the stress intensity factors from the finite element study to the crack growth rate. The relationships between fatigue behavior and joint geometry permitted the results of other studies to be correlated. In the case of certain welded joints, the influence of geometry upon the fatigue can be estimated quantitatively. Clearly weld imperfections, such as weld border cracks and weak regions along solidification boundaries, may cause large variations in fatigue life. Quantitative characterization of such defects in a fracture mechanics basis is possible by assigning an initial crack size corresponding to the observed fatigue life.

## 2.  <u>FATIGUE TESTS OF FILLET WELDED JOINTS</u>

Two cruciform shaped specimens were selected for investigation in this study. Figure 1 shows a schematic of the two specimens. The upper specimen is considered a non-load carrying specimen since the main plate is continuous. Consequently, the welds and cross plates only carry a small portion of the load. The lower specimen has a discontinuous main plate and the full load must be carried by the welds into the cross plate.

These specimens were selected due to their ease of fabrication and testing at high stress levels. They are representative of typical joints found in welded construction and have been used by numerous investigators. Their use permitted the results of this study to be directly compared with earlier work. The simple joint geometry facilitated the stress analysis and reduced the number of geometric parameters.

### 2.1  Specimen Fabrication

The specimens were fabricated from 5/8" thick ASTM grade A514F plate material. Table 1 summarizes the physical and mechanical properties. The specimens were fabricated from four sets of plates. The plates were cut so that the

direction of rolling of the main plate was the same as the direction of the appl load. After cutting, the plates were sand blasted to remove loose mill scale. The surfaces to be welded were then ground lightly to remove the remaining tight mill scale. The plate edges were left square.

One-half inch fillet welds were used to connect the cross plates to the main plate. The weld size was selected to provide a static weld strength greater than or equal to the capacity of the main plate. The welds were made in three passes in the sequence shown in Fig. 2. They were placed in the horizontal position with the legs inclined so that the plane of the electrode travel was 45° from the surface of the two plates.

The welds were made by the automatic gas metal arc process. One-sixteenth inch AX-110 welding wire was used with Argon plus 2% oxygen shielding gas. The average heat input was 40,000 joules/in with an interpass temperature of less than 150°F. These welding procedures were selected to provide a weld which slightly overmatched the strength of the base plate.

After welding, the joints were sliced into pieces 1 3/8 inches wide. The edges were then Blanchard ground to

a width of 1.200 inches $\pm$ 0.001. The nominal specimen dimensions are given in Fig. 1.

Figure 3 shows a polished and etched joint section. The three weld passes are readily apparent together with the heat affected zone and the lack of penetration at the weld roots. The variation of the weld profiles shown is typical of all the joints tested.

## 2.2  Testing Procedure

The specimens were tested in a 220 kip Amsler fatigue testing frame. The hydraulic power was supplied by a 220 kip Amsler Slow Cycling Unit. The specimens were tested under a constant amplitude cyclic stress. Due to the operating characteristics of the slow cycling unit the waveform was a rounded symmetrical saw tooth. The testing frequency varied between 20 and 60 CPM. The lower frequency was used for the highest stress range specimens and the higher frequency for the lower stress ranges.

The nominal stress in the main plate of the specimen was selected as the controlled experimental variable. The minimum stress of all the specimens was 20 ksi. Table 2 gives the values of stress range tested and the corresponding maximum stress. A minimum of three specimens of both types of specimens were tested at each stress level to provide a

measure of the variability. The order of testing and the
assignment of specimens to the stress levels was randomized
to minimize the effect of the uncontrolled variables such
as weld geometry, humidity, and ambient temperature.

Foil strain gages with a gage length of 1/4" were
applied to both sides of one end of the main plate. These
were located 3 inches from the cross plates. The gages were
used to measure the load in the main plate since the Slow
Cycling Unit's load indication was not accurate during cyclic
loading. The strain gage output was monitored on an x-y
recorder. The system allowed the loads to be set such that
stress range in the main plate was within 2% of the desired
range.

The tests were run continuously until either the
specimen fractured or its stiffness was reduced suddenly by
a failure of one weld causing the machine to shut off.

## 2.3  Failure Modes

The results of the fatigue tests are summarized in
Tables 3 and 4. The specimen designation is shown along with
the value of the nominal stress range and maximum stress in
the main plate. The failure mode of each specimen and its
cyclic life is also shown. Three failure modes were observed.
All of the non-load carrying welds failed from cracks

extending from the weld toe and are designated as the toe mode. Figure 4 shows a fracture corresponding to this mode of failure. The crack propagated through the thickness of the main plate until failure.

Most of the load carrying weld specimens failed from cracks which propagated from the initial flaw at the weld root. This discontinuity resulted from the incomplete penetration of the weld. These failures were designated as the root mode. The crack propagated perpendicular to the main plate into the weld metal. The final failure occurred by a shearing off across the weld. Figure 5 shows a typical root failure.

Two other failure modes were observed in the load carrying weld joints. Five joints failed from cracks extending from the weld toe and were similar to the failure shown in Fig. 4. A fourth failure mode observed in three load carrying joints was a shear failure as shown in Fig. 6. The failure plane was parallel to the main plate. The failure initiated at the weld toe from small cracks which were propagating into the plate until a few cycles before final failure. The crack growth direction abruptly changed to a direction parallel to the main plate. The failure occurring when the crack reached the weld's root.

## 2.4  Test Results

All test results are plotted in Fig. 7 where the
life of the specimen is plotted as a function of the nominal
stress range in the main plate.  The non-load carrying joints
are seen to yield a longer fatigue life.  The different
failure modes are indicated by the symbols in the legend.
Some of the welds exhibited marked amounts of porosity and
are indicated by vertical lines through their symbols.  They
are also marked by astericks in Table 3.  The shorter lives
of load carrying specimens with porous welds is seen to be
substantial at the higher stress ranges.

### 2.4.1  Effect of Weld Angle on the Cracking Behavior of the Non-Load Carrying Weld Joints.

All non-load carrying weld joints failed from
cracks starting at the weld toe.  Each joint had four weld
toes that provided potential failure sites.  Photoelastic
studies have shown that the stress at the weld toe is a
function of the weld angle.[8,9]  The influence of the weld
angle, $\theta$, on the failure location and specimen life was
examined to determine its affect.  The weld angle was defined
by the weld profile as shown in Fig. 8.  The measurements of
the weld height (H) and weld width (W) were made with a
machinist's scale to the nearest hundredth of an inch.

Figure 9 provides a histogram of the measured weld angles. The mean angle of all four welds of each joint is seen to be less than the mean weld angle where failure occurred. This difference suggests that the location of failure for a particular specimen is related to the weld angle.

The distribution of the ratio of each weld angle in a specimen to the failure weld angle is given in Fig. 10. Only 6 of the weld angles were greater than the weld angle at the weld where failure occurred. It is apparent that the larger the angle of a weld the more likely the failure will occur at that weld. Ninety-four percent of the joints in this test series failed at welds with the largest angle.

The fact that the failure location for a joint is dependent upon the angle of the welds suggests that the fatigue life is influenced by the weld angle. Figure 11 was constructed to examine this hypothesis. The ordinate defines the ratio of the weld angle at the failure location to the mean of the weld angles where failure occurred. The abscissa was taken as the ratio of the life of the specimen to the average life for that stress range. Although substantial scatter is apparent, a trend between weld angle and life is apparent. The solid line is a least square fit to the plotted data. The dashed line represents the mean line less the standard error of estimate. The life of a particular

specimen is therefore a function of the weld angle as well
as the applied stress.

The scatter in Fig. 11 seems reasonable since the
weld angle is only a gross indication of the weld profile.
Small irregularities at the toe along the length of the weld
such as undercut also affect the stress condition at the
weld toe and the initial crack condition and hence the
fatigue life. The weld angle defined in this study provides
a rough estimate of the variation in the stress at the weld
toe when the weld profile changes.

The influence of the weld angle upon the fracture
path of the toe failures was also investigated. The angle,
$\alpha$, which the crack made with the vertical was measured as
shown in Fig. 8. The measurements were made with a pro-
tractor to an estimated accuracy of $\pm 1°$. An attempt was
made to correlate the crack angle with the weld angle since
the state of stress at the toe is dependent upon the weld
angle. The crack plane was expected to be perpendicular to
the direction of the principal stress. Figure 12 shows a
plot of the weld angle and crack angle. No correlation is
apparent. An average angle of 13° seems to be a reasonable
estimate for all weld angles.

## 2.4.2   Fracture Path of Toe Failure

Failures from cracks at the weld toe occurred in both the load carrying and non-load carrying joints.  The origin of the crack was the same in both joints.  The cracks were observed to start from the intersection of the fusion line with the weld surface.  Figures 13 and 14 are photo micrographs of typical toe cracks.  Crack growth at the fusion line is visible in both figures.  Figure 13 is a fractured specimen that was tested at a stress range 30 ksi.  The crack grew away from the weld and the fusion line into the base metal of the main plate.  The crack shown in Fig. 14 is from a specimen tested at a stress range of 80 ksi.  The crack followed the fusion line and wash up zone into the weld metal.  The fracture path followed inclusions that were observed in this area.  The two fracture paths appear to be stress dependent.  Specimens tested at higher stress ranges showed a distinct tendency for the crack to follow the fusion line.  In the specimens tested at the lower stress levels the crack grew immediately into the base plate.  At the higher stress levels the crack followed the fusion line for a considerable distance before changing direction and growing in the plate.  Figure 15 shows the specimen which exhibited the longest fusion line growth of all the specimens tested.  In most of the specimens where crack growth was observed along the fusion line, the crack length along the fusion line was of the order of 0.05 inches.  Figure 16 shows

an enlargement of the area where the crack deviated from the fusion line into the plate.

The tendency for the crack to follow the fusion line at high stress levels seems to be related to the inclusion content of the heat affected zone. Figure 17 shows an unetched section of the weld metal and heat affected zone. A large number of inclusions are visible in the heat affected zone. Several elongated inclusions are parallel to the fusion line. An examination of the heat affected zone at a higher magnification can be made from the etched specimen shown in Fig. 18. The inclusions at the grain boundaries are easily seen. Heiser has shown that in banded steels the inclusions play an important role in fatigue crack propagation.[13] At high stress levels he found that the inclusion content had a significant effect upon fatigue crack growth rates and fracture paths. The crack tended to follow inclusions and grew intergranularly between the included grain boundary particles. He suggested that this behavior was due to the inability of the included particles to adjust to the stress conditions causing cracking around the particle. This cracking left a void which the crack propagated along. At lower stress conditions cracking at included particles was not observed.

The high inclusion content of the area adjacent to the fusion line seems to be responsible for the crack following that path.  Figure 19 shows a crack which formed at the toe and propagated in the HAZ following the fusion line.  The crack branching at inclusions is visually evident. Figure 20 is a higher magnification of the lower part of Fig. 19.

This study has shown that the length of the fracture path along the fusion line is dependent upon the stress level.  The higher the stress level the longer the crack followed this path before it grew through the thickness of the main plate.  This behavior was attributed to inclusion cracking at high stress levels.  The larger inclusion content of the HAZ at the fusion line caused the crack to follow this path at higher stress levels.  All toe cracks initiated at the intersection of the fusion line with the plate surface.

2.4.3  Fracture Path of Root Failures

Root failures only occurred in the load carrying weld joint.  No visible evidence of crack growth was found at the weld roots of the non-load carrying welds. Figures 21 and 22 show the region at the weld root for two untested load carrying joints.  The large separation at the right of the photos is due to the fit up of the

plates. The sharpness of this separation in Fig. 21 is seen to increase as it approaches the weld metal. Both figures indicate an extremely sharp crack immediately adjacent to weld metal. Cracks which caused the root failures propagated from these initial cracks.

Figures 23 and 24 show typical fracture paths of the root crack in the weld metal. The crack path has followed the columar grain boundaries in Fig. 23. This tendency is also evident in Fig. 24 but to a lesser degree. The path of the crack is nearly perpendicular to the main plate in both figures. A tendency for the crack to follow the grain boundaries in the weld metal was observed at all the root cracks examined. However the degree to which this influenced the macroscopic fracture path was found to be negligible. The crack would follow the grain boundaries when they were favorably oriented with respect to the macroscopic fracture path. If the grains of the weld were oriented perpendicular to the main plate at the weld root, as shown in Fig. 23, the fracture path was along the grain boundaries. When the grains were not perpendicular to the oriented plate, the crack would grow transgranularly across the grains as shown in Fig. 24.

These cracks grew vertically into the weld metal until failure occurred by a sudden tear as shown in Fig. 6.

Estimates of the stress on the final failure plane were
made and found to be smaller than the ultimate strength of
the weld metal. This fact suggests that weld metal may
have experienced fatigue damage during testing. This caused
the fracture to occur at a lower stress than its ultimate
capacity. No evidence of such damage was found, although
as shown in Fig. 15 the failure across this plane may have
been due to rapid crack growth.

Figure 25 shows the tip of a root crack at failure
after the crack has changed direction. The large open crack
is perpendicular to the main plate while the smaller branch
is almost parallel to the main plate. The final failure,
therefore, was due to rapid fatigue crack extension. The
change in the fracture path was attributed to a change in
the principal stress direction caused by the bending moment
introduced in the weld when the root crack is large.

The porosity of the weld also had a dramatic effect
upon the fatigue lives of specimens which failed from root
cracking. Figure 7 shows that at high stress levels
porosity in the weld caused failure to occur at much shorter
lives. This effect is believed to be due to crack growth
at the porosity. Crack growth was evident at the porosity
in all specimens with porous welds. These cracks weakened
the weld and decreased its faitue life. Figure 26 shows

the failure of a joint with a porous weld.  The failure oc-
curred by the rupture of the weld along the ligaments between
the extending cracks.  At lower stress levels the load on
these ligaments was less and failure was similar to the root
failures of welds without porosity.

### 2.4.4  Analysis of Shear Type Failures of the Load Carrying Weld Joint

Three load carrying welds exhibited a shear type
failure mode as shown in Fig. 6.  Examination of the welds
revealed that the leg of the weld (W in Fig. 1) was much
smaller than the average.  This fact along with the mode of
failure suggested that the failure of these specimens was
due to high shear stresses on the base of the weld.  Figure
27 shows the lives of the load carrying welds plotted
against the shear stress range of the weld with the smallest
leg.  The stress was calculated by dividing the total load
range per unit width by the smallest weld leg.  The line
shown in the figure is a least square fit of the shear
failure data.

The toe failures at high stress levels are the only
points above the least square line.  These failures occurred
by crack extension into the main plate after following the
fusion line for a portion of their life.  The shear failures
were similar to the toe failure except that the crack did

not propagate into the main plate. The failure occurred by cracking along the fusion line. At lower stress levels less cracking was evident along the fusion line. The line in Fig. 27 provides a reasonable estimate of the fatigue life of the weld in shear. At high stress levels, the crack propagated along the fusion line due to the inclusion cracking until the stress conditions favored through the plate thickness growth (toe failures).

If the inclusion orientation and spacing are favorable the crack may continue along the fusion line resulting in a shear mode failure. The tendency for inclusion cracking is less at lower stress levels and hence the specimens were not as critical in shear. Other failure modes were more critical as is apparent in Fig. 27.

## 3. <u>FRACTURE MECHANICS ANALYSIS OF FATIGUE BEHAVIOR</u>

Fracture mechanics, developed from the study of brittle fracture, has found increasing use in the study of structural fatigue.[32,33] Fracture mechanics is used to relate the materials fracture behavior by considering the energy balance of the energy released in fracture to the materials ability to absorb this energy. The use of fracture mechanics in structural fatigue is based on the assumption that the fatigue crack growth rate is a function of the crack tip stress field.

### 3.1 <u>Crack Tip Stress Field Equations</u>

The stress field in the region immediately adjacent to the crack tip for a two dimensional body is of the form:[34]

$$
\begin{Bmatrix} \sigma_x \\ \sigma_y \\ \tau_{xy} \end{Bmatrix} = \frac{1}{\sqrt{2\pi r}} \begin{bmatrix} \cos\theta/2[1-\sin\theta/2\sin3\theta/2] & -\sin\theta/2[2+\cos\theta/2\cos3\theta/2] \\ \cos\theta/2[1+\sin\theta/2\sin3\theta/2] & \sin\theta/2\cos\theta/2\cos3\theta/2 \\ \sin\theta/2\cos\theta/2\cos3\theta/2 & \sin\theta/2\cos\theta/2\cos3\theta/2 \end{bmatrix} \begin{Bmatrix} K_I \\ K_{II} \end{Bmatrix} \quad (1)
$$

where the coordinates "r" and $\theta$ are shown in Fig. 28. The parameters $K_I$ and $K_{II}$, called the crack tip stress-intensity factors, are two independent parameters which are functions of the body's geometry, crack length and linear functions of

the applied stress. $K_I$ represents the contribution of a symmetric and $K_{II}$ an antisymmetric stress distribution with respect to the crack plane on the crack tip stress field. The stress intensity factors are independent of the coordinates "r" and $\theta$ hence, represent the intensity of the stress field.

The stress-intensity factors are the leading terms of an expansion of the infinite series representing the total stress distribution of the body. The stress field adjacent to the crack is dominated by a square root singularity in "r" at the crack tip. The displacement field at the crack tip is also dependent on the stress intensity factor. Since the fatigue process takes place at the crack tip, it is reasonable to assume that it must be a function of the crack tip stress field and consequently the stress-intensity factors. [35]

## 3.2 Relationship Between the Stress-Intensity Factor and Fatigue Crack Growth Rate

Paris proposed the following relationship between the stress intensity range ($\Delta K$) and the crack growth rate (da/dN) [36]

$$da/dN = C\Delta K^n \qquad (2)$$

This relationship is a semi-empirical attempt to fit experimental data with the stress intensity factor. Numerous

crack growth studies on a variety of materials have shown that Eq. 2 provides a reasonable estimate of a material's crack growth rate response.[33,37,38] Other equations similar to Eq. 2 have been proposed. Some of these equations have been based on work hardening and fatigue damage considerations at the crack tip region. Other equations have been based on consideration of the crack tip displacements. Reference 39 gives an up-to-date review of these different models. Most models reduce to the general form of Eq. 2 for a particular material and environment.

## 3.3 Analysis of Fatigue Life Behavior Using Fracture Mechanics

The power law, (Eq. 2), relating the fatigue crack growth rate to a power of the range of stress-intensity provides the necessary relationship to estimate the fatigue life of a component. The range of the stress-intensity factor $\Delta K$ may, in general, can be expressed as

$$\Delta K = S_R \, g(a,w') \tag{3}$$

where
$S_R$ = nominal stress range

$a$ = crack length

$w'$ = a set of geometric constants for the body.

When Eq. 3 is substituted into Eq. 2 it yields

$$g(a,w')^{-n} da = C \, S_R^{\,n} dN \tag{4}$$

Integrating Eq. 4 between the limits of the initial crack

length $a_i$ and the final crack length $a_f$, defines the
component's fatigue life N as

$$N = \int_{a_i}^{a_f} g(a,w')^{-n} da / C \, S_R^{\ n} \tag{5}$$

Equation 5 provides a means to estimate the
fatigue life of a component if the value of $S_R$, $a_i$, $a_f$, C,
n, and the function g are known. It is also assumed that the
fatigue behavior of the component is totally a function of
crack growth. Crack initiation is not considered.

It is also interesting to note that the values of
C and n can be estimated from Eq. 5. If the values of $a_i$,
$a_f$, N, and $S_R$ are known from a series of fatigue tests, and
the function "g" is known for the geometry of the specimen,
then the values of C and n can be determined by fitting the
results of the fatigue tests to Eq. 5.

An alternate form of Eq. 5 is

$$N = \left[ S_R / n \sqrt{X} \right]^{-n} 1/C \tag{6}$$

where X

$$X = \int_{a_i}^{a_f} g(a,w')^{-n} da \tag{7}$$

Equation 6 is analogous to the log-log relationship between
$S_R$ and N normally observed for most structural details.

This provides a linear relationship of the form

$$\log N = \log B - m \log S_R \qquad (8)$$

or

$$N = B \, S_R^{-m} \qquad (9)$$

The constant B can be expressed as

$$B = X/C \qquad (10)$$

when the exponents "n" and "m" are equated. Equation 6 provides a means of including the effect of component geometry and initial flaw size, $a_i$, by the term $\sqrt[n]{X}$ . The consequences of this equation are explored and analyzed for fillet welded joints in this dissertation.

## 4. ESTIMATION OF STRAIN ENERGY RELEASE RATES USING THE FINITE ELEMENT TECHNIQUE

Irwin has shown that the stress-intensity factor, K, is related to the strain energy release rate, G. For a plane stress analysis this can be expressed as[34]

$$G = K_I^2 / E + K_{II}^2 / E \tag{11}$$

The value of the strain energy release is defined as the energy rate provided by a body containing an extending crack available for the crack-extension process. In other words the energy per unit of new crack area generated. This energy rate can be related to the change in compliance of the body for a load P as[34]

$$G = P^2/2 \; dC/dA \tag{12}$$

where dC/dA is the rate of change of compliance with crack area where the compliance is defined as

$$C = \Delta/P \tag{13}$$

### 4.1 Finite Element Analysis

The finite element technique has found wide spread use in the solution of boundary value problems. The

method is of a general nature and can be applied to any
boundary value problem.

The method of analysis can be divided into two
stages:

1.  The discretizing of the body to be solved into
    finite elements, and

2.  Minimization of a selected functional in the
    body.

The first stage in the analysis is done to make the second
stage more tractable.  By dividing the body into discrete
elements the functional to be minimized is represented
continuously in each element.  The result is a piecewise
continuous representation of the functional over the body.
The discrete elements are connected at nodes with the fields
in each element written as functions of nodal parameters.
The boundary value problem is therefore reduced to the
solution of a set of simultaneous equations in terms of the
nodal parameters connecting the finite elements.  These
sets of equations are of the form of

$$\{f\} = [A] \{\delta\} \tag{14}$$

where "f" is a vector of nodal forces and "$\delta$" the nodal
displacements.  The matrix "A" is the stiffness matrix of
the discretized body relating these parameters.  The
accuracy of a finite element solution depends on how well

the piecewise representation of the functional from the analysis approximate its true form.

## 4.2 Finite Element Compliance Analysis of Cruciform Weldments

The compliance of the cruciform joint was determined from a finite element analysis. The body was analyzed as a two dimensional plane stress problem. Figure 29 shows a schematic of the idealized shape of the two joints analyzed. The welds profiles were idealized as triangular shapes. The weldments were also assumed to be completely symmetric with respect to the planes shown as dashed lines in Fig. 29. The length of the main plate from the weld toe was taken as three times the thickness of the main plate. This located the loaded nodes far enough away from the weld toe and/or toe cracks so that the state of stress at those points would be uniform axial tension. Symmetry of the joint permitted a quarter section of the total joint to be used.

### 4.2.1. Element and Mesh Selection

The selection of the type of elements to be used and the mesh or discretizing of the body determines the accuracy of the finite element solution. The more sophisticated the element the larger the mesh can be for the same

accuracy. A more sophisticated element contains a higher order field and consequently can represent the functional over a larger area.

The crack tip stress field equations given in Chapter 3 show that at the crack tip a stress singularity of the form $1/\sqrt{r}$ exists. Consequently a displacement field of the form $r^{\frac{1}{2}}$ exists in the region of the crack tip. Due to the geometry of the weld joint, a complex stress distribution exists in the region of the weld and at the weld's toe and root.

The experimental study and the work of others have shown that cracking can occur at two locations in load carrying weld joints. Cracks may occur at the root of the weld or at the weld toe depending upon the geometry of the joint and the penetration of the weld. In non-load carrying weld specimens, cracking nearly always occurs at the weld toe. Hence, a finite element analysis of load carrying joints must provide for toe and root cracks. Only toe cracks need to be considered for the non-load carrying weld joints.

Due to the complexity of the stress distribution and the large number of geometries and crack lengths to be

analyzed, an element was selected that would minimize the time and cost of the analysis. The Constant Strain Triangle (CST) element is the simplest finite element available and was selected. Its chief advantages are that its element properties are easily and rapidly calculated and its triangular shape facilitated the matching of geometric boundaries.

The displacement field within the element is linear so consequently the strain and stress field are constant. Each element provides a constant strain energy density. Since the strain energy was selected as the functional to be minimized (as is normally done in the solution of boundary value problems whose solution is formulated from displacement fields) it is approximated stepwise by each element over the body.

The element mesh and size in the regions of high displacement gradients must be refined to insure that the true displacement field or strain energy density is adequately represented. Figure 30 shows the mesh used to evaluate the load carrying weld with a root crack. The element size near the crack tip and in the region of the weld toe is seen to be quite small. The elements within the weld were also made small to accommodate the complex

state of stress which existed. Figures 31 and 32 show the
meshes used for the analysis of toe cracks. Again the
refinement in the mesh at the crack tip is evident.

The crack in each of the joints was modeled by
two lines of nodal points immediately adjacent to each other
but not connected. Displacement boundary conditions were
applied along the planes of symmetry. The nodes at the
bottom of the figures at the mid-thickness of the main
plate were fixed in the vertical direction. The nodes at
the mid-thickness of the cross plate were restrained in the
horizontal direction. The nodes at the end of the main
plate were loaded by concentrated tension loads equivalent
to a uniform stress distribution.

The small elements used in the mesh near the crack
tip, although much smaller than normally used in finite
element analysis of bodies, are still larger than those
used by previous investigators of cracked bodies.[40,41,42]
This was not believed to invalidate the results since the
values of the stress intensity factors were determined from
a compliance analysis. Mowbray has recently demonstrated
that this method gives quite accurate results with rather
coarse meshes.[43]

The reason for this accuracy is due to the fact that although the finite element solution underestimates the strain energy near the crack tip, the compliance method of analysis examines the strain energy in the entire body. Since the crack tip singularity only dominates the region close to the tip the overall estimate of the strain energy is good. The strain energy at the crack tip region is only a small percentage of the total strain energy in the body. Consequently errors in its estimation do not have much effect on the total strain energy calculation. Methods suggested by other investigators focus on the local behavior at the crack tip and consequently require extremely small elements to accurately estimate the stress and displacement behavior in this region.[41,42,43] High order elements which include the stress singularity at the tip do not require the refinement in mesh size, however displacement discontinuities arise between these elements and adjacent ones which are also a source of error.[44]

The effect of the error in the estimation of the strain energy near the crack tip on the analysis can also be evaluated by comparison of compliance tests of actual specimens with analytical solutions. Srawley found the error to be small for a single edge-notch specimen.[45] The compliance was measured on a specimen where the crack tip

radius was 1/32 inch. The stress at the crack tip is
proportional to the ratio of the crack length to the crack
tip radius with the value of the stress intensity factor
being defined as the crack tip radius approaches zero.
Consequently the stress field in the vicinity of the crack
tip was less than that defined by equation 1. This is
similar to the effect of the underestimate of this stress
field by the finite element solution. Therefore,
the assumption that the error in estimating this energy will
not influence the accuracy of the compliance analysis seems
justified.

The second reason given by Mowbray for the accuracy
of the method is the fact that the values of G and K are
functions of the change in compliance with crack length.
Consequently, if the error in compliance is independent of
crack length, the slope of the compliance versus crack length
curve should be close to the true curve. The independence
of the error with crack length should hold if the finite
element mesh is similar for each crack length analyzed as it
was in this study.

4.2.2 Method of Solution of Finite Element Equations

The method of solution of the equations resulting
from the finite element formulation was selected to provide

rapid solution time. The quantities required for a
solution by a compliance analysis are the displacements of
the loaded nodes. The loads at these nodes were based on
the assumption that the state of stress was uniform. The
applied stress does not influence the resulting load-
displacement relationship so for convenience in checking
the results it was taken as 100 ksi for all geometries.
The load-displacement relationship was found by treating the
joint as a series of substructures. The load displacement
relationship was determined for each substructure and then
combined to give the load-displacement relationship for the
joint. Appendix A gives the details of the analysis. This
method reduces the size of the matrix inversions required
and eliminates most of the off diagonal zero terms. For
each crack length analyzed, only the substructures near the
crack are subjected to mesh changes, consequently only
those substructure stiffness matrices need be recomputed for
each crack length.

Each analysis provided the displacements of the
loaded nodes. A set of displacements was determined for
each joint geometry corresponding to a set of crack lengths.
The compliance of a particular geometry and crack length was
then determined by dividing the load, P, in the main plate
by the x-displacement of the loaded node at the plane of

symmetry of the main plate.  The x-displacement was
doubled since it represents the total extension of the
symmetric section.

### 4.3  Evaluation of the Stress Intensity Factor

The set of compliances and crack lengths were
fitted by least squares to a polynomial of the following
form

$$EBC = A_o + \sum_{n=2}^{m} A_{n-1} (a/w')^n \qquad (15)$$

where

C = P/Δ = specimen's compliance,

B = specimen's width,

E = Young's Modulus,

a = crack length

and  w'= a geometric constant with dimensions of
length.  The elastic Modulus and the specimen's thickness
were constant and taken equal to 30,000 ksi and unity
respectively.  The first order term of the polynomial was
not included since the stress intensity factor
must be zero when the crack length is zero.

Equation 12 can be rewritten as

$$G = \frac{P^2}{8EB^2 w'} \frac{d(EBC)}{d(a/w')} \qquad (16)$$

where the area of the new crack formed is

$$dA = 4Bw' \, d(a/w') \qquad (17)$$

The constant four in Eq. 17 is a consequence of the symmetry used in the finite element analysis. Each specimen contained four cracks.

Substituting Eq. 15 into Eq. 16 yields

$$G = P^2/8EB^2w' \sum_{n=2}^{m} n \, A_{n-1} \, (a/w')^{n-1} \qquad (18)$$

where G is the total strain energy release rate. The value of the stress intensity factor was evaluated using Eq. 18 as

$$K = [EG]^{\frac{1}{2}} = P/2B\sqrt{2w'} \sum_{n=2}^{m} [nA_{n-1} \, (a/w')^{n-1}]^{\frac{1}{2}} \qquad (19)$$

where K is an equivalent stress intensity factor equal to $K_I[1+(K_{II}/K_I)^2]^{\frac{1}{2}}$. The displacements of the nodes along the crack surface in the finite element analysis revealed that the ratio of $K_{II}$ to $K_I$ was less than 10 percent. Therefore the value K calculated by Eq. 19 is approximately **equal** to $K_I$. The stress intensity factors calculated from the finite element analysis are designated as K in this dissertation.

### 4.3.1 Stress Intensity Factors for Root Cracks of Load Carrying Fillet Welds

Thirty-two different joint geometries were analyzed to determine the effect of the joint geometry upon the stress intensity factor. The compliance of each geometry was determined for sixteen different crack lengths and the uncracked joint (full root penetration). Nine of the joint

geometries simulated the average geometry of the fatigue test specimens. The remaining geometric configurations correspond to specimens tested in previous investigations. Table 5 summarizes the dimensions of the joints analyzed and their source. The dimensions are defined in Fig. 1.

The analysis of the joints simulating the fatigue test specimens included a variation of the weld angle, $\theta$. The weld size was defined by the leg dimensions W and H. These parameters were determined by maintaining the weld cross sectional area constant and varying the weld angle. The weld area was equated to the average area of the specimens. One specimen was analyzed with an oversize weld with equal legs. It is identified with an asterisk in Table 5. The weld angle was assumed equal to 45 degrees for the earlier studies since its value was not reported.

The results for three test specimens are plotted in Fig. 33. The quantity EBC is shown as a function of a/w' for specimens with weld angles of 30, 40 and 45 degrees. The parameter w' was defined as

$$w' = T_p/2 + H \qquad (20)$$

for all the geometries analyzed. A fifth order polynomial of the form of Eq. 15 was used to fit the compliance (EBC) as a function of a/w' for all geometries. This order

polynomial was found to provide the minimum standard error of estimate.  The standard error of estimate of the fitted polynomial was less than 0.004 for all geometries which corresponds to an error of less than one-tenth of a percent.

The values of a/w' at which the compliance was determined were the same for all geometries.  The crack lengths included an uncracked joint (a/w'=0) and increments of a/w' between 0.115 and 0.692.  These crack lengths were believed to be in the most useful range based on visual examination of the test specimens.  The fitted polynomial provided a means of interpolating the value of the stress intensity factor for crack lengths smaller than w' x 0.115.  Accurate calculation of the compliance for cracks of this size would have required extremely small elements using the finite element technique.  Stress intensity factors were determined from Eq. 19.  The fitted polynomial permitted the stress intensity factor to be evaluated over a wide range of crack lengths.  Table 6 gives the values of the coefficients of the polynomial for K of each geometry.

Figure 34 shows the variation of the ratio of the stress intensity factor to nominal plate stress, $\sigma_{PL}$, as the crack length increased.  The five joint conditions shown in Fig. 34 correspond to different weld sizes.  The main and

cross plate thickness were equal and the weld angle is equal
to 45 degrees. The large variation of the stress intensity
factor with weld size is readily apparent. A decrease in
weld size resulted in a substantial increase in the ratio
of $K/\sigma_{PL}$ at all crack sizes.

Figure 35 shows the variation in stress intensity
with weld angle. The weld cross sectional area is the same
for each weld angle. The variation in the stress intensity
with weld angle is seen to be much less than the variation
predicted by changing the weld size ($H/T_p$) (see Fig. 34).
Increasing the weld angle from 30° to 50° results in approx-
imately a ten percent increase in $K/\sigma_{PL}$. This change in
weld angle represents a change in $H/T_p$ from 0.653 to 0.939.
A similar variation in $H/T_p$ in Fig. 34 for welds with equal
legs and increasing weld size would decrease the stress
intensity factor by approximately forty-five percent. The
effect of weld angle on the stress intensity factor for
welds of equal area is therefore small.

The similarity in the shape of the stress intensity
factor curves suggests that a functional relationship may
exist which describes the behavior for all joint geometries.
Harrison[28] suggested that the following expression could
be used to estimate the stress intensity factor at the root

of load carrying fillet welds

$$K = \sigma_w \sqrt{2w' \tan \pi a/2w'} \qquad (21)$$

$\sigma_w$ was defined as the nominal gross stress acting on the weld
and was equal to

$$\sigma_w = P/B \ (T_p + 2H) \qquad (22)$$

This estimate considers the joint to be equivalent to a
plate of breadth equal to $T_p$ + 2H containing a central crack
of length 2a.

An equation similar to Eq. 22 was found to provide
a reasonable estimate of the relationship between the stress
intensity factor and crack length. The more accurate secant
finite width correction was used in place of the tangent
correction used by Harrison. In addition, a non-dimensional
correction factor was developed to account for the difference
between the cruciform joint and the constant breadth plate.
This resulted in the following relationship for K at the
weld root:

$$K = \sigma_w \lambda_R \sqrt{\pi a \sec \pi a'/2w'} \qquad (23)$$

where $\lambda_R$ is non-dimensional correction factor for the
cruciform shape.

The value of $\lambda_R$ was observed to be a function of
$H/T_p$, the weld angle, the ratio of the thickness of the main

and cross plate, and the value of a/w'. The value of $\lambda_R$ was calculated for each geometry by equating Eq. 23 to the polynomial expression for K and solving for $\lambda_R$. The heavy lines in Fig. 36 show the variation in $\lambda_R$ with a/w' for different values of $H/T_p$.

A linear approximation was fitted to the values of correction factor using a least square fit. The fitted equation was

$$\lambda_R = C_1 + C_2 \ a/w' \qquad (24)$$

The linear approximation is also plotted in Fig. 36. The linear approximation for $\lambda_R$ yielded values of K within two percent of the values calculated from the polynomial expressions when substituted into Eq. 23. The average error was less than one percent and the maximum error occurred as a/w' approached zero.

The coefficients $C_1$ and $C_2$ were examined to find if they varied systematically with joint geometry. Figure 37 shows the variation of $C_1$ as a function of the ratio $H/T_p$. It is apparent that a continuous functional relationship exists between $C_1$ and $H/T_p$ over a wide range of plate thicknesses when the main and cross plates are of equal thickness and weld angle is 45 degrees. The values of $C_1$ for other weld angles are also shown for one plate thickness

and a constant weld area. A large variation in $C_1$ with weld angle is evident.

Only a single geometry with unequal plate thickness was evaluated since only one series of tests was available in the literature. This condition is indicated by the open circle with a horizontal line in Fig. 37. The value of $C_1$ for this geometry is seen to be slightly less than a joint with equal plate thicknesses for the same value of $H/T_p$.

Figure 38 shows the variation of $C_2$ with $H/T_p$. It is again apparent that a continuous relationship exists between $C_2$ and $H/T_p$ for a weld angle of 45 degrees and $T_p/T_c$ equal to unity. As observed with $C_1$, a change in weld angle results in a substantial change in $C_2$. The value of $C_2$ for the specimen with unequal plate thicknesses is seen to be greater for the same ratio of $H/T_p$.

The variation of $C_1$ and $C_2$ with weld angle as shown in Figs. 37 and 38 exaggerates the influence of the weld angle on the stress intensity factor. As was shown in Fig. 35, the actual variation in $K/\sigma_{PL}$ with weld angle was small. The large variation of $C_1$ and $C_2$ is due to the fact that K is expressed as a function of $\sigma_w$ in Eq. 23. Since the weld area was maintained constant in the analytical

study, an increase in the weld angle decreases the nominal gross weld stress, $\sigma_w$, since H is increased.

Generally the load carrying capacity of a joint is expressed in terms of the plate force. The variation of K with weld angle is small when expressed as a function of the plate stress as was shown in Fig. 35.

The values of $C_1$ and $C_2$ for weld angles of 45 degrees and $T_p/T_c$ equal to unity were fitted by least squares to polynomials of $H/T_p$. This yielded the following expressions:

$$C_1 = 0.52807 + 3.2872(H/T_p) - 4.3610(H/T_p)^2 + 3.6958(H/T_p)^3 - 1.8745(H/T_p)^4 + 0.41495(H/T_p)^5 \qquad (25)$$

and

$$C_2 = 0.21800 + 2.7173(H/T_p) - 10.171(H/T_p)^2 + 13.122(H/T_p)^3 - 7.7546(H/T_p)^4 + 1.7827(H/T_p)^5. \qquad (26)$$

These equations provide estimates of $C_1$ and $C_2$ for $H/T_p$ between 0.20 and 1.20. The stress intensity factor at the weld root can be estimated by the expression

$$K = \sigma_w \ [C_1 + C_2(a/w')] \ \sqrt{\pi a \ \sec \pi a'/2w'} \qquad (27)$$

for joints with equal plate thicknesses and weld angles of 45 degrees.

The value of K predicted by Eq. 27 is 20 to 70
percent greater than the estimate provided by Harrison's
approximation (Eq. 21). Equation 27 estimates K values
within two percent of the values predicted by the polynomial
expressions. The value of K for joints with equal plate
thicknesses and other weld angles ($\theta \neq 45°$) can also be
estimated from Eq. 27. The variation of $K/\sigma_{PL}$ for various
weld angles and constant weld area was observed to be small.
A reasonable approximation of K can be found by using a weld
height equivalent to a 45 degree weld of the same area. The
equivalent weld height, H, can be found from the relationship
$H = \sqrt{H^*W^*}$ where $H^*$ and $W^*$ are the legs of the actual weld.

Equation 27 can be expressed in a more useful
design form as

$$K = \frac{\sigma_{PL}}{(1+2H/T_p)} \ [C_1 + C_2(a/w')] \ \sqrt{\pi a \ \sec \pi a/2w'} \qquad (28)$$

where $\sigma_{PL}$ is the main plate stress. This equation provides
a reasonable estimate of the stress intensity factor at the
weld root in terms of weld and plate geometry and the nominal
plate stress.

### 4.3.2 Stress Intensity Factors for Toe Cracks of Load Carrying Fillet Welds

Table 7 summarizes the geometric variables for
the twenty-two load carrying fillet welded joints that were

available in the literature and this study. All joints had
main and cross plates of equal thickness. The effect of
weld angle was also studied. The average size reported in
the literature for each series was used. The weld size
parameters H and W were calculated from the average weld
area of the specimens. A comparable method was used for
the root crack analysis.

The influence of the weld penetration was also
included in the analysis. The average depth of root
penetration for each geometry is given in Table 7. The
penetration is expressed as a percentage of the half
thickness of the main plate. Thirteen geometric conditions
were analyzed with variable weld penetration. The effect
of weld penetration was included in the analysis since a
preliminary study had indicated that the stress
at the weld toe was a function of the weld penetration.
Increasing the weld penetration decreased the stress at the
weld toe. Thirteen of the twenty-two geometries were an-
alyzed with full and approximately zero weld penetration to
determine its effect. The other remaining geometries were
analyzed using the average penetration they were fabricated
with.

The cracks at the toe of the weld were assumed to

be inclined from the vertical at the angle of 13 degrees.
This angle corresponded to the condition observed during
the experimental phase of this investigation.  This angle
was also compatible with the inclination of the principle
stress axis at the weld toe.

The geometric constant w' in the compliance
polynomial was defined as

$$w' = T_p/[2 \cos 13°] \tag{29}$$

The compliance of each joint was determined for thirteen
crack lengths including the uncracked joint.  The ratios of
crack length to w' included in the analysis varied from 0.15
to 0.70 in increments of 0.05.

A sixth order compliance polynomial was found to
provide the minimum standard error of estimate.  The
standard error of estimate was less than one-tenth of a
percent of the measured compliances.  The coefficients of
the polynomial expressions for the stress intensity factor
(see Eq. 19) for each geometry is given in Table 8.

Figure 39 shows the predicted variation of $K/\sigma_{PL}$
with a/w' for two different plate thicknesses.  The effect
of weld size for full and small penetration welds is also
shown.  The variation of $K/\sigma_{PL}$ for joints with full

penetration welds was not affected by weld size. However, for joints with small penetration the value of $K/\sigma_{PL}$ is seen to increase as the weld size decreased. As the weld size approached the plate thickness, the effect of penetration on the ratio $K/\sigma_{PL}$ decreased. Partial and full penetration welds provided about the same conditions at the weld toe for large welds ($H/T_p \simeq 1$).

An equation comparable to Eq. 23 was used to express the stress intensity factor in terms of the applied stress, crack size and plate geometry

$$K/\sigma_{PL} = \lambda_T \sqrt{\pi a \ \sec \pi a/2w'} \qquad (30)$$

where w' is defined in Eq. 29 and $\lambda_T$ is a non-dimensional correction factor that is analogous to the stress concentration. The form of Eq. 30 was based on the known relationship for a finite width plate with a through crack. This relationship is an approximate solution for a double edge crack plate.

Equation 30 was equated to the polynomials that defined K as a function of a/w'. This permitted the variation of $\lambda_T$ with crack length and geometry to be determined. Figure 40 shows the scatter band of the variation of $\lambda_T$ with a/w' for all the geometries analyzed with 45 degree weld angles and full root penetration. The

maximum difference between $\lambda_T$ for all these geometries was
less than 5% for all crack sizes. The magnitude of $\lambda_T$ was
determined at values of a/w' equal to 0.02 through 0.10
in increments of 0.02 and from 0.10 through 0.70 in
increments of 0.05. These values were then fitted with a
polynomial of a/w'. The polynomial which provided the
minimum standard error of estimate was

$$\lambda_T = 2.164 - 6.957 \, (a/w) + 17.09 \, (a/w)^2 - 20.10 \, (a/w)^3$$
$$+ 8.842 \, (a/w)^4 \tag{31}$$

This equation is plotted in Fig. 40 as a solid line and is
seen to provide a reasonable estimate of the value of $\lambda_T$.

Figure 41 shows the variation of $\lambda_T$ with weld
angle. The weld area was constant for each joint and each
joint had full root penetration. Increasing the weld angle
is seen to increase $\lambda_T$ for small cracks. This effect
diminishes as the crack grows. As a/w' approaches 0.30 there
is no significant difference due to the angle of the weld.

Figure 42 shows the variation of $\lambda_T$ with a/w' for
joints with small root penetration. The value of $\lambda_T$ is seen
to increase with decreasing weld size. This behavior was
found for all the geometries analyzed. The stress intensity
factor at the weld root also increases with smaller weld

sizes and may represent a more critical condition when the weld penetration is small.

A stress analysis was performed on selected joints to determine if the behavior of the stress intensity factor could be related to the stress concentration at the weld toe. Figure 43 shows the finite element mesh used in the stress analysis. Constant strain triangular elements were used. The method of solution is given in Appendix A. The stress at the weld toe, $\sigma_{TOE}$, was taken as the maximum principle stress in the shaded element (Fig. 43). Figure 44 shows the variation of the stress concentration at the weld toe ($\sigma_{TOE}/\sigma_{PL}$) with $H/T_p$ for full and zero penetration welds. The plotted points are from joints with weld angles of 45 degrees. The variation of the stress concentration with $H/T_p$ for joints with full penetration welds is small. This is the same behavior that was found for $\lambda_T$ with full penetration joints. Joints with zero penetration yielded a dramatic increase in the stress concentration with decreasing weld size. The values of the stress concentration for zero penetration welds also seem to lie on the same curve for all the plate thicknesses included in the analysis.

The variation in the stress concentration at the weld toe was investigated further. Figure 45 shows the variation of the stress concentration factor with weld angle

for constant area welds. Increasing the weld angle
increases the stress concentration for joints with full
and zero penetration welds. The joints with full penetration
welds have lower stress concentrations. The variation of
the stress concentration factor with the weld angle is
approximately linear for both weld conditions.

Figure 46 shows the variation of the stress
concentration with root penetration for four values of $H/T_p$.
The stress concentration for small welds is seen to increase
much more rapidly with decreasing weld penetration than the
larger welds.

The value of the stress concentrations at the weld
toe were compared to the values of $\lambda_T$ as the ratio $a/w'$
approached zero. This limiting value of $\lambda_T$, which was
labeled $\overline{\lambda}_T$, was found by taking the limit of Eq. 30 as $a/w'$
approached zero. This yields

$$K = \sigma_{PL} \; \lambda_T \; \sqrt{\pi a} \tag{32}$$

The polynomial expression for K as $a/w'$ approaches zero
yields

$$K = \sigma_{PL} \; \frac{T_p}{2\sqrt{w'}} \; [A_1 (a/w')]^{\frac{1}{2}} \tag{33}$$

Equating Eqs. 32 and 33 provides an estimate for $\overline{\lambda}_T$ as

$$\overline{\lambda}_T = [A_1/\pi]^{\frac{1}{2}} T_p / [2w'] \tag{34}$$

Figure 47 compares $\overline{\lambda}_T$ with the stress concentration at the weld toe for joints of various plate thickness, weld penetrations, and weld angle. The values of $\overline{\lambda}_T$ are compatible with the stress concentration factor although they appear to be slightly larger. Hence the stress concentration factor provides a reasonable estimate of $\overline{\lambda}_T$.

This correlation seems reasonable since the stress intensity factor for small cracks at the weld toe should be a function of the local stress field. The toe stress from the finite element at the weld toe provides an estimate of this local stress. Since a rather coarse mesh was used to estimate the stress concentration, (element area $\simeq$ $(w'/10)^2$) the true stress state was underestimated. A better estimate of the stress concentration factor would provide better agreement with $\overline{\lambda}_T$. The dashed line in Fig. 47 represents a least squares fit of limiting value of $\lambda_T$ and the stress concentration factor predicted by the finite element analysis. $\overline{\lambda}_T$ can be estimated by

$$\overline{\lambda}_T = (\sigma_{TOE}/\sigma_{PL}) + 0.2 \tag{35}$$

for the stress concentrations estimated in this study. If more refined methods of calculating the stress are used the value of the stress concentration should approach $\overline{\lambda}_T$.

The correlation of the stress concentration factor with $\overline{\lambda}_T$ provides a method to estimate the stress intensity factor K for various crack lengths and geometric conditions which were not considered in the compliance analysis.

Figure 48 shows the variation of the ratio of $\lambda_T$ and the limiting value $\overline{\lambda}_T$ with a/w'. The relationships correspond to joints with 45 degree weld angles and small weld penetrations. For small cracks, a/w' less than 0.20, the ratio is seen to be approximately the same for all values of $H/T_p$. The curves tend to diverge at larger crack sizes.

For fatigue crack growth the estimate of K for small cracks is more critical since the largest portion of the life is consumed in propagating small cracks. An attempt was made to correlate the stress intensity factors at the weld toe for both full and partial penetration in terms of $\lambda_T/\overline{\lambda}_T$ and a/w'.

Equation 31 was modified by expressing the ratio $\lambda_T/\overline{\lambda}_T$ as a function of a/w'. This permitted $\lambda_T$ to be expressed in terms of its value as a/w' approaches zero $(\overline{\lambda}_T)$ for various crack lengths. Equation 31 in this form yields

$$\lambda_T/\overline{\lambda}_T = 1 - 3.215(a/w') + 7.897(a/w')^2 - 9.288(a/w')^3$$
$$+ 4.086(a/w')^4 \tag{36}$$

The dashed line in Fig. 48 compares this polynomial with the predicted values of $\lambda_T/\overline{\lambda}_T$. Equation 36 is seen to provide a reasonable estimate of the $\lambda_T/\overline{\lambda}_T$ ratio for these joints.

The stress intensity factor for cracks at the toe of load carrying fillet welds with partial root penetration can be estimated from:

$$K = \sigma_{PL} \; \overline{\lambda}_T \; [1 - 3.215(a/w') + 7.897(a/w')^2 - 9.288(a/w')^3$$
$$+ 4.086(a/w')^4] \; \sqrt{\pi a \; \sec \; \pi a/2w'} \tag{37}$$

$\overline{\lambda}_T$ can be estimated from the stress concentration at the weld toe. The magnitude of the stress concentration for a particular geometry can be estimated from Figs. 45 and 46. Equation 37 is accurate within 2% for full penetration welds with 45 degree angle. The average value of $\overline{\lambda}_T$ for all the joints analyzed with full penetration 45 degree welds was found to be 2.16. This value is a reasonable estimate of all joints with full penetration welds. The accuracy for joints with smaller weld penetration is less. For crack lengths less than 0.30w', Eq. 37 provides an estimate within 5% of the values determined from the polynomials.

### 4.3.3  Stress Intensity Factors for Toe Cracks of Non-Load Carrying Fillet Welds

Test data were available for thirteen non-load carrying weld joints. The joint geometries are summarized in Table 9. Specimens NT-1 through NT-9 were evaluated based on the average dimensions of the fatigue specimens. The weld angle was varied from 30 to 53 degrees with a constant weld area. Specimen's NT-10 geometry was based on the average size of the load carrying weld fatigue specimen. Specimens NT-14 through NT-19 were selected to provide an indication of variation due to a wide range of geometric parameters.

The weld root penetration was taken to be zero for all joints. The load carrying weld joints with full penetration provide information that would be directly applicable to the non-load carrying joints with full penetration.

The parameter w' in the compliance polynomial was defined in the same manner for load carrying and non-load carrying joints for crack growth at the toe (see Eq. 20). This assumed the crack plane to be 13 degrees from the vertical. The same increments of a/w' were used for the compliance analysis of both weld types.

A sixth order polynomial was again found to provide the minimum standard error of estimate. The standard error of estimate was less than one-tenth of a percent of the measured compliances. The coefficients for the stress intensity polynomials for each joint geometry are summarized in Table 10.

Figure 49 shows the typical variation of $K/\sigma_{PL}$ with a/w'. The value of $K/\sigma_{PL}$ is seen to increase slightly with an increase in the cross plate thickness. Figure 50 shows the variation of $K/\sigma_{PL}$ with weld angle. The scale of the abscissa has been enlarged to show the variation for small values of a/w'. The value of $K/\sigma_{PL}$ is seen to increase with increasing weld angle. The sensitivity of the value of K to weld angle is about the same order magnitude that was found in the load carrying joints. The effect of weld angle diminishes with increasing crack lengths. This behavior with weld angle was also noted in the load carrying weld joints.

The effect of weld root penetration on $K/\sigma_{PL}$ is illustrated in Fig. 51. The full penetration joint is seen to have a substantially higher value of $K/\sigma_{PL}$ than the zero penetration joint at all crack sizes.

within the range of the values plotted.  The value of
$\lambda_T/\bar{\lambda}_T$ is seen to be approximately the same for all
geometries for a/w' less than 0.25.  Some divergence is
apparent for larger cracks for the different ratios of $H/T_p$.

Equation 36 which was developed from the analysis
of load carrying joints with toe cracks is plotted in
Fig. 54.  This estimate of $\lambda_T/\bar{\lambda}_T$ is seen to provide a
conservative estimate of the variation of $\lambda_T/\bar{\lambda}_T$ when a/w'
is less than 0.35.  The value for larger crack sizes falls
within the band of the values for the various ratios of
$H/T_p$.  Equation 36 provides a reasonable estimate of the
variation of $\lambda_T/\bar{\lambda}_T$ for toe cracks in both load carrying
and non-load carrying joints.

The value of $\bar{\lambda}_T$ was found to correlate reasonably
well with the stress concentration factor for load carrying
joints.  No such correlation was found for the non-load
carrying joints.  The stress concentration factor increased
with $H/T_p$ for joints with equal plate thicknesses, $T_c/T_p=1$,
and with the weld angle.  This is similar to the behavior
which was observed for load carrying joints (see Figs. 44
and 45).

Attempts to correlate the stress concentration factor at the weld toe with $\bar{\lambda}_T$ were unsuccessful as is apparent in Fig. 55. The stress concentration is seen to decrease with increasing $\bar{\lambda}_T$. The stress concentration overestimates the value of $\bar{\lambda}_T$ for most of the geometric conditions examined.

The stress intensity factor for toe cracks in non-load carrying joints for the geometries analyzed can be estimated from Eq. 37. The value of $\bar{\lambda}_T$ for these geometries can be found using Eq. 34 with the leading term of the stress intensity polynomial given in Table 11. The value of $\bar{\lambda}_T$ for other similar geometries can be estimated from these values. When estimating values of $\bar{\lambda}_T$, consideration should be given to the fact that $\bar{\lambda}_T$ increased with smaller welds and increasing weld penetration increased the value of $\bar{\lambda}_T$

5.  COMPARISON OF TEST RESULTS WITH BEHAVIOR PREDICTED
    BY THE FRACTURE MECHANICS OF STABLE CRACK GROWTH

The fatigue behavior of the joints tested in this
study as well as the results of previous investigations were
evaluated using the principles of the fracture mechanics of
stable crack growth.  The equations developed from the simple
power law of crack growth were used to relate the fatigue
life of the test specimens to the applied stress.  The
influence of joint geometry and location of the failure were
included in the analysis using the relationships for the
stress intensity factor developed in this dissertation.

5.1  Crack Growth Behavior of Structural Steels

Figure 56 summarizes the results from five crack
growth investigations and defines the crack growth rate,
da/dN, as a function of the range of the stress intensity
factor, $\Delta K$.[37,46,47,48,49]  The growth rates are for
materials with yield strengths between 24 ksi and 125 ksi.
Also included are data from Ref. 49 where the growth rate was
measured in the weld metal and heat affected zone.  The weld
metal yield strengths varied from 70 to 90 ksi.  The welds
were made using the manual shielded metal arc process and
the gas metal arc process.

The data is seen to fall in a narrow scatterband.
The slope of the scatterband is about one-third.  This slope
corresponds to an exponent, "n", equal to 3 in Eq. 2.
Barsom and Klingerman observed that an exponent of three
provided the best fit to their test data when the power law
was used to describe the relationship between growth rate
and the range of the stress intensity factor.  Gurney and
Maddox found that the exponent varied slightly with material
strength.  Their studies showed a variation in "n" between
2.4 and 3.4.  A fatigue study of the effect of weldments
on steel beams has shown that the relationship between the
stress range at the detail and its life yielded a value of
"m" close to three for the exponential stress-life model, in
Eq. 8.[25]  The equivalence of the exponent "n" in the
power law of crack propagation to the exponent "m" in the
exponential stress life relationship was discussed in part
three.  This assumption was tested by Hirt in his analysis
of the behavior of welded beams.[50]  He found that an
exponent of three provided a reasonable estimate of both
"n" and "m" in Eqs. 2 and 8 respectively.  An exponent
equal to 3 was also selected for this fatigue study.

Little information is available about the crack
growth rate at the extreme values of $\Delta K$.  At low levels of
$\Delta K$ a threshold in crack growth rate has been suggested.  This

has been investigated by Paris in ASTM 9310 steel.[51]
He found that the growth rate decreased significantly at
$\Delta K \simeq 5.2$ ksi $\sqrt{in}$ . Harrison has estimated the value of this
threshold level from an analysis of rotating beam fatigue
results.[52] He estimates a threshold value of $\Delta K$ between
3.5 and 5.5 ksi $\sqrt{in}$ for steels. These estimates are shown
in Fig. 56 as horizontal lines near the ordinate.

At higher levels of $\Delta K$, Parry, Klingerman and
Barsom observed that the crack growth rate increased
markedly.[37,46,47] Parry and Klingerman observed this
change to occur when the net section stress approached the
yield point. Barsom suggested that the increase occurred
at a critical value of $\Delta \delta$, the range of crack opening-
displacement. The bands plotted in Fig. 56 also include
the data from these studies at high $\Delta K$ values. The rate of
crack growth observed at high $\Delta K$ levels falls within the
same general scatterband as the lower levels of $\Delta K$. The
assumption that the $\Delta K$-da/dN is governed by Eq. 2 at all
levels of $\Delta K$ seems to be reasonable in view of the
available experimental evidence.

## 5.2 Analysis of Load Carrying Joints Failing from the Weld Root

Six different joint geometries were included in

the analysis. Table 11 gives the average dimensions of the joints analyzed and their references. In addition, the analysis included data from a crack growth experiment on a center crack plates by Klingerman.[46] The dimensions of the plate are also given in Table 11. $T_p$ was taken as the plate width and the initial crack length is expressed as a percentage of the half width under the column giving the value of the percentage of root penetration. This data was included in the analysis since Eq. 27, which expresses the value of K for root cracks, is based on the known relationship for K for a center cracked plate. By equating the coefficients $C_2$ and the weld height, H, equal to zero and $C_1=1$, Eq. 27 yields the K value for the center cracked plate.

The plate geometry provides a means of evaluating the error in the estimate of the stress intensity factor for the welded joints. The stress conditions and the geometry of the plate specimens were carefully controlled thereby minimizing any associated error in their analysis.

Equation 6 can be expressed in the following form for an exponent of 3:

$$N = (S_R/\sqrt[3]{x})^{-3} \; 1/C \tag{38}$$

where $S_R$ refers to the gross section stress at the weld. The integral "X" is defined in Eq. 5 as

$$X = \int_{a_i}^{a_f} g(a,w')^{-n} da$$

$$= \int_{a_i}^{a_f} \left\{ [C_1 + C_2(a/w')] \sqrt{\pi a \sec \pi a/2w'} \right\}^{-3} da \tag{39}$$

where $w'$ is defined by Eq. 20. The coefficients $C_1$ and $C_2$ are defined by Eqs. 25 and 26 respectively as functions of $H/T_p$.

It is convenient to express Eq. 38 in terms of a "modified stress range" defined as

$$S_R^* = S_R/X^{1/3} \tag{40}$$

where the units of $S_R^*$ are KSI $in^{1/6}$. Substituting Eq. 40 into Eq. 38 yields:

$$N = S_R^{*-3}/C \tag{41}$$

This equation reduces to a linear form with the following logaithnic transformation

$$\log N = -\log C - 3 \log S_R^* \tag{42}$$

The load carrying joints were evaluated by determining $S_R^*$ for each joint. The integration to determine "X" was performed numerically using twelve point Gaussian Quaduature. Tests of the integration routine for

comparable integrals have yielded results to within 0.1%

of the closed form solution.  The error in "X" is believed

to be less than 1%.  The average values of $X^{1/3}$ for the test

specimens analyzed is given in Table 11.  The final crack

size, $a_f$, was taken as the value when the net section stress

at the weld was equal to the yield stress.  The influence of

the final crack size on the value of "X" using other

approximations such as the ultimate strength caused less than

a 2% variation in "X".  The crack size calculated from the

yield stress criterion gave closer agreement to the measured

size in the fatigue specimens tested in this study.  The

value of $a_i$ was taken as half the thickness of the main plate

minus the weld penetration.

Figure 57 summarizes the results of the analysis.

The "modified stress range" $S_r^*$ is plotted as a function of

cycle fife.  The results are seen to fall within a narrow

scatter band.  The two parallel lines shown in Fig. 57

represent the variation in the coefficient "C" found by

Barsom in his study of the crack growth behavior of ferrite-

pearlite steels.  These lines are plotted at a slope of -1/3,

corresponding to the exponent n=3 in the crack growth power

law.

The results from Klingerman's cracked plate study,

shown as the open squares, are seen to fall within the

limits for the welded joints. The estimates of the K relationship for welded joints developed in this study seem to be reasonable.

The large scatter in the data reported in Ref. 15 is believed to be due to the use of average values of the initial crack size, $a_i$, and weld size. The welding process was the same for all the specimens plotted from Ref. 15. Since wide variations in the average values existed for each joint of this study, comparable variation in the four welds could be expected for the joints reported in Ref. 15. The fatigue failure should occur at the weld with the smallest penetration (largest $a_i$) and size. The use of average geometry and crack size would obviously lead to increased scatter as observed in Fig. 57. The degree of weld penetration and consequently the initial crack size was more precisely defined by the other investigators.

The linear form of the log $S_R$* and log life relationship is seen to be valid over a wide interval of life. Lives from $10^3$ to $5x10^6$ cycles are seen to follow the linear relationship predicted by Eq. 42. The equation is seen to be valid in both the high stress-low cycle life and low stress-high cycle life regions. The results from a fatigue study in either of these regions can be

extrapolated over a wide range of stress and fatigue life.

At low levels of $S_R{}^*$ and high cycle life the scatter is seen to increase. The estimate of $\Delta K$ for the average initial crack size for joints from Ref. 15 tested at $S_R{}^*=11$ is 7.0 ksi $\sqrt{in}$ . The crack growth rate at this level of $\Delta K$ has not been established experimentally. Figure 56 indicates that at these low levels of $\Delta K$, the threshold of crack growth predicted by Paris and Harrison is approached.

The fatigue life of other load carrying joints that exhibit failure from the weld root can be estimated from Fig. 57. The magnitude of "X" can be estimated by integrating Eq. 39 between the limits provided by the initial crack size, $a_i$, and the final crack size, $a_f$. The final crack size can be estimated as the crack size at which the net section stress of the weld is equal to the yield stress. The initial crack size, $a_i$, is a function of the weld root penetration. Therefore, for a given weld size, plate size and alternating plate load, the degree of weld penetration necessary to provide the desired fatigue life can be determined.

## 5.3 Analysis of Load and Non-Load Carrying Weld Toe Failures

Three non-load and three load carrying fillet welded joints were analyzed for crack growth at the weld toe. The joint geometries are summarized in Table 12. The analysis of crack growth at the fillet weld toe was analogous to the study of root cracks. The stress intensity factor, K, was estimated from Eq. 37. The equation can be expressed in the following form

$$K = \sigma_{PL} \, \overline{\lambda}_T \, h(a, a/w') \tag{43}$$

where

$$h(a, a/w') = \lambda_T/\overline{\lambda}_T \, \sqrt{\pi a \, \sec \pi a/2w'} \tag{44}$$

The function $\lambda_T/\overline{\lambda}_T$ was defined by Eq. 36 in terms of $a/w'$. The expression for the fatigue life can be obtained from Eq. 5 and is

$$N = (\overline{\lambda}_T \, S_R)^{-3} \, Y/C \tag{45}$$

where

$$Y = \int_{a_i}^{a_f} h(a, a/w')^{-3} da \tag{46}$$

The parameter Y is a function of the initial and final crack size and w'.

The initial crack size, $a_i$, existing at the toe of fillet welds has been examined at the Welding Institute.[21,27] The toes of fillet welds made be several welding processes were examined metalographically by taking

slices through the thickness at the toe. These studies confirmed that crack like instrusions of slag and other inpurities existed at the weld toe. These intrusions as well as crack like cold laps and undercut were observed to provide initiation sites for fatigue crack growth. The depth of these defects were found to range from 0.0004 in.to 0.02 in. Welded specimens tested with artificial notches cut at the weld toe to a depth of 0.005 in. yielded fatigue lives comparable to those observed from specimens without notches.[27] The fatigue life was shown to increase when the toes were treated by grinding or peening to remove or reduce the initial flaw. Also the life increased when the welding process was modified to decrease the initial flaw size. The fatigue behavior of a fillet weld joint is consequently a function of crack growth since the initial crack like defects exist at the weld toe.

The integral Y which expresses the relationship between the fatigue life and applied stress range is a function of $a_i$, $a_f$ and $w'$. The value of Y was determined numerically for various values of $a_i$, $a_f$ and $w'$. Integration was again performed by the twelve point Gaussian Quadrature A singularity in the integrand exists as $a_i$ approaches z ro. The integration was performed by dividing the crack interval between $a_i$ and $a_f$ into four parts. The first increment was

taken as $a_i$ to $2a_i$ to account for the singularity.

Figure 58 shows the variation of Y with $a_i$ for two plate thickness. The final crack size, $a_f$, was also varied. $a_f$ was taken as $0.50w'=0.0641$ in. for the $\frac{1}{4}$ in. plate and $0.80w'=0.821$ in. for 2 in. thick plate. These values provide an extreme variation in plate thickness and final crack size. Values of Y for other plate thickness and final crack sizes were bounded by the curves shown in Fig. 58. The variation of Y with plate thickness and final crack size is seen to be negligible compared to the influence of the initial crack size. This is particularly true for small crack sizes. At larger crack sizes the value of Y was approximately constant. Hence, Y is primarily a function of $a_i$, the initial crack size.

The value of $a_i$ and the corresponding value of Y was not estimated directly in the analysis. The fatigue behavior of joints failing from the weld toe was estimated by assuming that Y was the same for all specimens. Hence, the cyclic life of each specimen was plotted as a function of the parameter $\bar{\lambda}_T S_R$. Figure 59 summarizes the available test data. The data shown includes both load and non-load carrying fillet welded specimens. The value of $\bar{\lambda}_T$ for each geometry was estimated as outlined in part four. The value

of $\bar{\lambda}_T$ estimated for each geometry is given in Table 12.

The scatter bands provided by the test data are plotted at a slope of -1/3. The data all fall within a reasonably narrow band. The use of a slope equal to -1/3 is seen to provide a reasonable estimate of the linear relationship between $\bar{\lambda}_T S_R$ and the cycle life. The variation in the test data is greater than predicted for the root cracks shown in Fig. 57. This increase in the scatter can be attributed to the variation in initial flaw size, $a_i$, and the variation of the crack growth constant for the steels used in the fabrication of the specimens. Obviously differences in the welding processes could substantially affect the initial crack size, $a_i$. The quality of the weld for a particular welding process can also vary due to uncontrolled variables such as operator performance. Manual shielded arc welds were used in Refs. 11 and 18. The manual welded specimens from Ref. 11 are plotted as open circles. These data define the lower limit of the scatter. The upper limit of the data is provided by manually welded specimens from Ref. 18. These data are shown by the closed circles. The automatic welds used in the fabrication of the specimens of the experimental study fall near the center of the scatter bands.

The initial crack size can be estimated by eval-

uating the ratio Y/C in terms of the scatter bands shown in
Fig. 59. The value of Y/C corresponding to the upper band
is $1.1 \times 10^{11}$ and the lower band is $1.2 \times 10^{10}$. Barsom's crack
growth data provided an estimate of the magnitude of C. He
observed C to vary between 1.37 to $3.6 \times 10^{-10}$ for ferrite-
pearlite steels. The corresponding values of Y vary
between 1.65 and 39.5. If average values are used, $Y/C =$
$6.1 \times 10^{10}$, $C = 2.5 \times 10^{-10}$, then $Y \simeq 15$. These values of Y are
compatible with the measured initial crack sizes found at
fillet weld toes as shown in Fig. 58.[21,27] A value of 15
for Y corresponds to an initial crack size of about 0.001 in.
in Fig. 58.

The scatter for the results from an individual
study are seen in Fig. 59 to be much less than the total
scatter for all results plotted. The dashed lines in Fig.
59 show the scatter in the results from the fatigue tests
from this study. Consequently the values of Y calculated
from the overall scatterbands and the limits of the C values
from Barsom's study overestimate the variation of the initial
flaw size for a particular test series. However, unless the
initial flaw size is measured for each specimen or an
estimate of the value of C corresponding to the material used
to fabricate the specimen, the two parameters Y and C are
confounded. An estimate of the variation in $a_i$ for the
results of the present study's fatigue specimens was made by

taking C equal to $3.6 \times 10^{-10}$. This value of C was estimated from Barsom's study and was felt to be a reasonable estimate for A514 steel. Using this value for C and the values of $\overline{\lambda}_T$ $S_R$ and cycle life defined by the dashed lines in **Fig.** 59 yielded a variation of $a_i$ between 0.0015 in. and 0.007 in. These values of $a_i$ correspond to values of Y of 12.6 and 7.31 respectively. They provide a more concise measure of the variability of initial flaw size at the weld toe. These flaw sizes correspond to equivalent lengths of sharp cracks at the weld toe. A blunt intrusion at the weld toe of greater depth may provide a longer life then inferred from this analysis since fatigue crack initiation may consume an appreciable portion of the life.

The linear trend between $\overline{\lambda}_T$ $S_R$ and cycle life in Fig. 59 is seen to be valid over a large range of cycle lives. The range of lives included in the analysis were $2 \times 10^3$ to $2 \times 10^6$ cycles of load. These lives cover the full range of the high cycle fatigue and into the low cycle regime of fatigue.

The fatigue life of a load and non-load carrying weld joint can be estimated directly from Fig. 59 when failure occurs from crack growth at the weld toe. The factor $\overline{\lambda}_T$ can be estimated from the relationships developed in this study.

## 6.  CONCLUSIONS

The main findings of this study are summarized in this chapter.  They are based on the analysis of the fatigue performance of fillet welded joints stressed perpendicular to the weld line.

1. The stress intensity factor for root cracks in load carrying joints was found to be a function of weld size, weld angle, and the thickness of the cross plates.  A relationship was developed which permitted the stress intensity factor, K, to be estimated for equal leg welds and equal thickness plates.

2. The stress intensity factor for toe cracks in load carrying joints was found to be proportional to the local stress at the weld toe.  This stress was estimated from a finite element analysis and found to be a function of weld angle, weld size, plate thickness and weld penetration.  Increasing the weld penetration decreased the stress and the K value as did increasing weld size.  The value of K for full penetration welds was found to be

approximately the same for all geometries.  The
stress intensity relationship was developed in
terms of a non-dimensional correction factor $\lambda_T$.
The value of $\lambda_T$ was observed to decay as crack
length increased.  $\overline{\lambda}_T$, the value of $\lambda_T$ as the
crack length approached zero, was found to be
proportional to the stress concentration at the
weld toe.  The decay function of $\lambda_T$ as crack
length increased was found to be the same for all
geometries.

3. The stress intensity factor for several non-load
   carrying joints was obtained.  The relationship
   developed to predict K for load carrying weld with
   toe cracks was found to be applicable.  However
   no correlation was found between the stress at
   the weld toe and the stress intensity factor.
   Further study is desirable.  The value of K at the
   weld toe was observed to increase as the weld
   penetration increased and weld size was decreased.

4. The failure mode of load carrying welds at high
   stress levels is dependent upon the weld size and
   the heat affected zone inclusion content.  A
   shearing mode of failure along the fusion line was

exhibited by joints with small welds. This behavior was attributed to cracking along included particles at high stress levels.

5. The fatigue behavior of both the non-load carrying and load carrying joints was analyzed using fracture mechanics principles. The fatigue behavior of many different specimen geometries were correlated. The results provide a rational means of estimating the fatigue performance of a joint for lives between $10^3$ and $5 \times 10^6$ cycles of load application. The correlation provided at low cycle lives provides a means to determine the fatigue performance of structural joints subjected to high stress ranges from a knowledge of their low stress performance.

6. The influence of the initial crack size on the life of toe crack failures was found to be great. The life increased rapidly as the initial crack size approaches zero. At crack sizes greater than 0.01, the effect was much less. Treatment of the weld toe by grinding and peening to reduce the initial crack size offer means

of substantially increasing the fatigue life.

7. The threshold value of $\Delta K$ for toe cracks appeared
   to be about 2 ksi $\sqrt{in}$ , much lower than estimated
   by others.  The value for root cracks appeared to
   be about 7 ksi $\sqrt{in}$ .  The fatigue behavior of
   welded joints at low stress ranges is dependent
   upon the crack growth behavior at these low levels
   of $\Delta K$.  Crack growth studies at low levels of $\Delta K$
   are needed to allow the accurate prediction of the
   fatigue performance of joints at low levels of
   stress.

8. The finite element technique of stress analysis
   was shown to provide a method of estimating the
   stress intensity factor for cracks in fillet
   welded joints.  This technique provides a
   powerful and straight forward means to estimate
   the stress intensity factor for other complex
   geometries.  The analysis of the
   cracking behavior of structures by fracture
   mechanics need no longer be restricted to simple
   geometries with known stress intensity factors
   since these may be estimated by a finite element
   analysis.

TABLES

# TABLE 1

## MECHANICAL AND PHYSICAL PROPERTIES OF PLATE MATERIAL

### ASTM GRADE A514F

COMPOSITION
(PERCENTAGE)

| C | Mn | P | S | Cu | Si | Ni | Mo | V | B |
|---|----|---|---|----|----|----|----|----|----|
| 0.15 | 0.85 | 0.010 | 0.018 | 0.17 | 0.17 | 0.75 | 0.45 | 0.06 | 0.0045 |

MECHANICAL PROPERTIES

YIELD STRENGTH    =108 KSI

TENSILE STRENGTH  =118 KSI

ELONGATION IN 2 IN.= 36%

REDUCTION IN AREA  = 54%

## TABLE 2

### EXPERIMENT DESIGN FOR FATIGUE TESTS

|  | NOMINAL STRESS RANGE MAIN PLATE KSI | | | | | | |
|---|---|---|---|---|---|---|---|
| MAXIMUM NOMINAL STRESS MAIN PLATE KSI | 30 | 40 | 50 | 60 | 70 | 80 | 90 |
| 50 | 3* | | | | | | |
| 60 | | 3 | | | | | |
| 70 | | | 3 | | | | |
| 80 | | | | 3 | | | |
| 90 | | | | | 3 | | |
| 100 | | | | | | 3 | |
| 110 | | | | | | | 3 |

*Number of Specimens Tested.

TABLE 3

FATIGUE TEST RESULTS

LOAD CARRYING WELD JOINTS

| Specimen | Stress Range KSI | Maximum Stress KSI | Fatigue Life Cycles | Failure Mode |
|---|---|---|---|---|
| L-34 | 90 | 110 | 610 | Shear |
| L-28 | 90 | 110 | 1,548 | Root |
| L-7 | 90 | 110 | 1,515 | Shear |
| L-19 | 80 | 100 | 4,224 | Toe |
| L-17 | 80 | 100 | 4,726 | Toe |
| L-39 | 80 | 100 | 740 | Root* |
| L-33 | 80 | 100 | 2,425 | Toe |
| L-1 | 70 | 90 | 1,267 | Root* |
| L-29 | 70 | 90 | 3,147 | Root |
| L-36 | 70 | 90 | 3,737 | Shear |
| L-5 | 70 | 90 | 2,900 | Toe |
| L-18 | 60 | 80 | 6,948 | Root |
| L-10 | 60 | 80 | 7,497 | Root |
| L-14 | 60 | 80 | 6,681 | Root* |
| L-6 | 50 | 70 | 7,721 | Root |
| L-26 | 50 | 70 | 13,060 | Root* |
| L-21 | 50 | 70 | 17,839 | Toe |
| L-4 | 40 | 60 | 22,026 | Root |
| L-9 | 40 | 60 | 19,878 | Root |
| L-20 | 40 | 60 | 23,422 | Root |
| L-23 | 30 | 50 | 36,091 | Root |
| L-24 | 30 | 50 | 35,526 | Root |
| L-11 | 30 | 50 | 42,959 | Root |

*Porous Welds.

# TABLE 4
## FATIGUE TEST RESULTS
### NON-LOAD CARRY WELD JOINTS

| Specimen | Stress Range KSI | Maximum Stress KSI | Fatigue Life Cycles | Failure Mode |
|---|---|---|---|---|
| N-6 | 90 | 110 | 8,683 | Toe |
| N-18 | 90 | 110 | 6,852 | Toe |
| N-35 | 90 | 110 | 5,319 | Toe |
| N-25 | 80 | 100 | 16,550 | Toe |
| N-7 | 80 | 100 | 13,896 | Toe |
| N-17 | 80 | 100 | 13,370 | Toe |
| N-10 | 70 | 90 | 19,945 | Toe |
| N-12 | 70 | 90 | 22,107 | Toe |
| N-33 | 70 | 90 | 11,780 | Toe |
| N-16 | 60 | 80 | 42,331 | Toe |
| N-37 | 60 | 80 | 35,536 | Toe |
| N-30 | 60 | 80 | 22,205 | Toe |
| N-8 | 50 | 70 | 41,195 | Toe |
| N-26 | 50 | 70 | 61,858 | Toe |
| N-4 | 50 | 70 | 34,830 | Toe |
| N-21 | 40 | 60 | 99,446 | Toe |
| N-3 | 40 | 60 | 58,321 | Toe |
| N-9 | 40 | 60 | 87,485 | Toe |
| N-29 | 30 | 50 | 225,878 | Toe |
| N-11 | 30 | 50 | 217,998 | Toe |
| N-39 | 30 | 50 | 182,390 | Toe |

## TABLE 5

### DIMENSIONS OF LOAD CARRYING JOINTS ANALYZED FOR ROOT CRACKS

| SPECIMEN | $T_p$ in. | $T_c$ in. | w in. | H in. | $H_c$ in. | θ Degrees | $H/T_p$ | Ref. |
|---|---|---|---|---|---|---|---|---|
| LR – 1 | 0.786 | 0.786 | 0.378 | 0.378 | 1.18 | 45 | 0.481 | 15 |
| LR – 2 | 0.786 | 0.786 | 0.372 | 0.372 | 1.18 | 45 | 0.473 | 15 |
| LR – 3 | 0.786 | 0.786 | 0.333 | 0.333 | 1.18 | 45 | 0.424 | 15 |
| LR – 4 | 0.786 | 0.786 | 0.339 | 0.339 | 1.18 | 45 | 0.431 | 15 |
| LR – 5 | 0.786 | 0.786 | 0.328 | 0.328 | 1.18 | 45 | 0.417 | 15 |
| LR – 6 | 0.629 | 0.629 | 0.478 | 0.478 | 1.26 | 45 | 0.760 | 15 |
| LR – 7 | 0.629 | 0.629 | 0.483 | 0.483 | 1.26 | 45 | 0.768 | 15 |
| LR – 8 | 0.394 | 0.394 | 0.394 | 0.394 | 0.788 | 45 | 1.000 | 17 |
| LR – 9 | 0.590 | 0.590 | 0.200 | 0.200 | 1.38 | 45 | 0.339 | 3 |
| LR – 10 | 0.590 | 0.590 | 0.470 | 0.470 | 1.38 | 45 | 0.797 | 3 |
| LR – 11 | 0.590 | 0.590 | 0.710 | 0.710 | 1.38 | 45 | 1.203 | 3 |
| LR – 12 | 0.630 | 0.630 | 0.157 | 0.157 | 1.46 | 45 | 0.249 | 16 |
| LR – 13 | 0.630 | 0.630 | 0.236 | 0.236 | 1.46 | 45 | 0.375 | 16 |
| LR – 14 | 0.630 | 0.630 | 0.315 | 0.315 | 1.46 | 45 | 0.500 | 16 |
| LR – 15 | 0.630 | 0.630 | 0.394 | 0.394 | 1.46 | 45 | 0.625 | 16 |
| LR – 16 | 0.630 | 0.630 | 0.472 | 0.472 | 1.46 | 45 | 0.749 | 16 |
| LR – 17 | 0.630 | 0.630 | 0.551 | 0.551 | 1.46 | 45 | 0.875 | 16 |
| LR – 18 | 1.260 | 1.260 | 0.394 | 0.394 | 3.31 | 45 | 0.313 | 16 |
| LR – 19 | 1.260 | 1.260 | 0.590 | 0.590 | 3.31 | 45 | 0.468 | 16 |
| LR – 20 | 1.260 | 1.260 | 0.787 | 0.787 | 3.31 | 45 | 0.625 | 16 |
| LR – 21 | 1.260 | 1.260 | 0.984 | 0.984 | 3.31 | 45 | 0.781 | 16 |
| LR – 22 | 1.260 | 1.260 | 1.180 | 1.180 | 3.31 | 45 | 0.937 | 16 |
| LR – 23 | 0.750 | 0.875 | 0.3125 | 0.3125 | 0.625 | 45 | 0.417 | 2 |
| LR – 24 | 0.662 | 0.662 | 0.7492 | 0.4325 | 2.00 | 30 | 0.653 | |
| LR – 25 | 0.662 | 0.662 | 0.6803 | 0.4763 | 2.00 | 35 | 0.719 | |
| LR – 26 | 0.662 | 0.662 | 0.6440 | 0.5032 | 2.00 | 38 | 0.760 | |
| LR – 27 | 0.662 | 0.662 | 0.6212 | 0.5214 | 2.00 | 40 | 0.788 | |

## TABLE 5 (CONTINUED)

## DIMENSIONS OF LOAD CARRYING JOINTS ANALYZED FOR ROOT CRACKS

| SPECIMEN | $T_p$ in. | $T_c$ in. | W in. | H in. | $H_c$ in. | $\theta$ Degrees | $H/T_p$ | Ref. |
|---|---|---|---|---|---|---|---|---|
| LR - 28 | 0.662 | 0.662 | 0.5999 | 0.5402 | 2.00 | 42 | 0.816 | |
| LR - 29 | 0.662 | 0.662 | 0.5692 | 0.5692 | 2.00 | 45 | 0.860 | |
| LR - 30* | 0.662 | 0.662 | 0.6214 | 0.6214 | 2.00 | 45 | 0.939 | |
| LR - 31 | 0.662 | 0.662 | 0.5214 | 0.6214 | 2.00 | 50 | 0.939 | |
| LR - 32 | 0.662 | 0.662 | 0.4962 | 0.6558 | 2.00 | 53 | 0.991 | |

*Oversize Weld.

## TABLE 6

STRESS INTENSITY FACTOR POLYNOMIAL COEFFICIENTS FOR

ROOT CRACKS OF LOAD CARRYING WELD JOINTS

$nA_i$

| SPECIMEN | $2A_1$ | $3A_2$ | $4A_3$ | $5A_4$ |
|---|---|---|---|---|
| LR - 1 | 11.812 | 24.199 | - 71.383 | 121.45 |
| LR - 2 | 11.671 | 24.270 | - 71.220 | 121.21 |
| LR - 3 | 10.856 | 24.377 | - 71.858 | 122.38 |
| LR - 4 | 10.930 | 24.859 | - 73.045 | 123.26 |
| LR - 5 | 10.690 | 24.853 | - 73.181 | 123.53 |
| LR - 6 | 15.495 | 19.418 | - 68.691 | 121.62 |
| LR - 7 | 15.535 | 19.655 | - 69.761 | 122.67 |
| LR - 8 | 17.655 | 11.122 | - 54.809 | 114.20 |
| LR - 9 | 9.1429 | 26.497 | - 81.572 | 131.96 |
| LR - 10 | 15.899 | 18.088 | - 66.556 | 120.39 |
| LR - 11 | 18.816 | 4.8185 | - 41.964 | 106.31 |
| LR - 12 | 6.8059 | 32.931 | -106.76 | 151.33 |
| LR - 13 | 9.9418 | 24.911 | - 74.884 | 125.69 |
| LR - 14 | 12.078 | 24.254 | - 71.443 | 121.15 |
| LR - 15 | 13.831 | 23.329 | - 73.408 | 123.55 |
| LR - 16 | 15.345 | 20.071 | - 70.008 | 122.50 |
| LR - 17 | 16.631 | 15.635 | - 63.019 | 118.91 |
| LR - 18 | 8.5541 | 27.607 | - 86.785 | 136.55 |
| LR - 19 | 11.612 | 24.112 | - 70.835 | 120.93 |
| LR - 20 | 13.835 | 23.200 | - 72.980 | 123.12 |
| LR - 21 | 15.680 | 19.120 | - 68.723 | 121.94 |
| LR - 22 | 17.171 | 13.373 | - 59.038 | 116.67 |
| LR - 23 | 9.8997 | 28.347 | - 79.376 | 127.81 |
| LR - 24 | 10.062 | 9.9706 | - 40.911 | 63.710 |
| LR - 25 | 11.848 | 11.184 | - 46.738 | 76.725 |
| LR - 26 | 13.127 | 11.796 | - 49.835 | 85.765 |
| LR - 27 | 14.031 | 12.560 | - 52.662 | 93.196 |
| LR - 28 | 14.932 | 14.184 | - 57.879 | 103.51 |
| LR - 29 | 16.489 | 16.211 | - 63.962 | 119.34 |
| LR - 30 | 17.207 | 13.087 | - 58.234 | 115.97 |
| LR - 31 | 19.322 | 22.630 | - 80.913 | 158.91 |
| LR - 32 | 21.199 | 27.955 | - 93.722 | 190.66 |

## TABLE 7

### DIMENSIONS OF LOAD CARRYING JOINTS ANALYZED FOR TOE CRACKS

| SPECIMEN | $T_p$ in. | $T_c$ in. | W in. | H in. | $H_c$ in. | θ Degrees | $H/T_p$ | Root Penetration % | Ref. |
|---|---|---|---|---|---|---|---|---|---|
| LT - 1 | 0.630 | 0.630 | 0.236 | 0.236 | 1.46 | 45 | 0.375 | 100 / 5.8 | 16 |
| LT - 2 | 0.630 | 0.630 | 0.394 | 0.394 | 1.46 | 45 | 0.625 | 100 / 4.7 | 16 |
| LT - 3 | 0.630 | 0.630 | 0.551 | 0.551 | 1.46 | 45 | 0.875 | 100 / 26.0 | 16 |
| LT - 4 | 1.26 | 1.26 | 0.394 | 0.394 | 3.31 | 45 | 0.313 | 100 / 12.5 | 16 |
| LT - 5 | 1.26 | 1.26 | 0.590 | 0.590 | 3.31 | 45 | 0.468 | 100 / 10.6 | 16 |
| LT - 6 | 1.26 | 1.26 | 0.984 | 0.984 | 3.31 | 45 | 0.781 | 100 / 11.3 | 16 |
| LT - 7 | 1.26 | 1.26 | 1.18 | 1.18 | 3.31 | 45 | 0.937 | 100 / 0.5 | 16 |
| LT - 8 | 0.662 | 0.662 | 0.749 | 0.433 | 2.00 | 30 | 0.653 | 100 / 2.4 | |
| LT - 9 | 0.662 | 0.662 | 0.621 | 0.521 | 2.00 | 40 | 0.788 | 100 / 1.0 | |
| LT - 10 | 0.662 | 0.662 | 0.5999 | 0.540 | 2.00 | 42 | 0.816 | 100 / 19.0 / 8.9 | |

## TABLE 7 (CONTINUED)

### DIMENSIONS OF LOAD CARRYING JOINTS ANALYZED FOR TOE CRACKS

| SPECIMEN | $T_p$ in. | $T_c$ in. | W in. | H in. | $H_c$ in. | $\theta$ Degrees | $H/T_p$ | Root Penetration % | Ref. |
|---|---|---|---|---|---|---|---|---|---|
| LT - 11 | 0.662 | 0.662 | 0.569 | 0.569 | 2.00 | 45 | 0.860 | 100 / 5.9 | |
| LT - 12 | 0.662 | 0.662 | 0.496 | 0.656 | 2.00 | 53 | 0.990 | 100 / 19.7 | |
| LT - 13 | 0.786 | 0.786 | 0.378 | 0.378 | 1.18 | 45 | 0.481 | 47.2 | 15 |
| LT - 14 | 0.786 | 0.786 | 0.328 | 0.328 | 1.18 | 45 | 0.417 | 77.8 | 15 |
| LT - 15 | 0.629 | 0.629 | 0.478 | 0.478 | 1.26 | 45 | 0.756 | 100 | 15 |
| LT - 16 | 0.629 | 0.629 | 0.483 | 0.483 | 1.26 | 45 | 0.768 | 100 | 15 |
| LT - 17 | 0.590 | 0.590 | 0.200 | 0.200 | 1.38 | 45 | 0.339 | 48.4 | 3 |
| LT - 18 | 0.590 | 0.590 | 0.470 | 0.470 | 1.38 | 45 | 0.797 | 20.2 | 3 |
| LT - 19 | 0.590 | 0.590 | 0.710 | 0.710 | 1.38 | 45 | 1.203 | -4.8 | 3 |
| LT - 20 | 0.787 | 0.787 | 0.296 | 0.493 | 2.36 | 59 | 0.626 | 100 | 18 |
| LT - 21 | 0.787 | 0.787 | 0.315 | 0.528 | 2.36 | 59 | 0.670 | 100 | 18 |
| LT - 22 | 0.787 | 0.787 | 0.284 | 0.498 | 2.36 | 60° | 0.632 | 100 | 18 |

-88

## TABLE 8

STRESS INTENSITY FACTOR POLYNOMIAL COEFFICIENTS FOR TOE CRACKS OF

LOAD CARRYING WELD JOINTS $nA_i$

| SPECIMEN | Root Penetration % | $2A_1$ | $3A_2$ | $4A_3$ | $5A_4$ | $6A_5$ |
|---|---|---|---|---|---|---|
| LT – 1 | 100<br>5.8 | 29.575<br>129.75 | -163.73<br>-680.55 | 491.97<br>1966.1 | - 657.25<br>-2474.3 | 340.25<br>1131.4 |
| LT – 2 | 100<br>4.7 | 30.312<br>72.641 | -173.77<br>-428.37 | 536.95<br>130.58 | - 751.56<br>-1820.6 | 406.72<br>955.55 |
| LT – 3 | 100<br>2.6 | 30.906<br>42.878 | -177.49<br>-250.89 | 549.76<br>768.99 | - 771.60<br>-1075.7 | 417.82<br>574.51 |
| LT – 4 | 100<br>12.5 | 28.872<br>130.42 | -157.56<br>-660.14 | 478.14<br>1948.2 | - 648.12<br>-2411.1 | 341.27<br>1056.5 |
| LT – 5 | 100<br>10 6 | 29.743<br>92.245 | -165.10<br>-512.94 | 493.51<br>1519.7 | - 662.74<br>-2032.4 | 346.87<br>1018.4 |
| LT – 6 | 100<br>11.3 | 30.710<br>52.904 | -176.31<br>-311.79 | 545.87<br>951.66 | - 765.77<br>-1329.2 | 414.71<br>704.86 |
| LT – 7 | 100<br>0.5 | 31.025<br>48.156 | -178.22<br>-283.61 | 552.06<br>865.58 | - 774.97<br>-1209.1 | 419.59<br>643.26 |
| LT – 8 | 100<br>2.4 | 23.306<br>28.385 | -112.32<br>-137.12 | 337.74<br>405.87 | - 468.69<br>- 560.59 | 258.80<br>305.46 |
| LT – 9 | 100<br>1.0 | 28.707<br>43.323 | -157.70<br>-242.94 | 484.10<br>733.30 | - 676.95<br>-1019.7 | 367.91<br>543.75 |
| LT – 10 | 100<br>19.0<br>8.9 | 29.608<br>41.656<br>44.464 | -165.58<br>-237.66<br>-254.41 | 509.50<br>723.06<br>772.29 | - 712.53<br>-1008.5<br>-1076.3 | 386.11<br>538.79<br>573.65 |

-89

## TABLE 8 (CONTINUED)

STRESS INTENSITY FACTOR POLYNOMIAL COEFFICIENTS FOR TOE CRACKS OF

LOAD CARRYING WELD JOINTS

$$nA_i$$

| SPECIMEN | Root Penetration % | $2A_1$ | $3A_2$ | $4A_3$ | $5A_4$ | $6A_5$ |
|---|---|---|---|---|---|---|
| LT - 11 | 100<br>5.9 | 30.876<br>50.366 | -177.31<br>-296.86 | 549.18<br>905.87 | - 770.75<br>-1265.3 | 417.37<br>672.15 |
| LT - 12 | 100<br>19.7 | 33.332<br>55.970 | -201.43<br>-347.15 | 631.78<br>1077.6 | - 891.41<br>-1516.2 | 481.36<br>804.76 |
| LT - 13 | 47.2 | 46.605 | -257.72 | 770.22 | -1027.4 | 552.39 |
| LT - 14 | 71.8 | 34.027 | -184.93 | 544.62 | - 707.31 | 356.14 |
| LT - 15 | 100 | 30.659 | -175.95 | 544.52 | - 763.48 | 413.34 |
| LT - 16 | 100 | 30.677 | -176.06 | 544.89 | - 764.05 | 413.65 |
| LT - 17 | 48.4 | 49.344 | -255.88 | 740.86 | - 882.40 | 388.78 |
| LT - 18 | 20.2 | 48.071 | -282.30 | 863.48 | -1206.9 | 641.92 |
| LT - 19 | -4.8 | 40.567 | -237.07 | 726.10 | -1015.4 | 543.42 |
| LT - 20 | 100 | 26.068 | -159.08 | 493.98 | - 673.89 | 349.84 |
| LT - 21 | 1000 | 26.052 | -158.65 | 491.23 | - 669.46  q | 347.68 |
| LT - 22 | 100 | 26.244 | -161.27 | 503.17 | - 688.78 | 358.19 |

## TABLE 9

### DIMENSIONS OF NON-LOAD CARRYING JOINTS ANALYZED FOR TOE CRACKS

| SPECIMEN | $T_p$ in. | $T_c$ in. | $W$ in. | $H$ in. | $H_c$ in. | $\theta$ Degrees | $H/T_p$ | Ref. |
|---|---|---|---|---|---|---|---|---|
| NT – 1 | 0.662 | 0.662 | 0.7437 | 0.4294 | 2.00 | 30 | 0.649 | |
| NT – 2 | 0.662 | 0.662 | 0.6753 | 0.4728 | 2.00 | 35 | 0.714 | |
| NT – 3 | 0.662 | 0.662 | 0.6393 | 0.4995 | 2.00 | 38 | 0.754 | |
| NT – 4 | 0.662 | 0.662 | 0.6169 | 0.5176 | 2.00 | 40 | 0.782 | |
| NT – 5 | 0.662 | 0.662 | 0.5852 | 0.5457 | 2.00 | 43 | 0.824 | |
| NT – 6 | 0.662 | 0.662 | 0.5651 | 0.5651 | 2.00 | 45 | 0.854 | |
| NT – 7 | 0.662 | 0.662 | 0.5457 | 0.5852 | 2.00 | 47 | 0.884 | |
| NT – 8 | 0.662 | 0.662 | 0.5176 | 0.6169 | 2.00 | 50 | 0.935 | |
| NT – 9 | 0.662 | 0.662 | 0.4905 | 0.6510 | 2.00 | 53 | 0.983 | |
| NT – 10 | 0.662 | 0.662 | 0.5692 | 0.5692 | 2.00 | 45 | 0.860 | |
| NT – 11 | 0.500 | 0.375 | 0.3125 | 0.3125 | 1.50 | 45 | 0.625 | 11 |
| NT – 12 | 0.625 | 0.375 | 0.3125 | 0.3125 | 2.00 | 45 | 0.500 | 1 |
| NT – 13 | 0.500 | 0.500 | 0.3125 | 0.3125 | 2.00 | 45 | 0.625 | 27 |
| NT – 14 | 1.000 | 0.375 | 0.500 | 0.500 | 3.00 | 45 | 0.500 | |
| NT – 15 | 0.250 | 0.375 | 0.250 | 0.250 | 2.00 | 45 | 1.000 | |
| NT – 16 | 0.375 | 0.375 | 0.250 | 0.250 | 2.00 | 45 | 0.667 | |
| NT – 17 | 2.000 | 0.500 | 0.375 | 0.375 | 4.00 | 45 | 0.188 | |
| NT – 18 | 0.500 | 0.500 | 0.250 | 0.250 | 2.00 | 45 | 0.500 | |
| NT – 19 | 0.500 | 0.250 | 0.250 | 0.250 | 2.00 | 45 | 0.500 | |

## TABLE 10

### STRESS INTENSITY FACTOR POLYNOMIAL COEFFICIENTS FOR
### TOE CRACKS OF NON-LOAD CARRYING JOINTS

$$nA_i$$

| SPECIMEN | $2A_1$ | $3A_2$ | $4A_3$ | $5A_4$ | $6A_5$ |
|----------|--------|--------|--------|--------|--------|
| NT - 1  | 15.347 | - 73.968 | 222.40 | -308.61 | 170.38 |
| NT - 2  | 17.240 | - 89.506 | 271.99 | -378.81 | 207.07 |
| NT - 3  | 18.288 | - 98.451 | 300.94 | -420.06 | 228.70 |
| NT - 4  | 18.936 | -104.12  | 319.47 | -446.59 | 242.64 |
| NT - 5  | 19.824 | -112.12  | 345.88 | -484.55 | 262.64 |
| NT - 6  | 20.352 | -117.04  | 362.29 | -508.25 | 275.16 |
| NT - 7  | 20.827 | -121.58  | 377.60 | -530.46 | 286.90 |
| NT - 8  | 21.434 | -127.63  | 398.26 | -560.59 | 302.89 |
| NT - 9  | 21.912 | -132.69  | 415.91 | -586.55 | 316.72 |
| NT - 10 | 20.365 | -117.12  | 362.53 | -508.59 | 275.34 |
| NT - 11 | 14.475 | - 82.982 | 275.24 | -360.02 | 194.92 |
| NT - 12 | 17.086 | - 96.572 | 295.32 | -402.93 | 213.33 |
| NT - 13 | 14.964 | - 85.953 | 265.97 | -372.09 | 201.15 |
| NT - 14 | 25.678 | -144.86  | 444.11 | -605.80 | 321.46 |
| NT - 15 | 8.0191 | - 46.212 | 142.83 | -200.35 | 108.30 |
| NT - 16 | 11.300 | - 64.902 | 200.80 | -281.14 | 152.09 |
| NT - 17 | 45.063 | -275.68  | 912.88 | -1318.9 | 728.01 |
| NT - 18 | 14.730 | - 83.529 | 254.31 | -346.75 | 183.00 |
| NT - 19 | 13.361 | - 75.433 | 230.87 | -314.88 | 166.81 |

## TABLE 11

### AVERAGE DIMENSIONS OF ROOT CRACK FATIGUE SPECIMENS ANALYZED

| NUMBER OF SPECIMENS | $T_P$ in. | $T_C$ in. | W in. | H in. | $H_C$ in. | ROOT PENE-TRATION % | x 1/3* $in^{-1/6}$ | REF. |
|---|---|---|---|---|---|---|---|---|
| 5 | 0.630 | 0.630 | 0.394 | 0.394 | 1.46 | 0 | 0.289 | 16 |
| 4 | 1.260 | 1.260 | 0.984 | 0.984 | 3.31 | 0 | 0.264 | 16 |
| 4 | 0.630 | 0.630 | 0.354 | 0.354 | 1.46 | 56 | 0.475 | 16 |
| 4 | 1.260 | 1.260 | 0.708 | 0.708 | 3.31 | 56 | 0.409 | 16 |
| 4 | 0.630 | 0.630 | 0.197 | 0.197 | 1.46 | 63 | 0.486 | 16 |
| 6 | 1.260 | 1.260 | 0.394 | 0.394 | 3.31 | 63 | 0.439 | 16 |
| 20 | 0.786 | 0.786 | 0.328 | 0.328 | 1.18 | 70 | 0.520 | 15 |
| 9 | 3.75 | - | - | - | - | 89 | 0.585 | 46** |
| 18 | 0.662 | 0.662 | 0.569 | 0.569 | 2.00 | 18 | 0.252 | |

*Average Value
**Crack Growth Study of Plate with a Through Crack

## TABLE 12

### AVERAGE DIMENSIONS OF TOE CRACK FATIGUE SPECIMENS ANALYZED

| NUMBER OF SPECIMENS | $T_P$ in. | $T_C$ in. | W in. | H in. | $H_C$ in. | ROOT PENE- TRATION % | $\bar{\lambda}_T$ | REFERENCE |
|---|---|---|---|---|---|---|---|---|
| 3 | 0.630 | 0.630 | 0.708 | 0.708 | 1.46 | 0 | 2.40 | 16 |
| 2 | 1.260 | 1.260 | 1.180 | 1.180 | 3.31 | 0 | 2.73 | 16 |
| 7 | 0.630 | 0.630 | 0.550 | 0.550 | 1.46 | 88 | 2.25 | 16 |
| 4 | 1.260 | 1.260 | 1.100 | 1.100 | 3.31 | 88 | 2.25 | 16 |
| 4 | 0.630 | 0.630 | 0.275 | 0.275 | 1.46 | 88 | 2.40 | 16 |
| 4 | 1.260 | 1.260 | 0.550 | 0.550 | 3.31 | 88 | 2.40 | 16 |
| 2 | 0.500 | 0.500 | 0.313 | 0.313 | 1.50 | * | 1.52 | 27 |
| 11 | 0.500 | 0.375 | 0.313 | 0.313 | 1.50 | * | 1.50 | 11 |
| 96 | 0.787 | 0.787 | 0.298 | 0.506 | 2.36 | 100 | 2.01 | 18 |
| 5 | 0.662 | 0.662 | 0.569 | 0.569 | 2.00 | 18 | 2.78 | 11 |
| 21 | 0.662 | 0.662 | 0.565 | 0.565 | 2.00 | * | 1.81 | 18 |

*Non Load Carrying Welds-Zero Penetration Assumed

FIGURES

(a) Non-Load Carrying
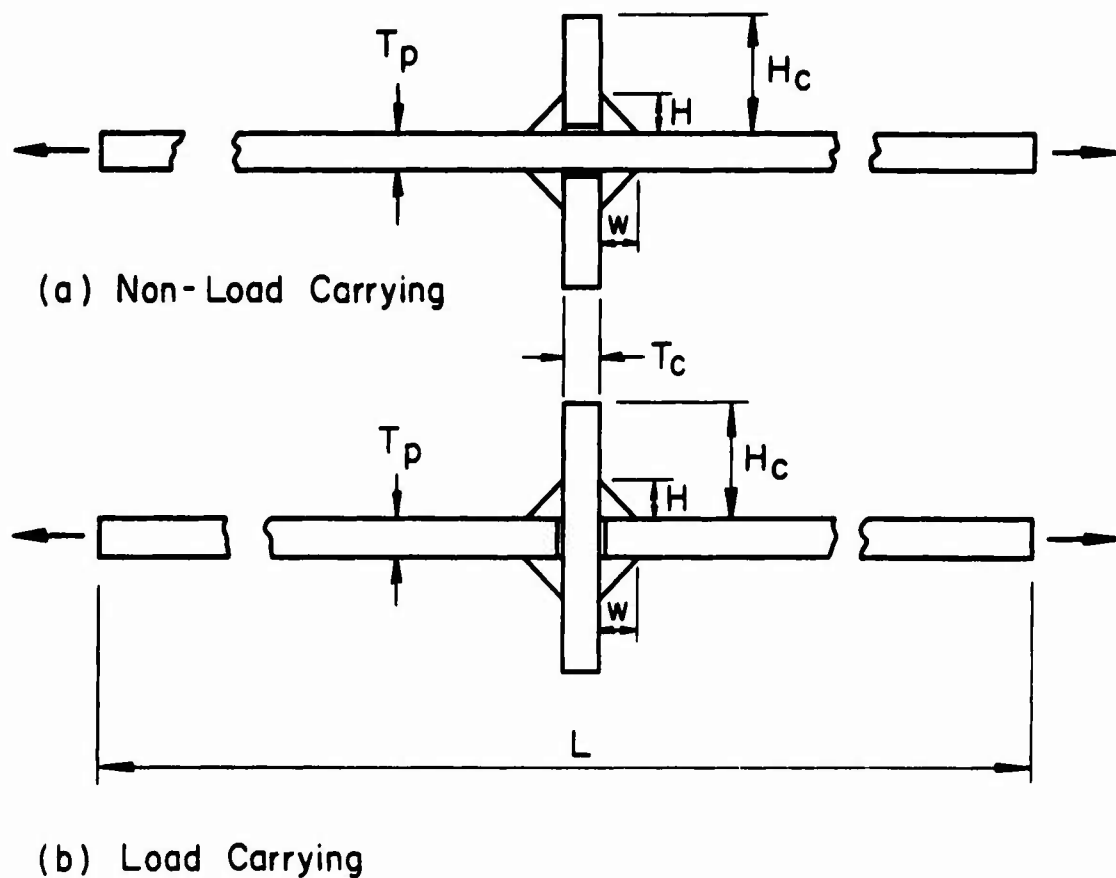
(b) Load Carrying

Nominal Dimensions

$T_p = T_c = 0.625$ in.

$W = H = 0.500$ in.

$H_c = 2.00$ in.

$L = 24.0$ in.

Width $= 1.200$ in.

Fig. 1   Fatigue Specimen Dimensions
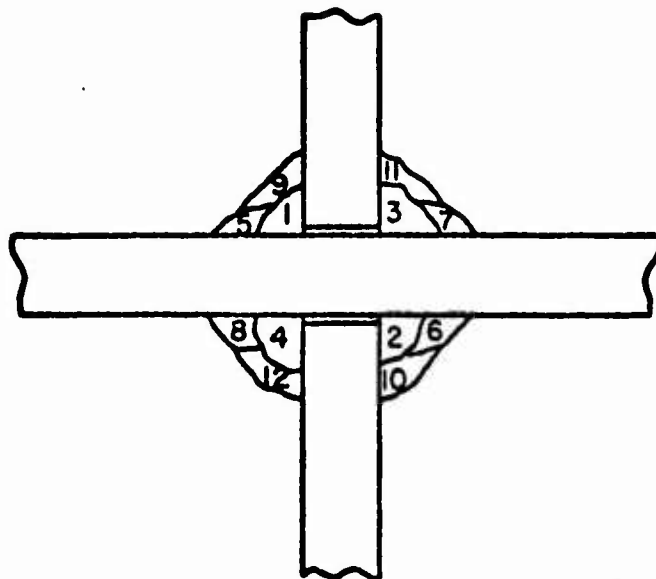
**Fig. 2  Welding Sequence**
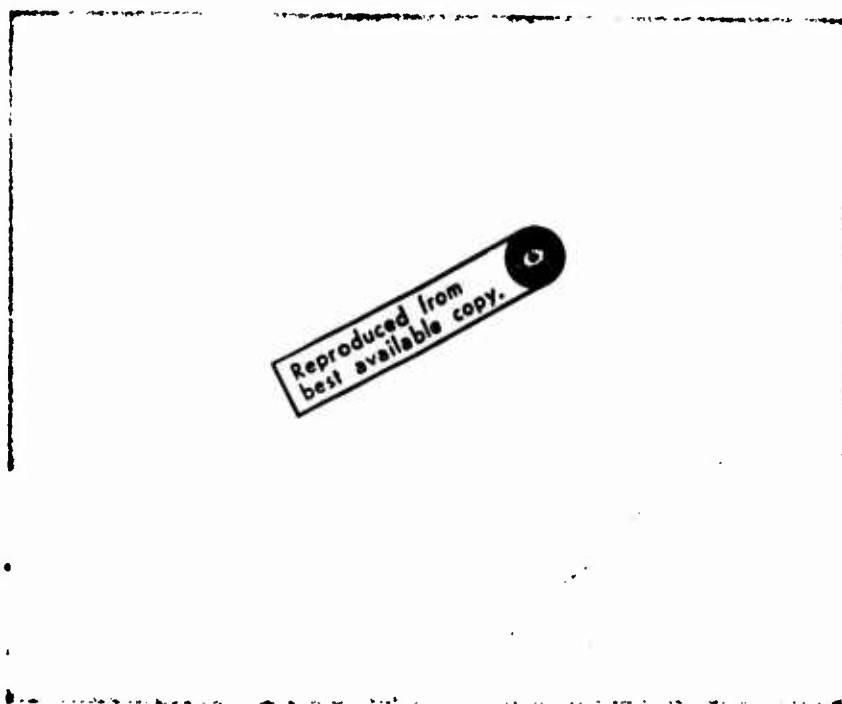
**Fig. 3  Etched Cross Section of Typical Joint**
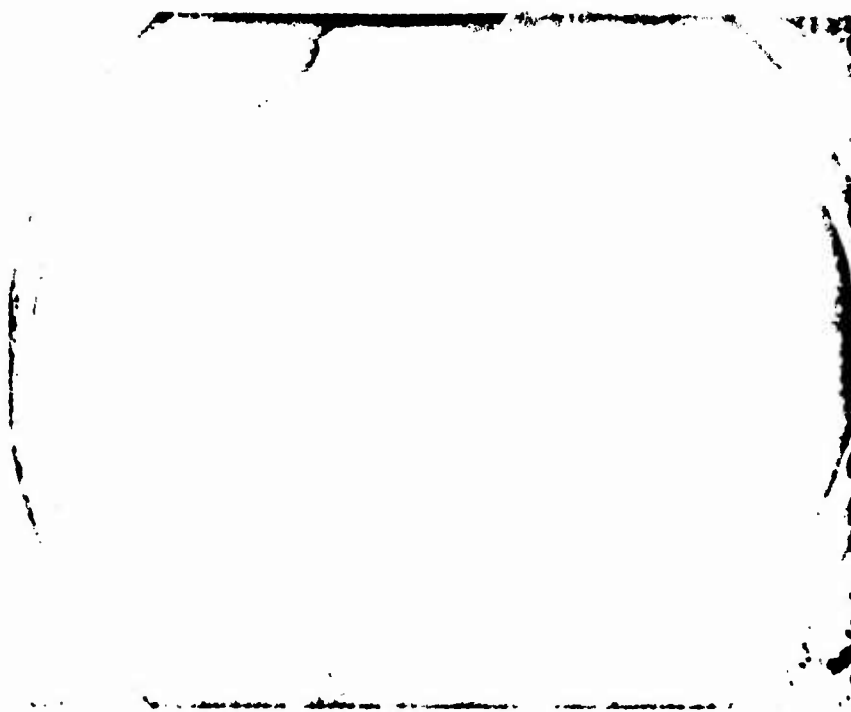
**Fig. 4**   Toe Failure-Non-Load Carrying Joint

**Fig. 5**   Root Failure-Load Carrying Joint
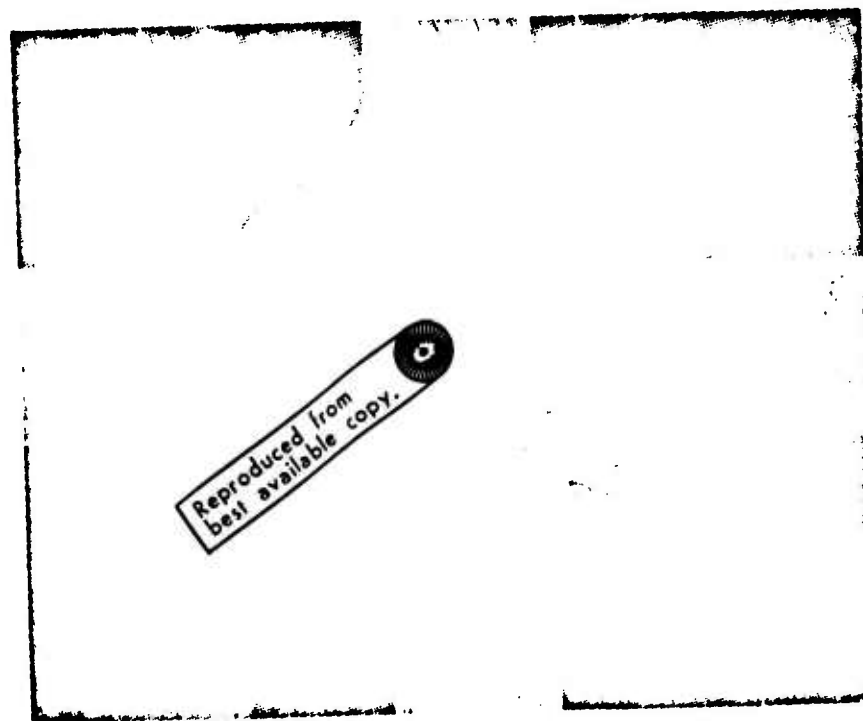
Fig. 6  Shear Failure-Load Carrying Joint
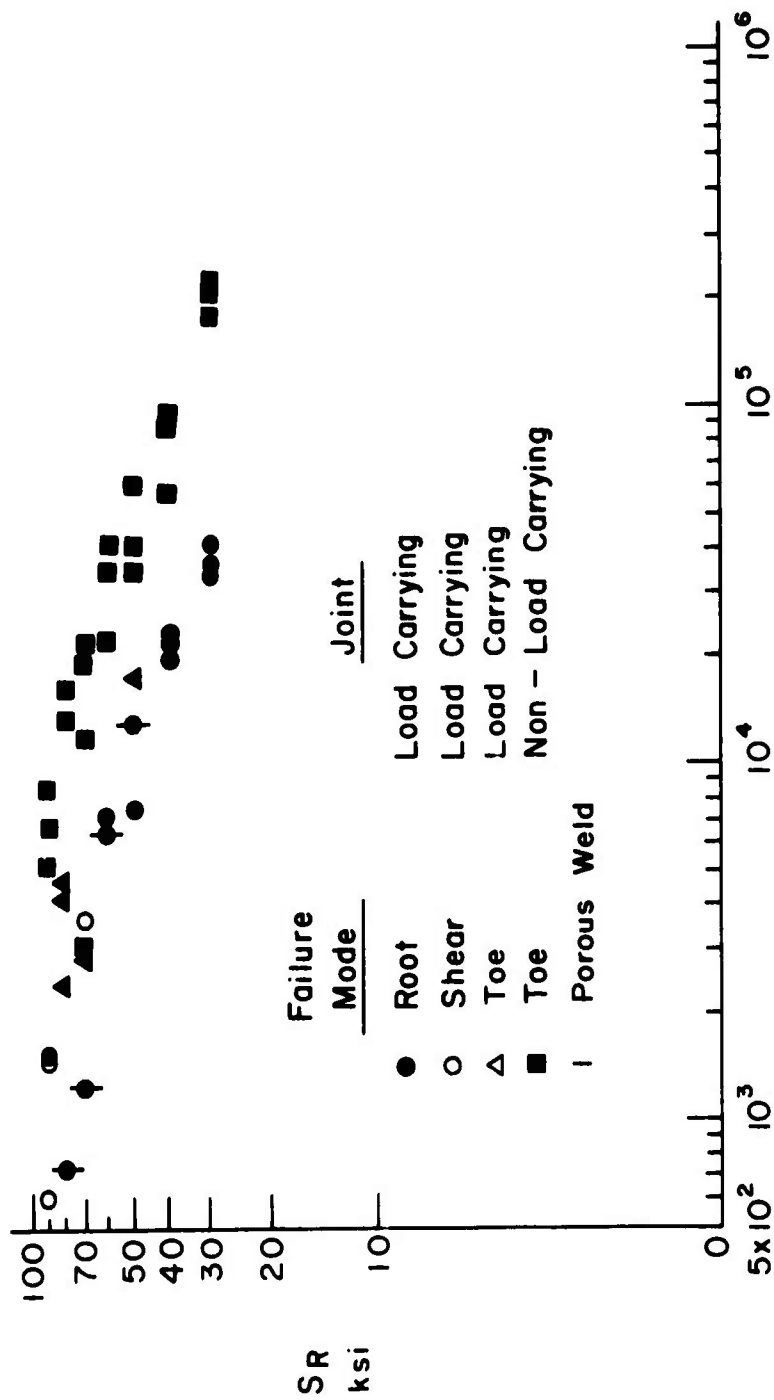
Fig. 7 Fatigue Life of Load and Non-Load Carrying Joints
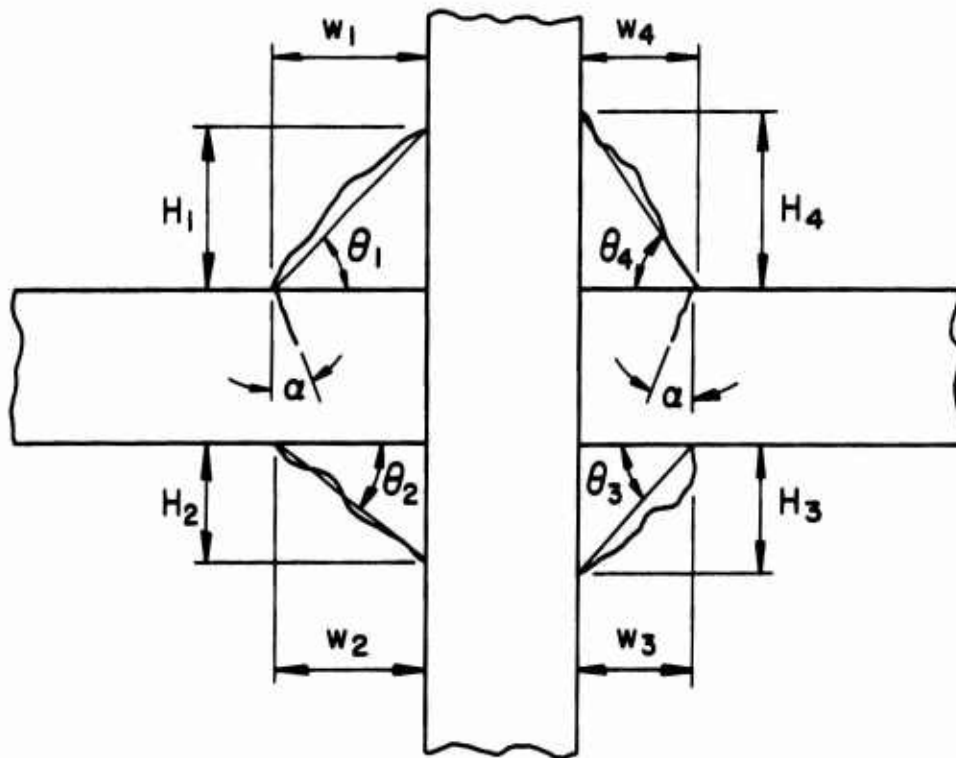
Weld Angle $= \theta_i = \text{Arctan}\left[H_i/w_i\right]$

Angle of Toe Crack $= \alpha$

Fig. 8  Definition of Weld and Crack Angle
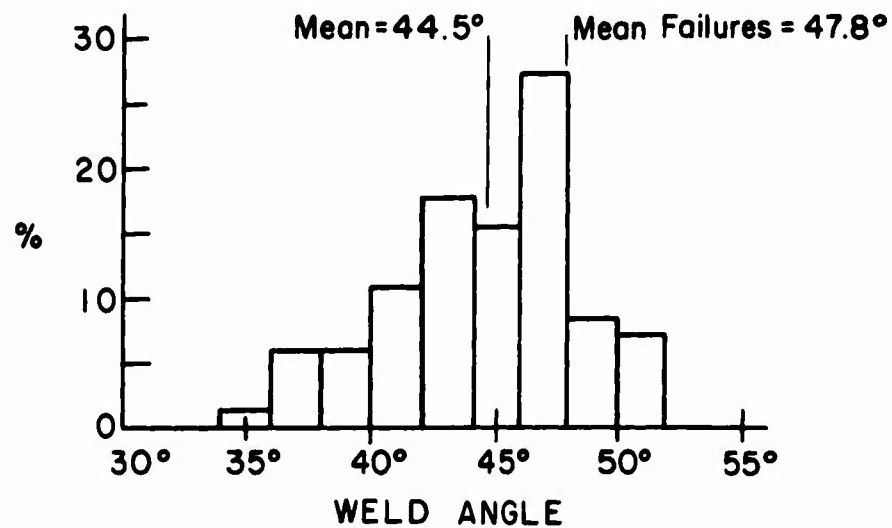
Fig. 9   Histogram of Weld Angle-Non-Load Carrying Joints
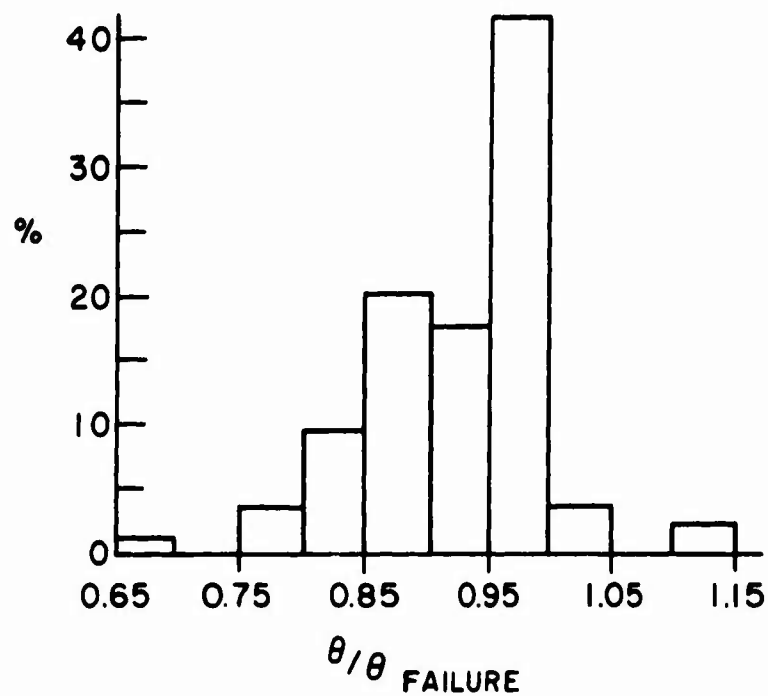


Fig. 10   Histogram of $\theta$ to $\theta_{Failure}$-Non Load Carrying Joints
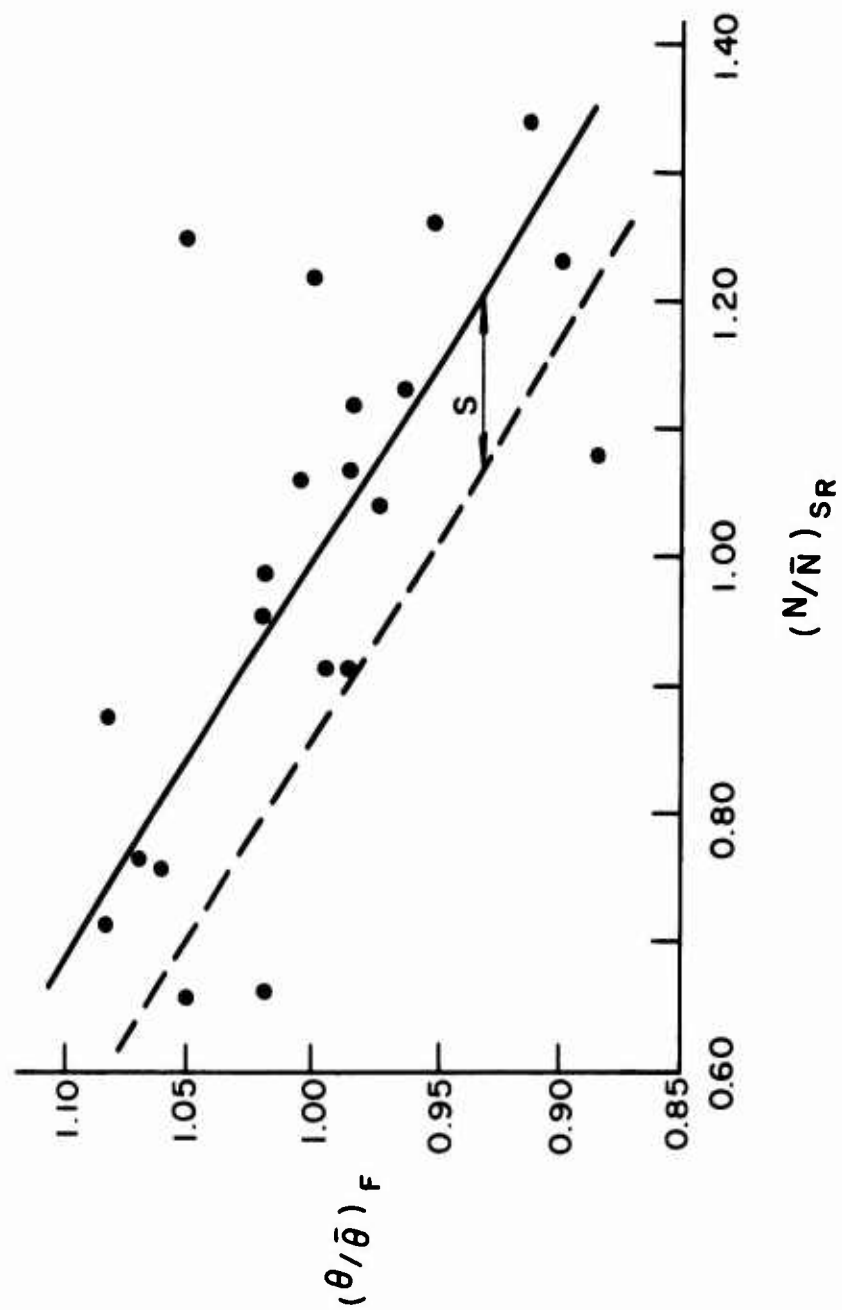
Fig. 11  Variation of Fatigue Life of Non-Load Carrying
Joints
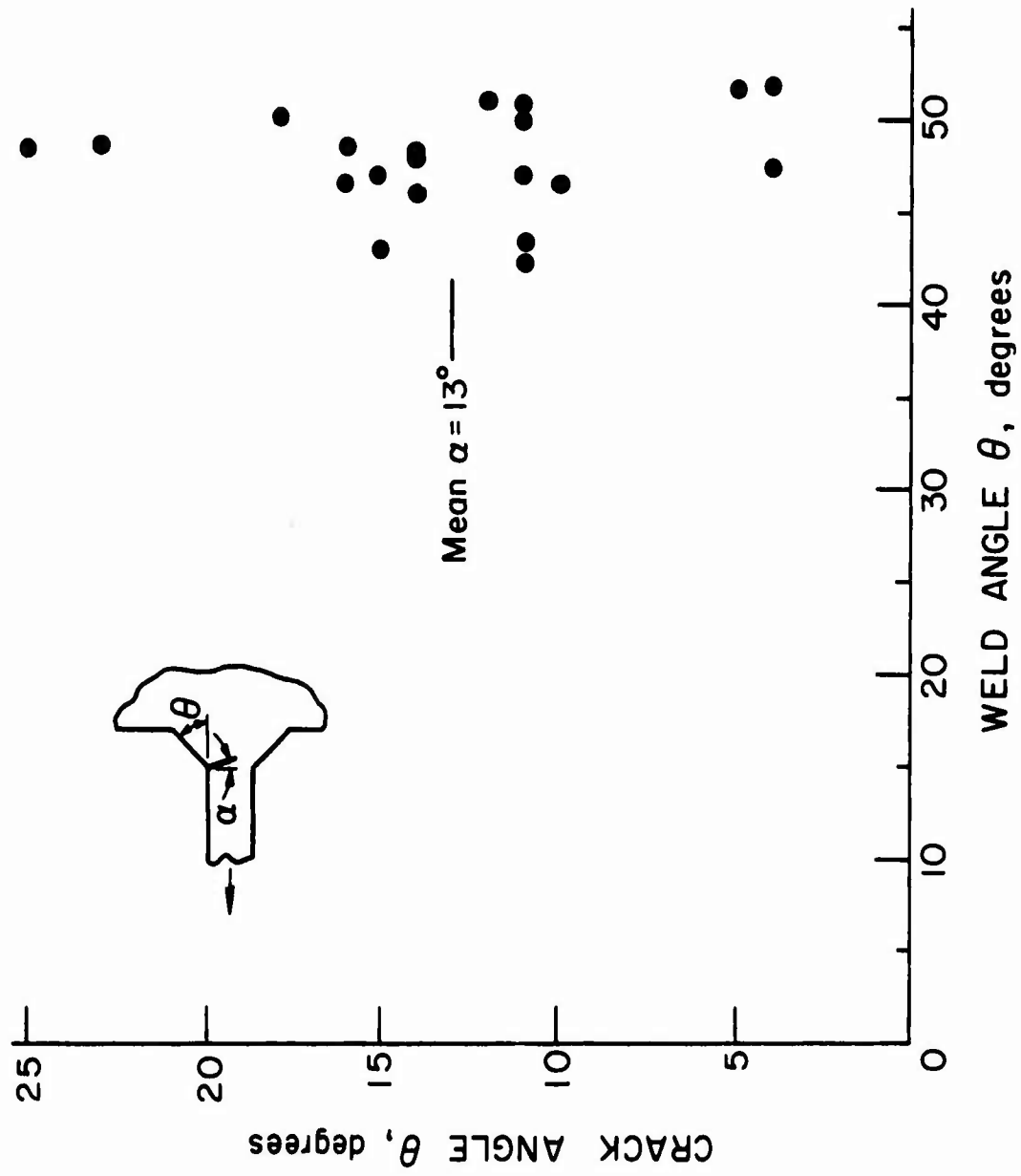
Fig. 12  Toe Crack Angle Variation With Weld Angle
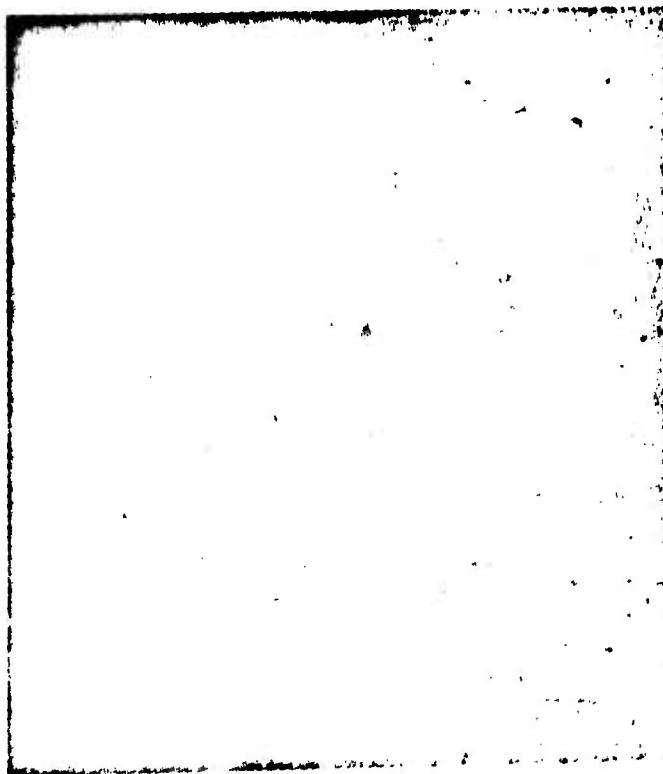
Fig. 13  Low Stress Toe Crack Failure
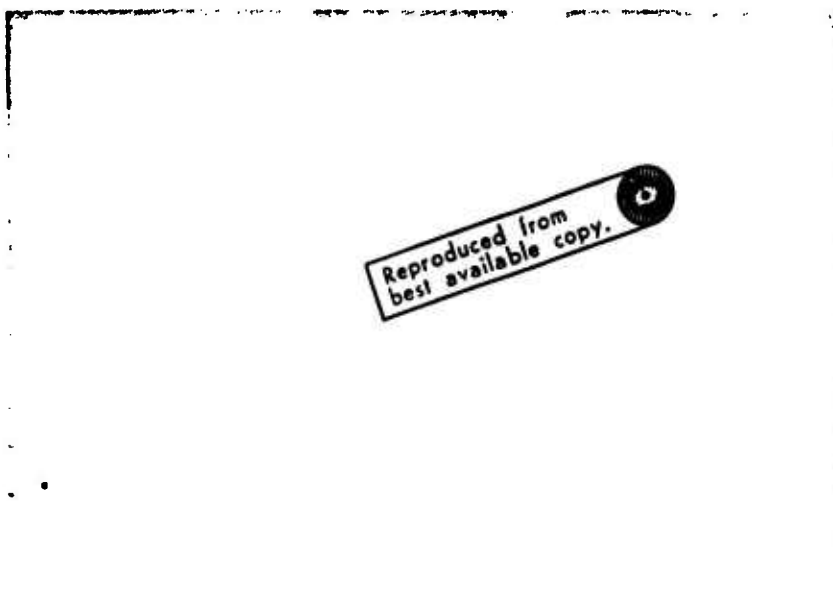
Fig. 14  High Stress Toe Crack Failure
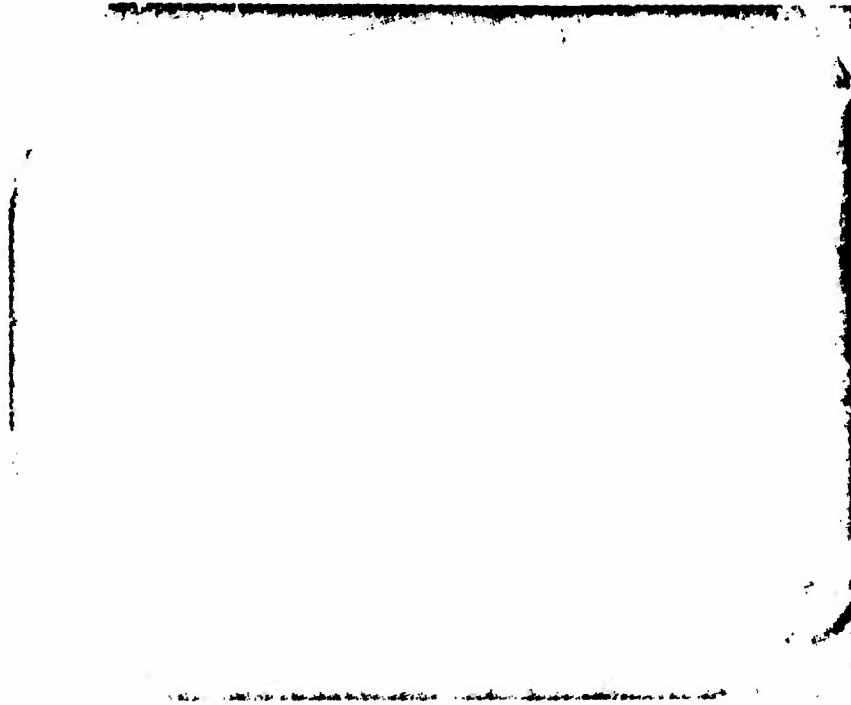
Fig. 15   Toe Crack Growth Along Fusion Line
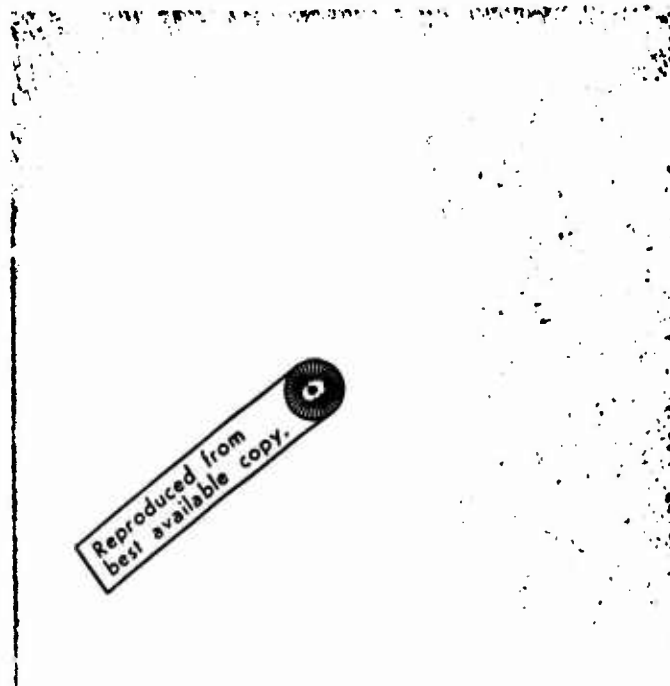


Fig. 16   End of Fusion Line Crack - 66X
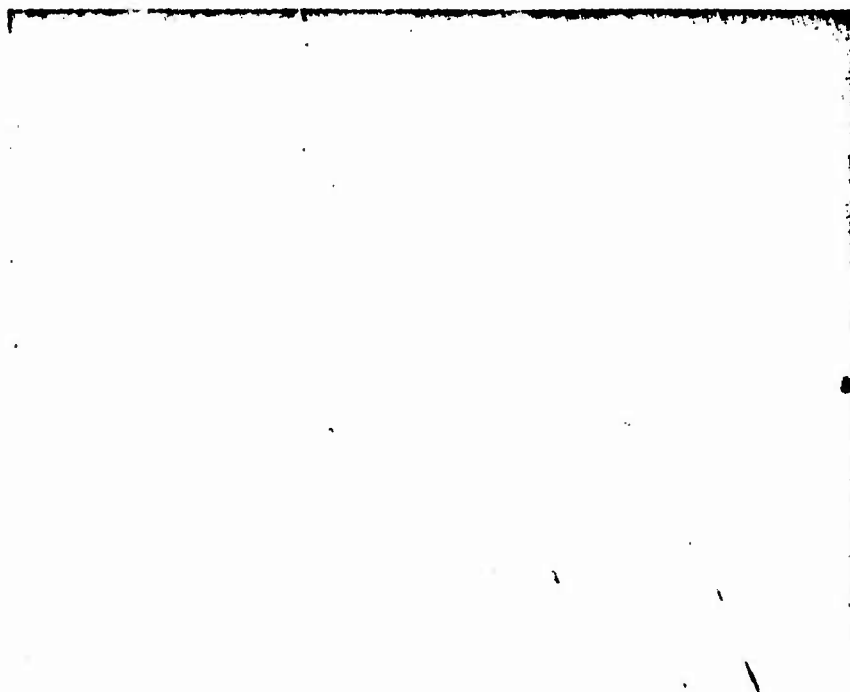
Fig. 17   Unetched Heat Affected Zone - 133X
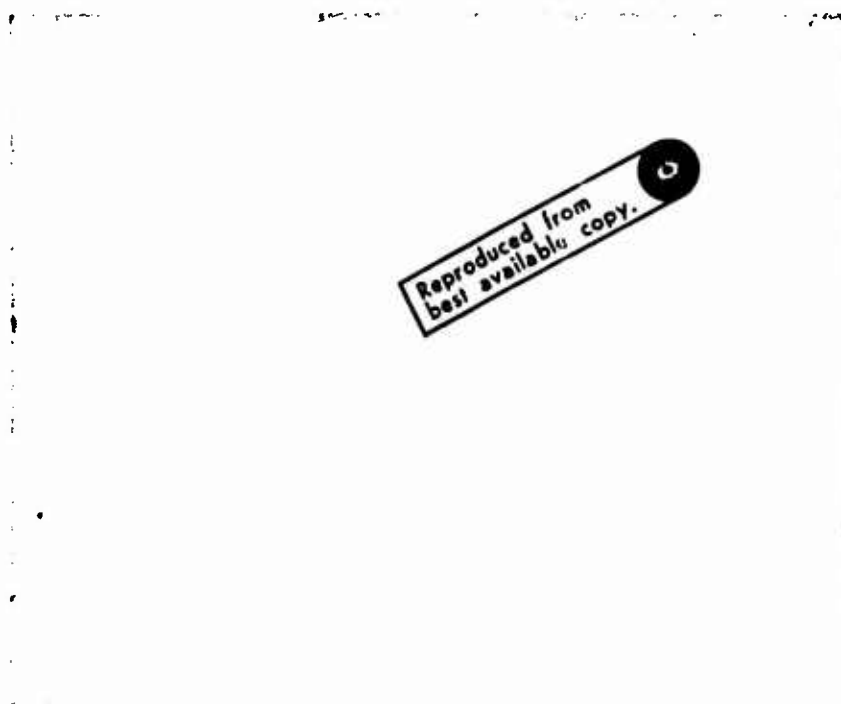
Fig. 18   Etched Heat Affected Zone - 532X
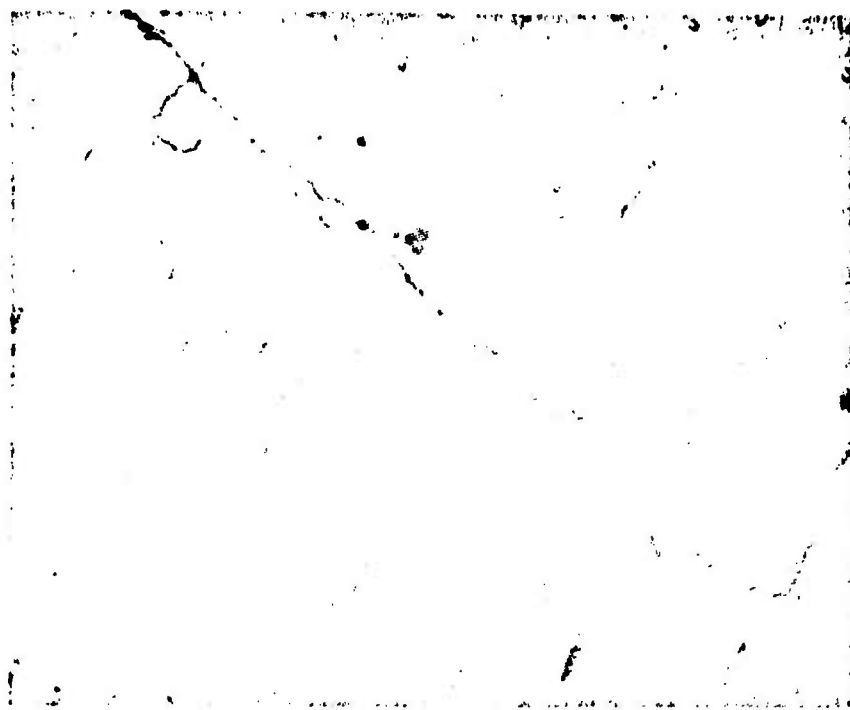
Fig. 19  Crack Branching to Included Particles - 66X



Fig. 20  Crack Growth Path at Included Particles - 133X
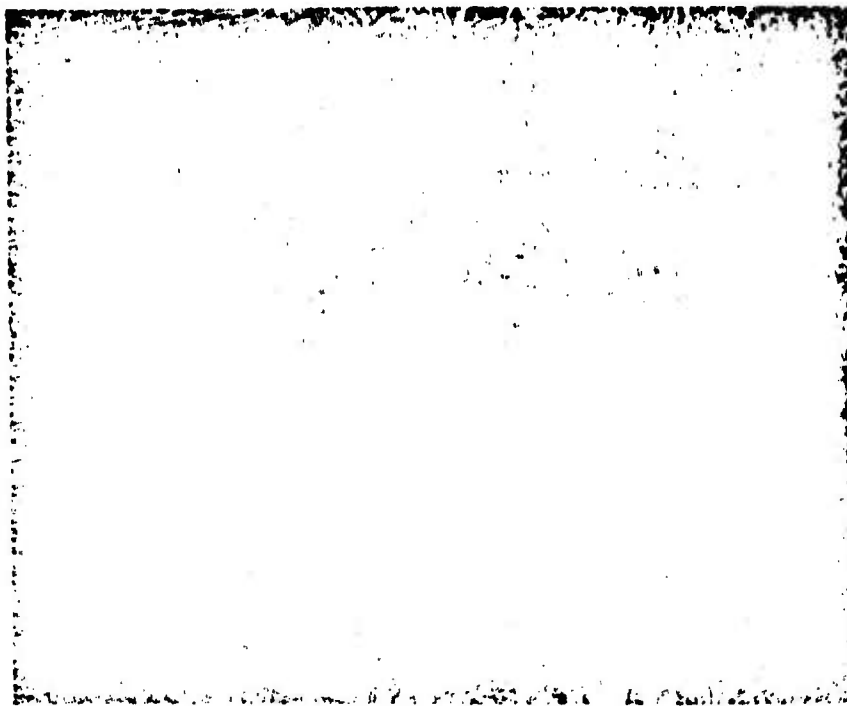
Fig. 21   Root Crack Tip Untested Specimen 133X

Fig. 22   Root Crack Tip Untested Specimen With Large Plate
Gap - 133X

Fig. 23   Root Crack Growth Along Grain Boundaries - 133X
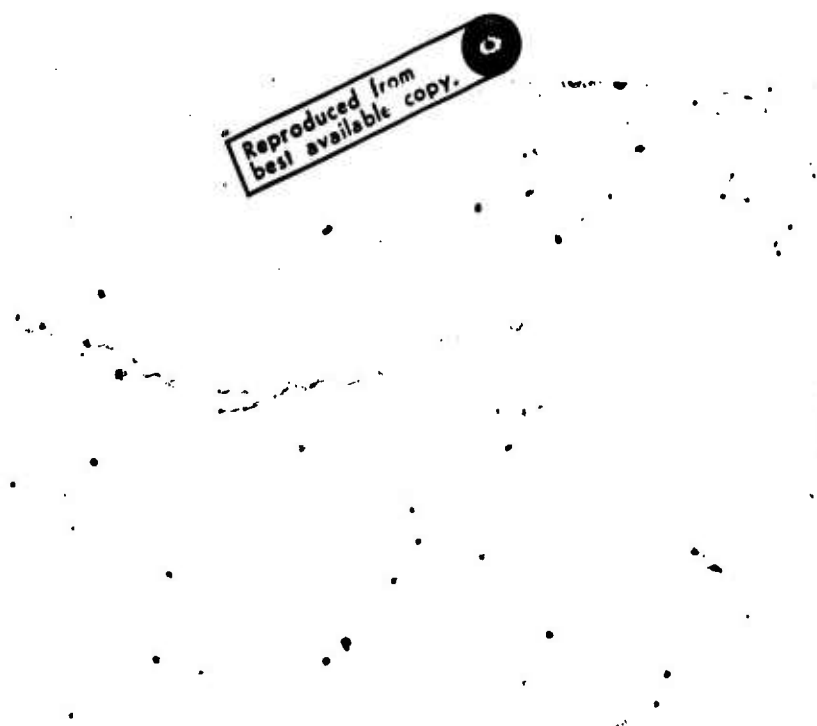
Fig. 24   Transgranular Root Crack Growth - 133X
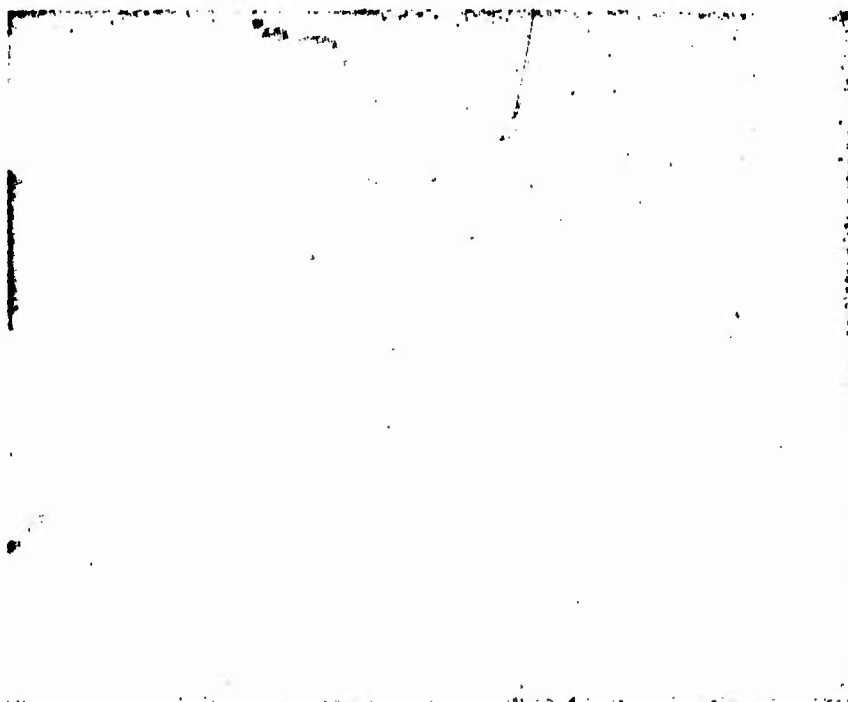
**Fig. 25** Vertical End of Root Crack At Failure - 66X

**Fig. 26** Failure of Joint With Porous Weld
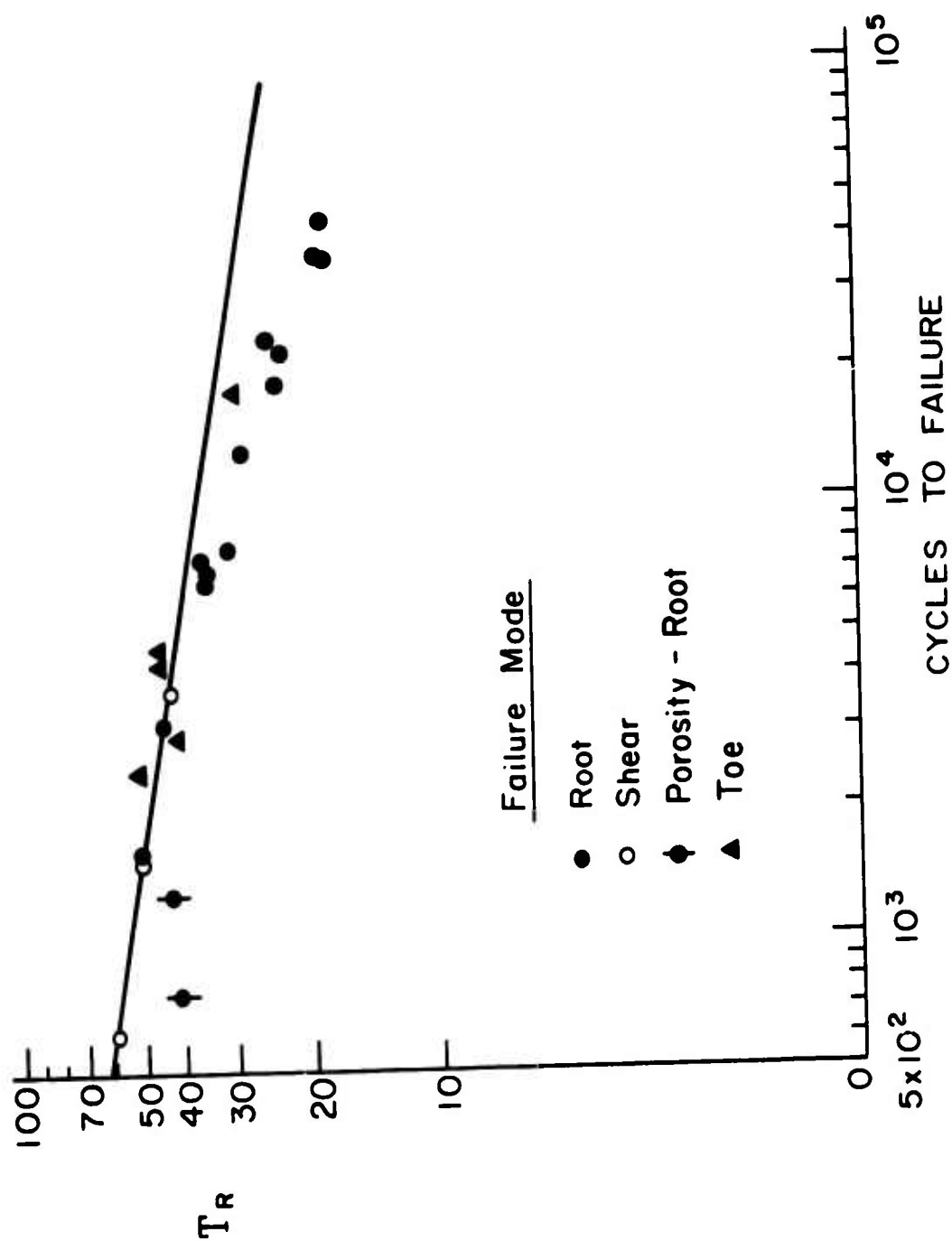
Fig. 27  Weld Shear Stress Range versus Cycle Life
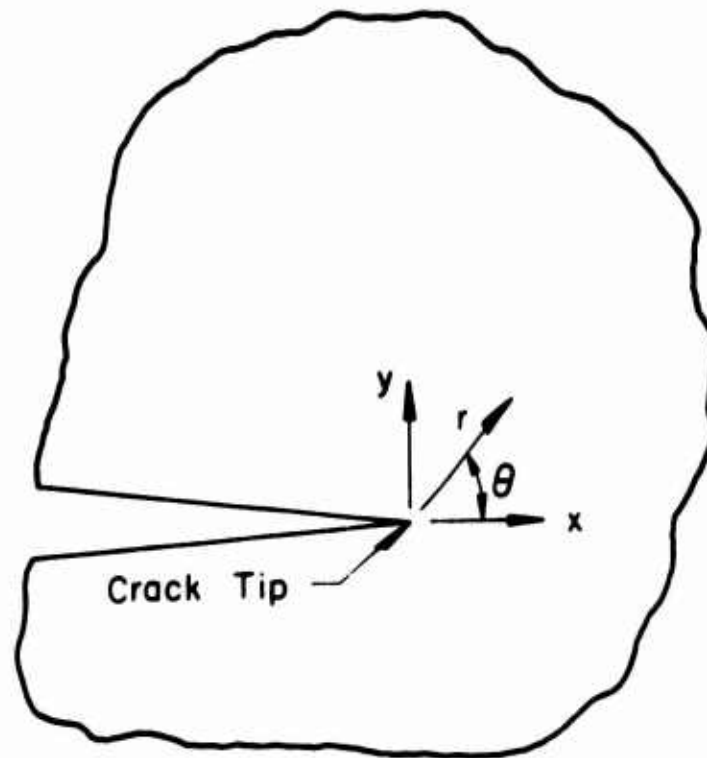
$$\{\sigma\} = \left[ f(r,\theta) \right] \{K\}$$

Fig. 28   Crack Tip Stress Field Coordinates
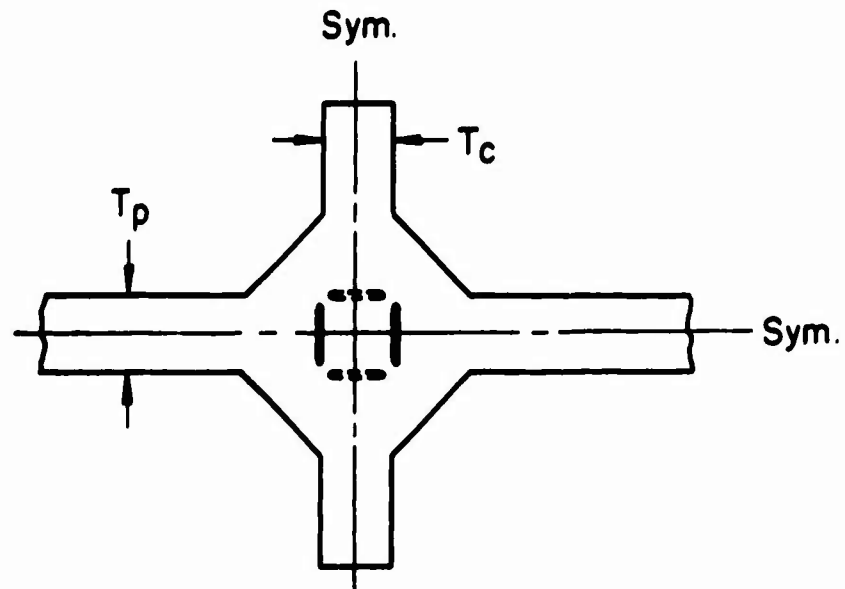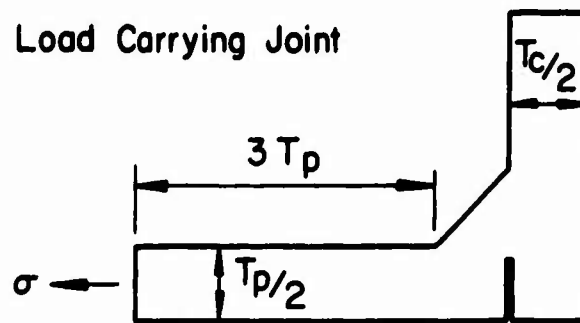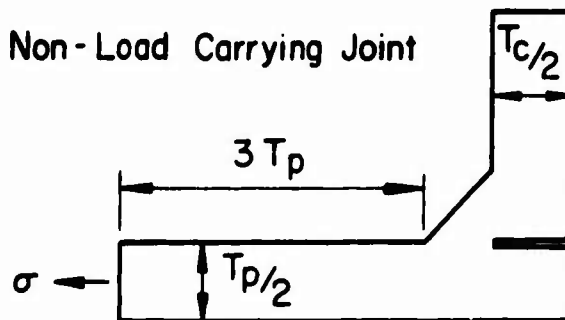
Fig. 29 Symmetric Joints Analyzed

-114

CRACK TIP MESH

$3\,T_p$

$T_p/2$
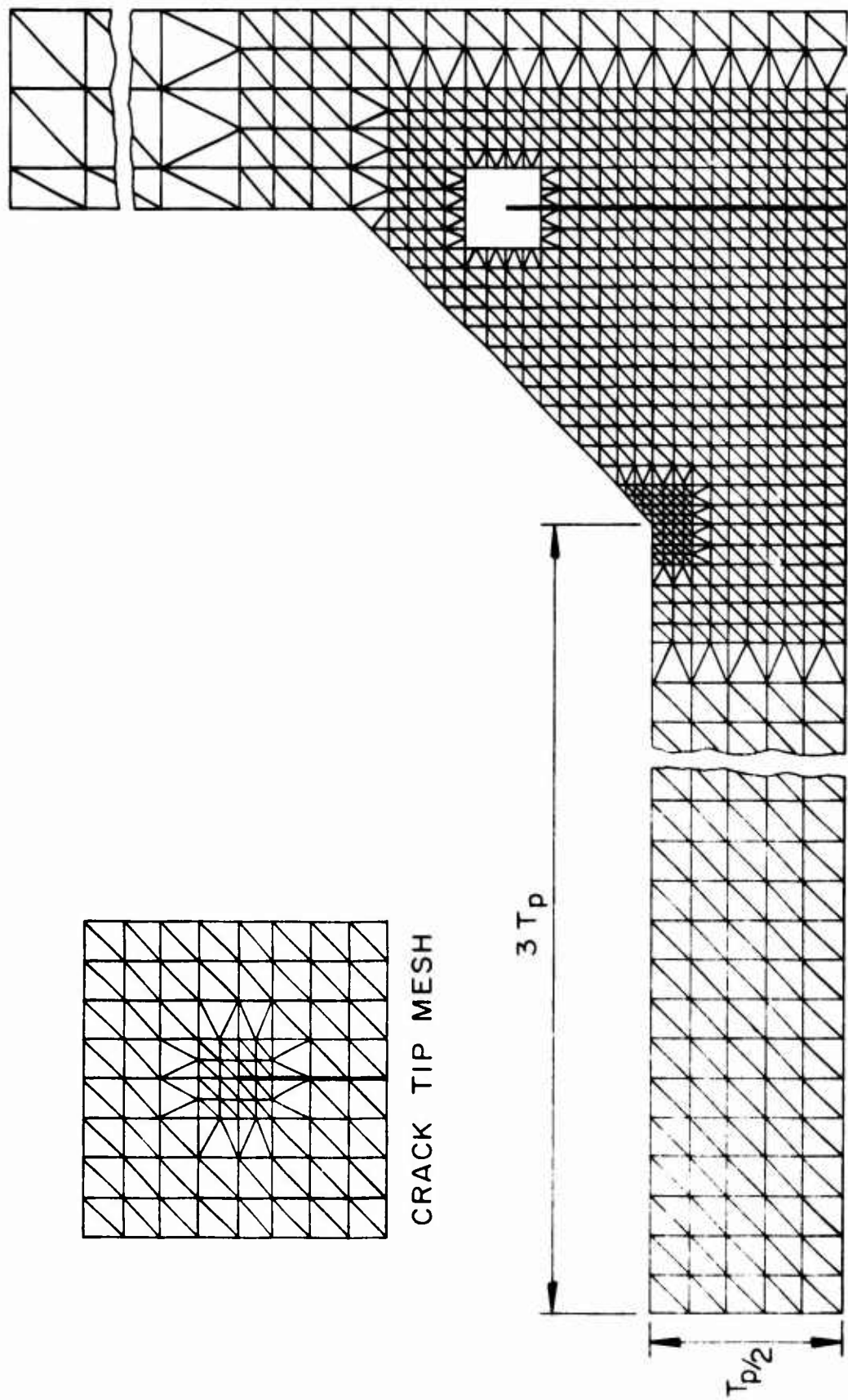
Fig. 30 Load Carrying Joint Root Crack Finite Element Mesh

-115

CRACK TIP MESH
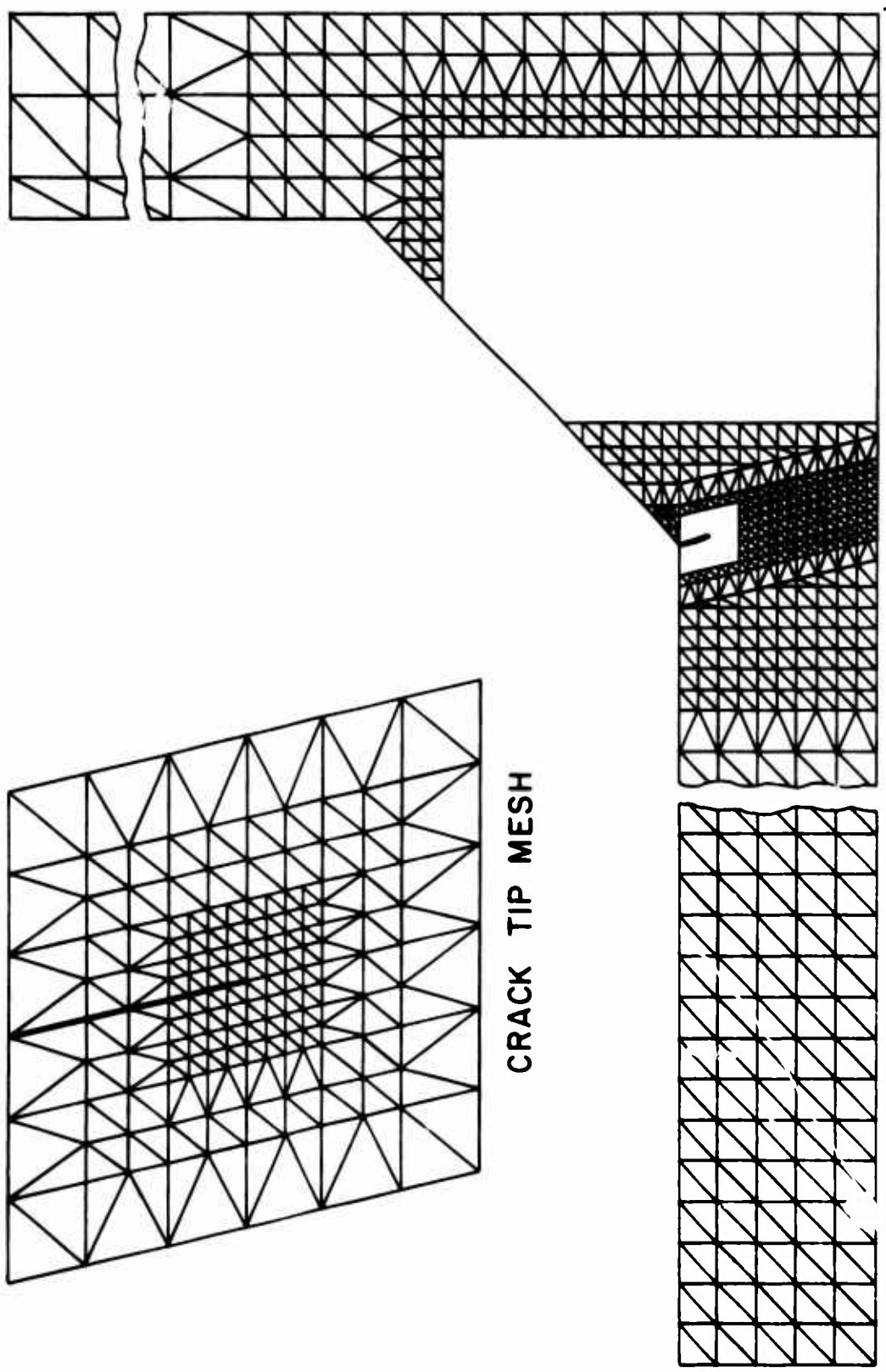
Fig. 31  Load Carrying Joint Toe Crack Finite Element Mesh
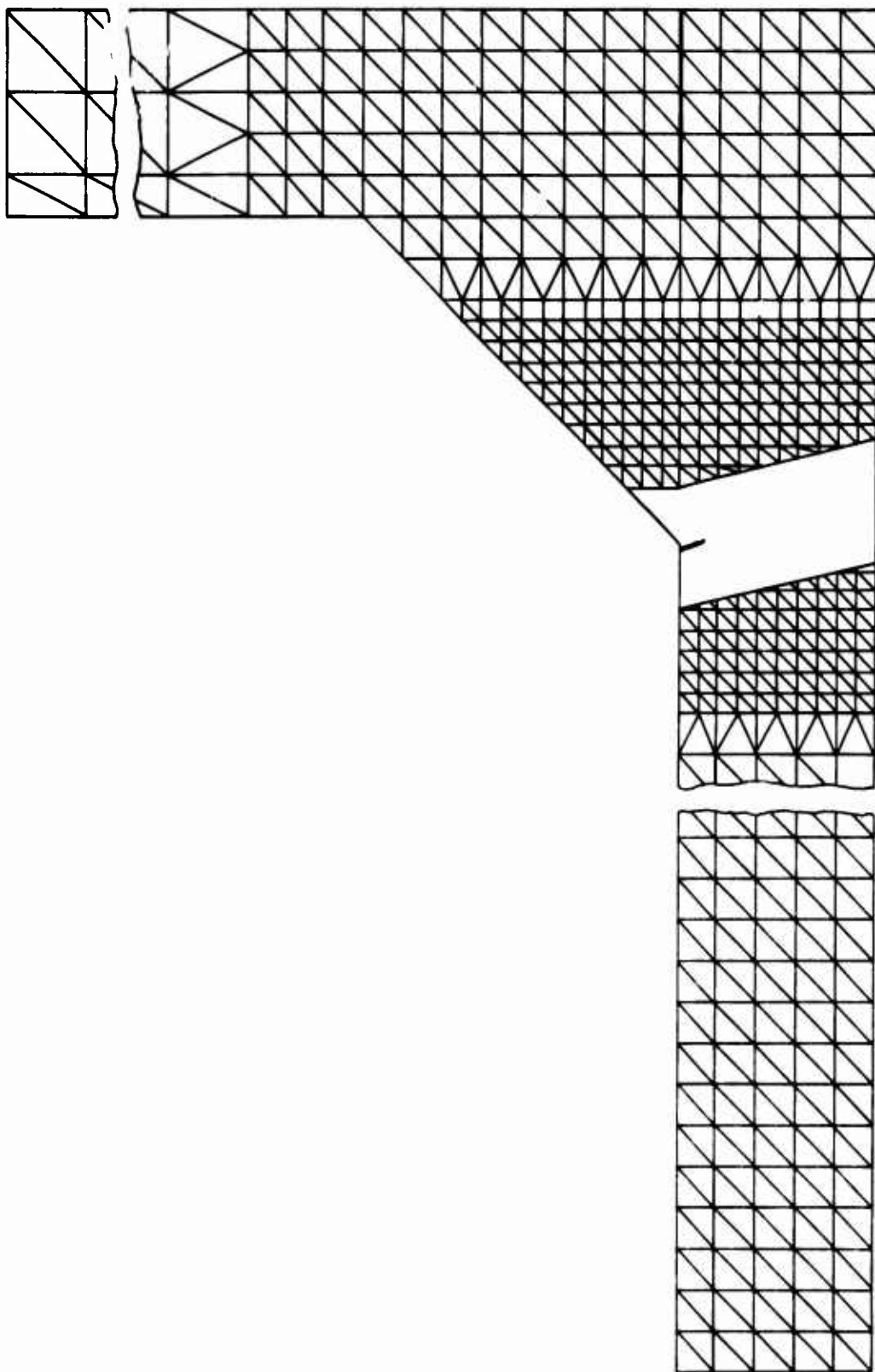
Fig. 32  Non-Load Carrying Toe Crack Finite Element Mesh
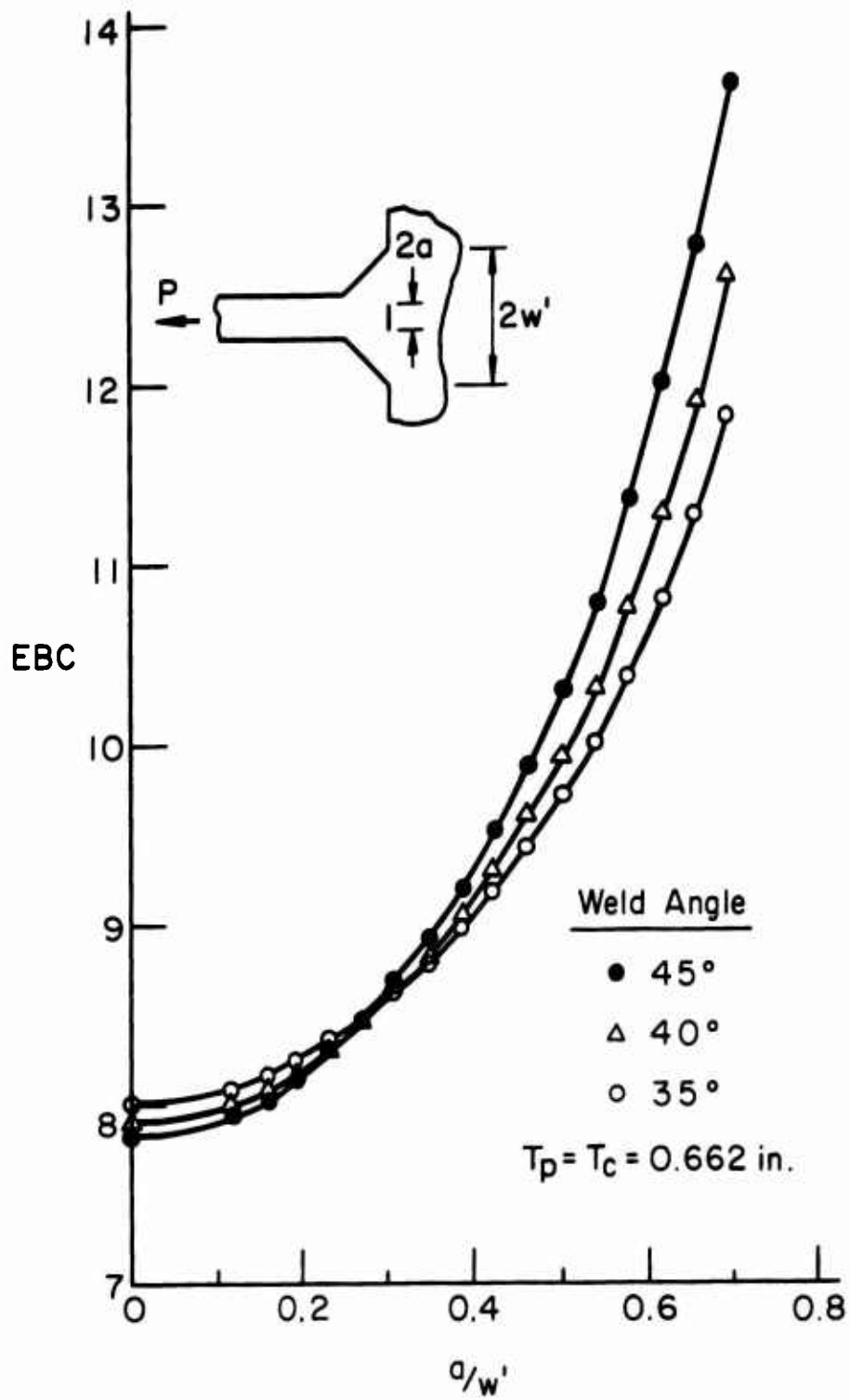
Fig. 33  Change of Compliance With Crack Length
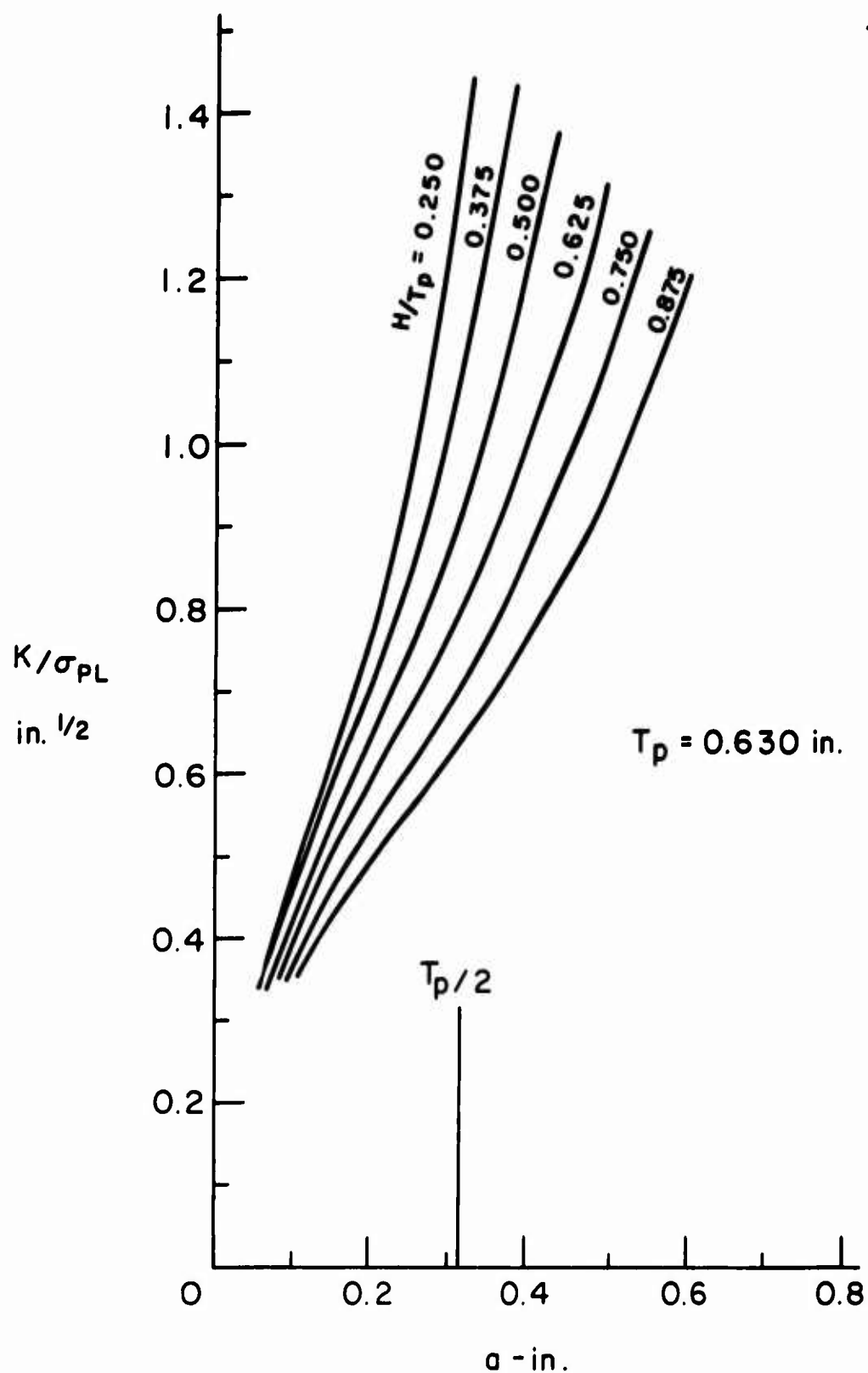
Fig. 34   Variation of $K/\sigma_{PL}$ With $H/T_p$ for Root Cracks in Load Carrying Joints
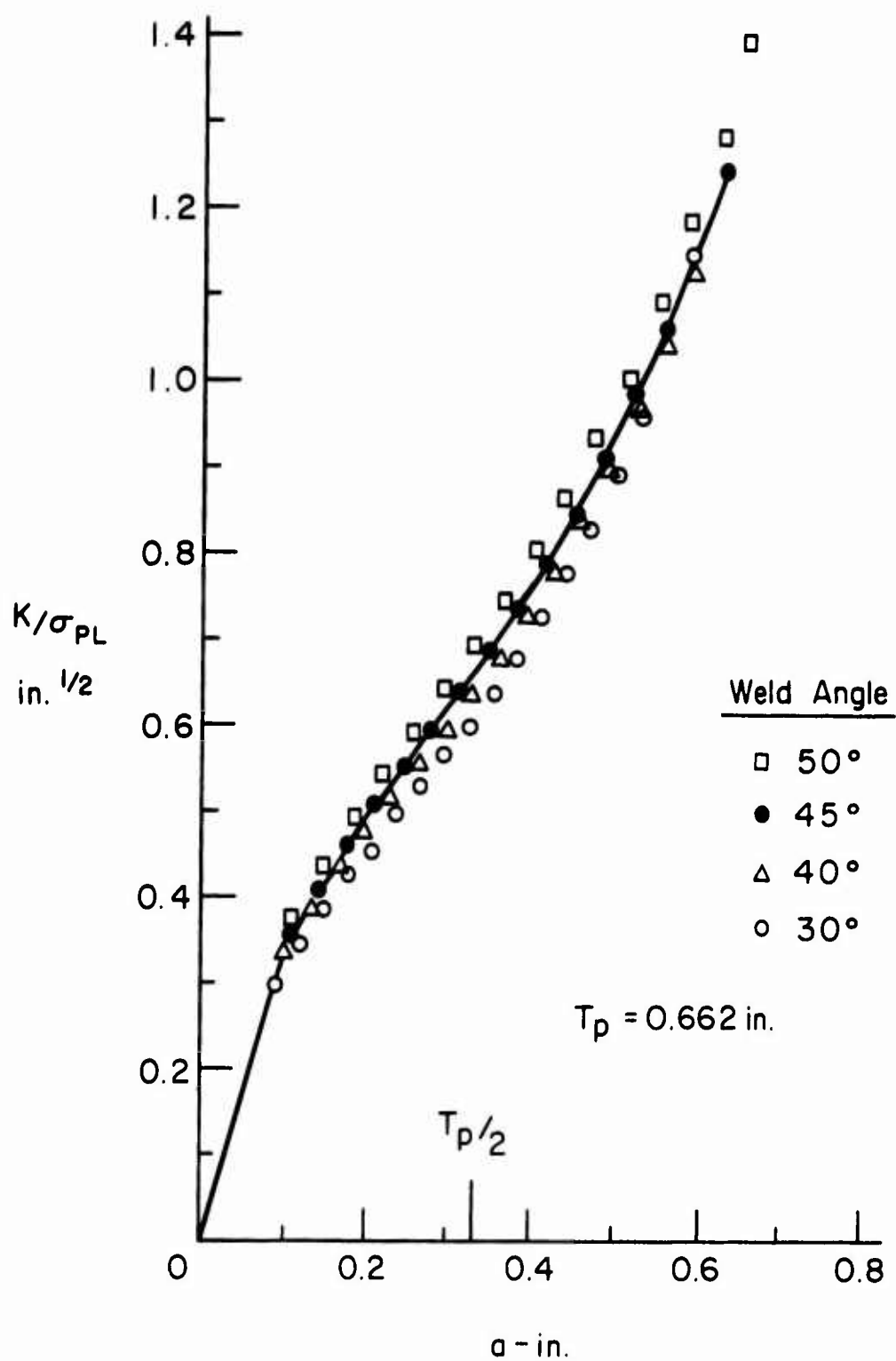
Fig. 35 Variation of $K/\sigma_{pl}$ With Weld Angle for Root Cracks in Load Carrying Joints
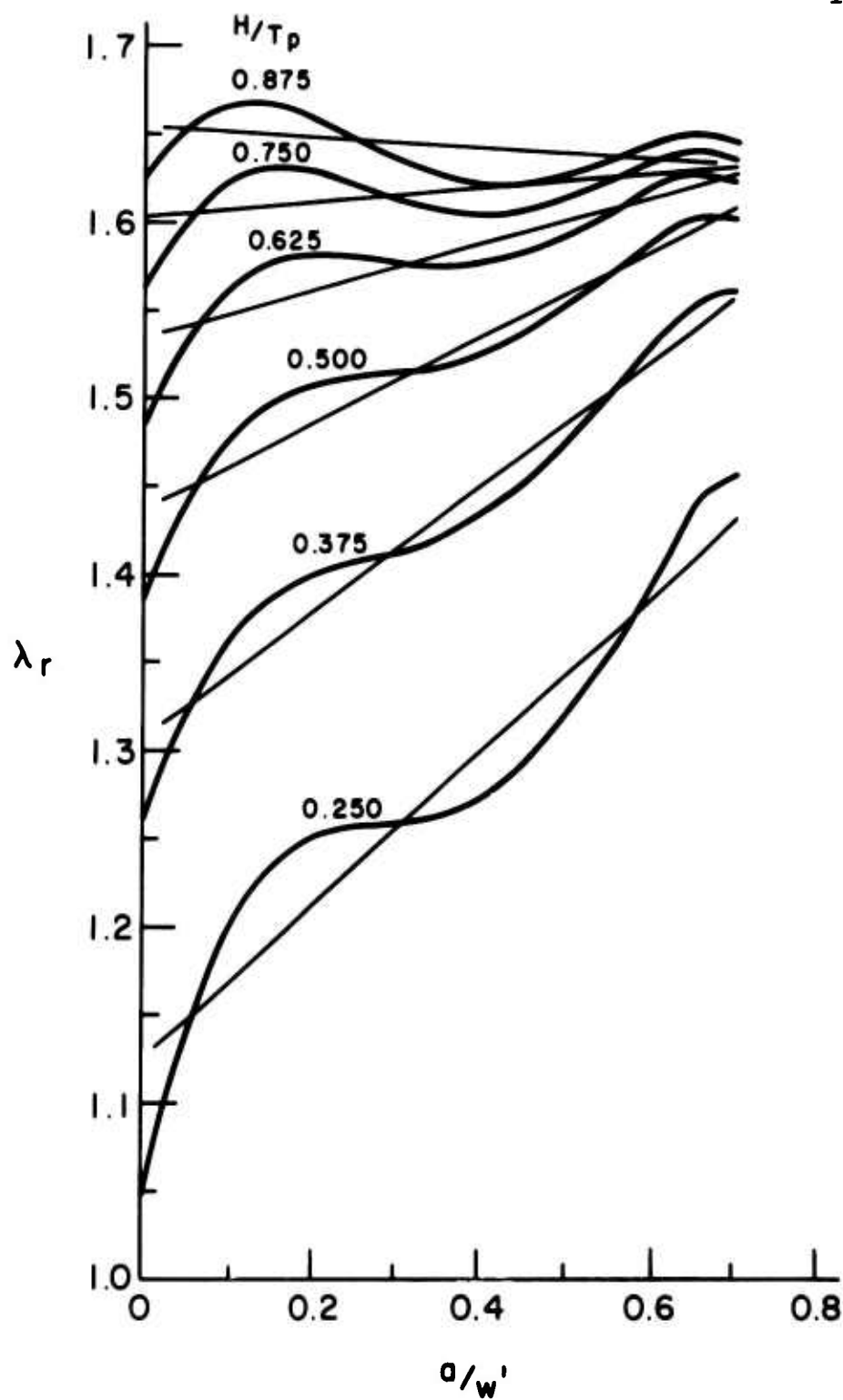
Fig. 36   Change in $\lambda_R$ With Crack Length and Weld Size
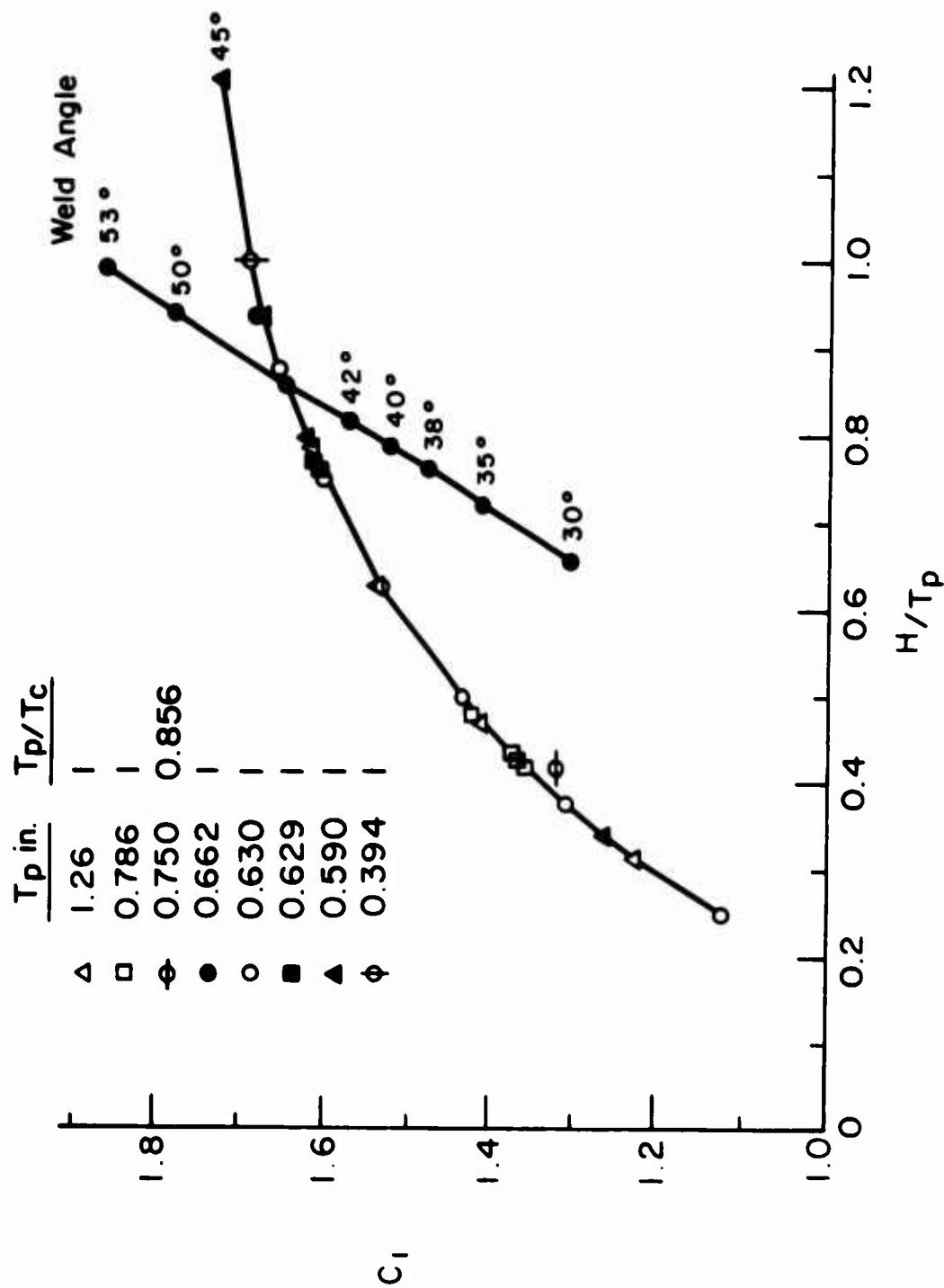
Fig. 37  Variation of the Coefficient $C_l$ With $H/T_p$
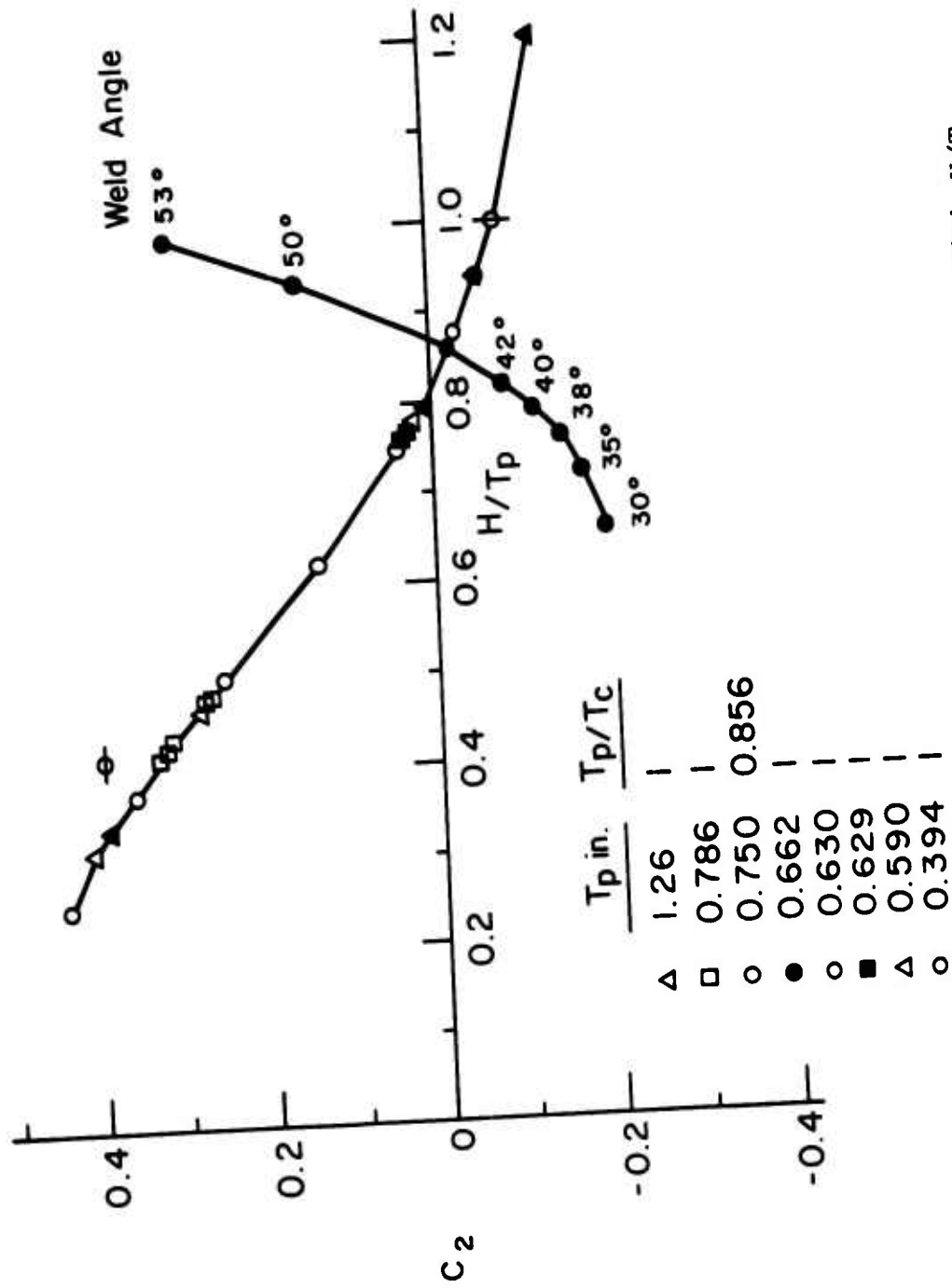
Fig. 38  Variation of the Coefficient $C_2$ with $H/T_p$
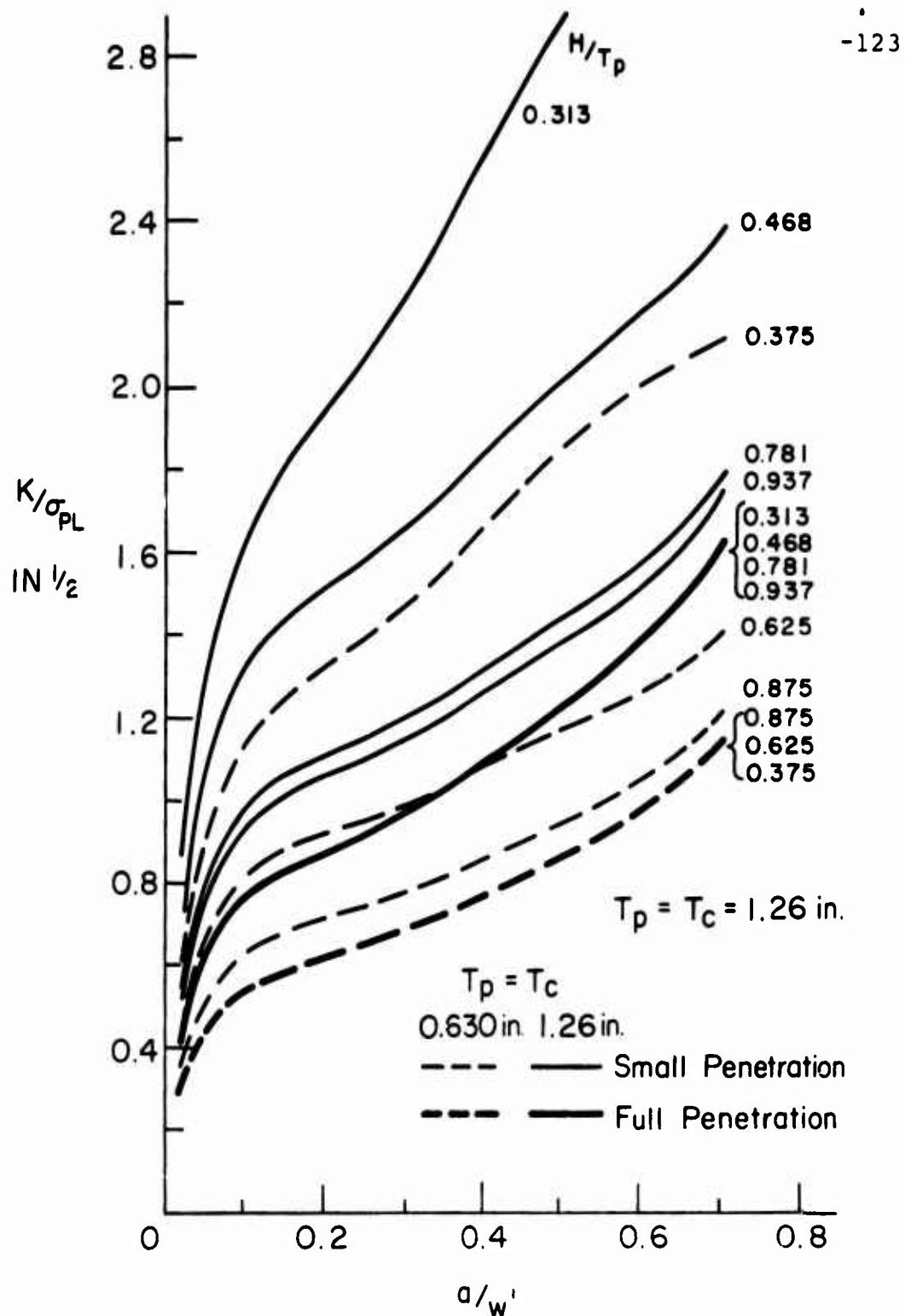
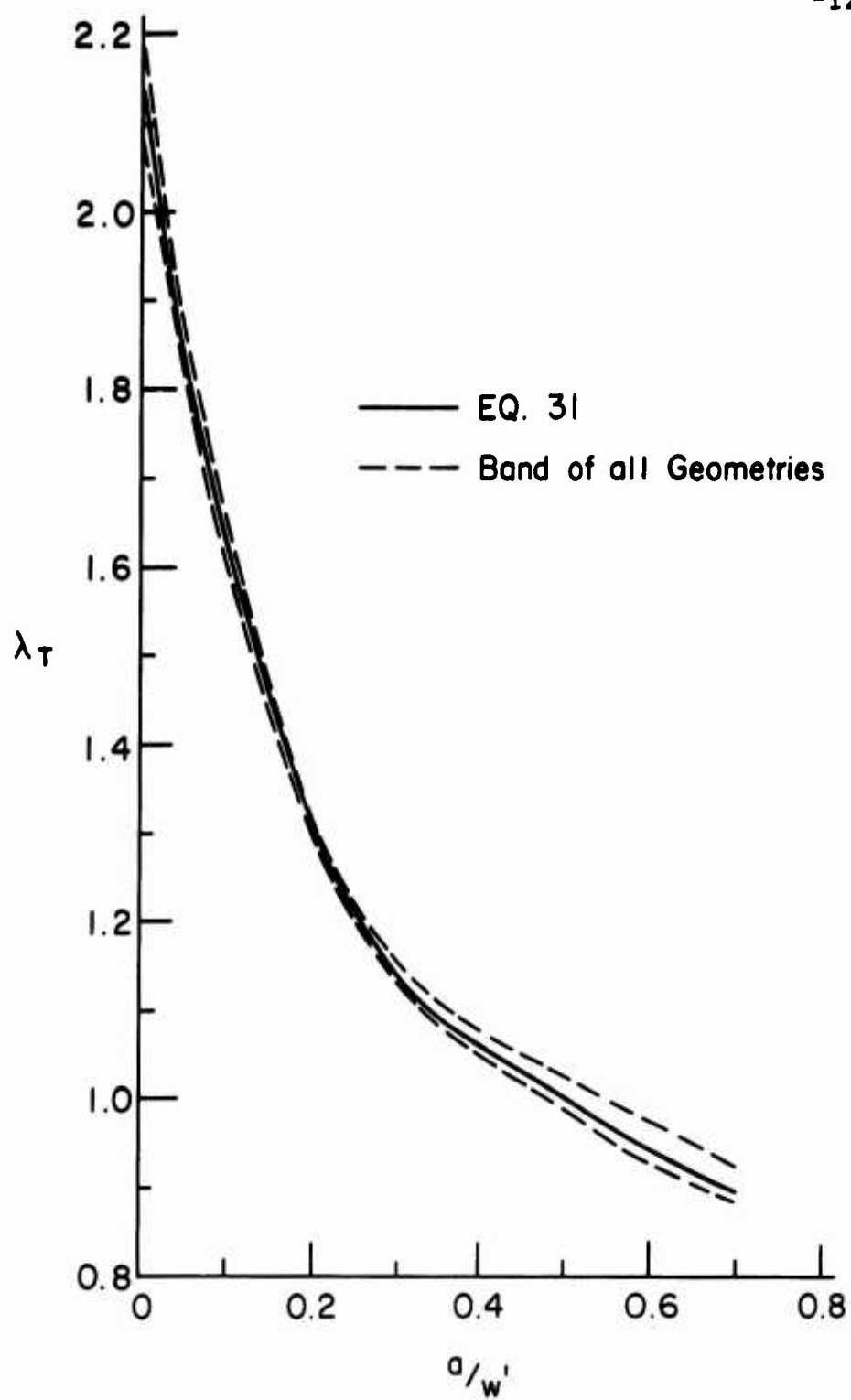Fig. 39  Variation of $K/\sigma_{pl}$ With Weld Penetration and a/w' for Two Plate Thicknesses for Toe Cracks in Load Carrying Joints

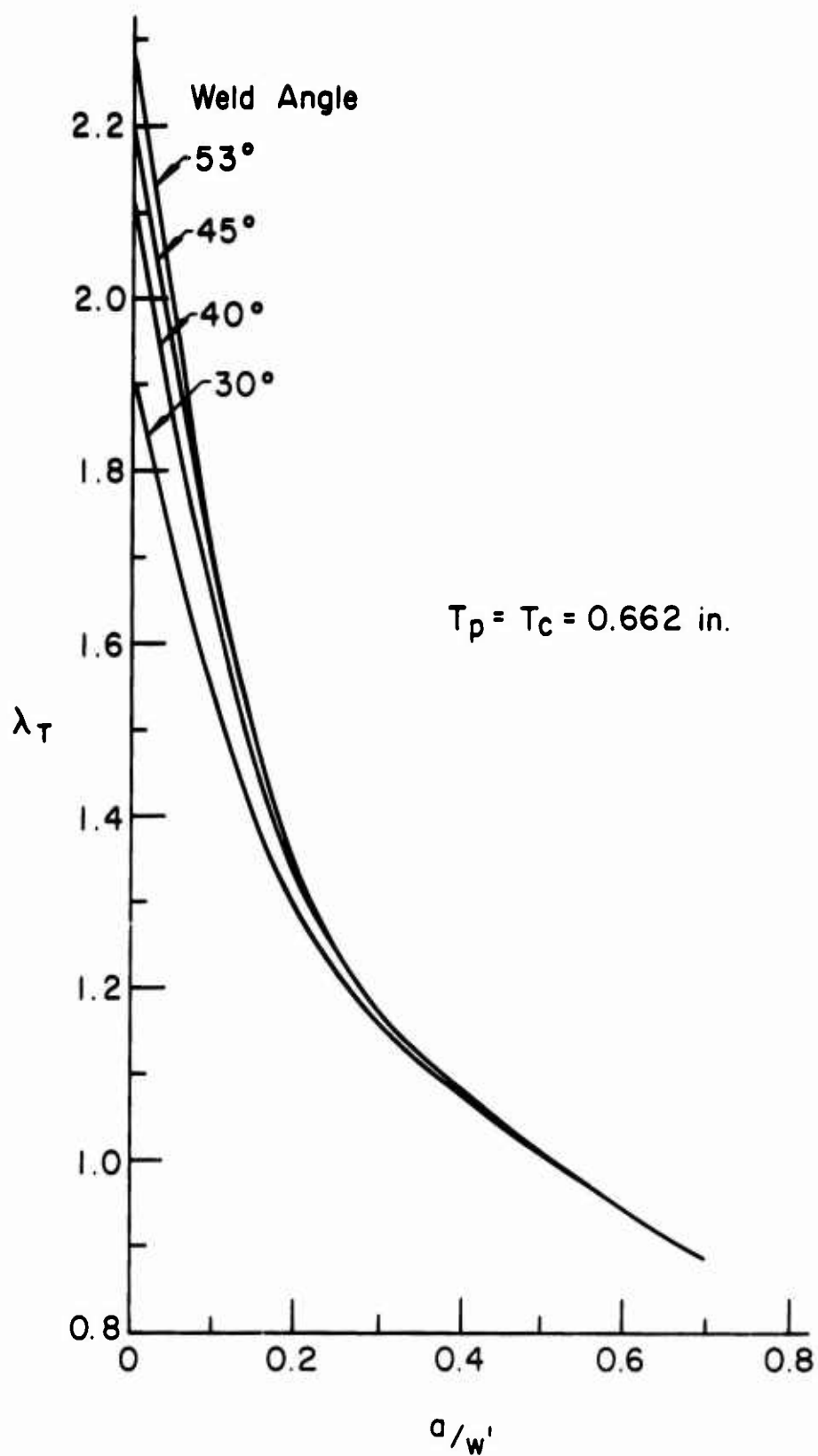Fig. 40   Variation of $\lambda_T$ for Load Carrying Joints with Full Penetration and 45° Degree Welds

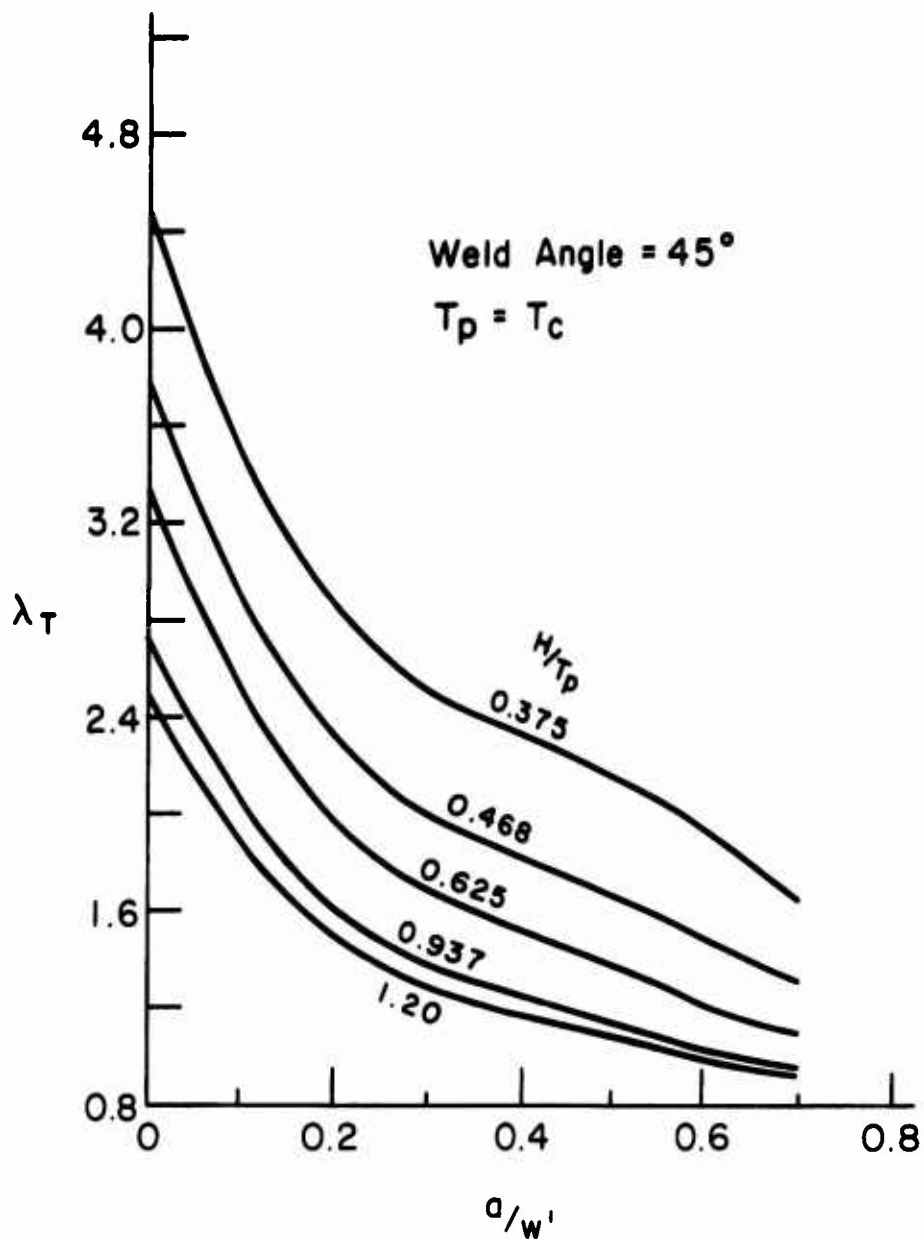Fig. 41   Change in $\lambda_T$ With Weld Angle for Full Penetration Welds

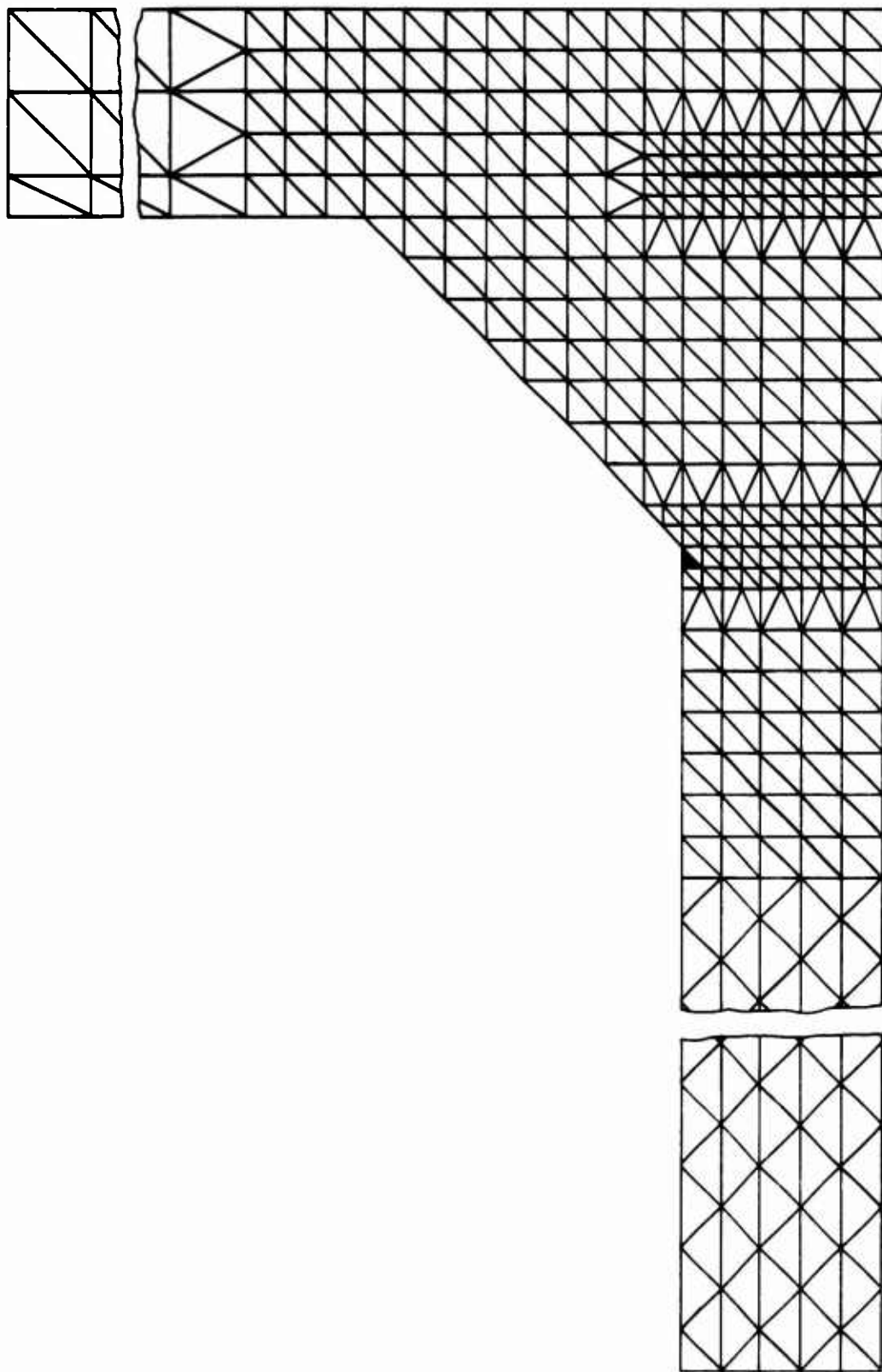Fig. 42 Change in $\lambda_T$ With Weld Size for Load Carrying Joints With Small Root Penetration

Fig. 43   Finite Element Used for Stress Analysis of Load
Carrying Weld Joints

| Penetration | | TP=TC |
|:---:|:---:|:---:|
| Full | Zero | in. |
| ▲ | △ | 1.260 |
| ◕ | ◒ | 0.786 |
| ⬤ | ⊖ | 0.764 |
| ■ | □ | 0.662 |
| ● | ○ | 0.630 |
| ◗ | □ | 0.625 |

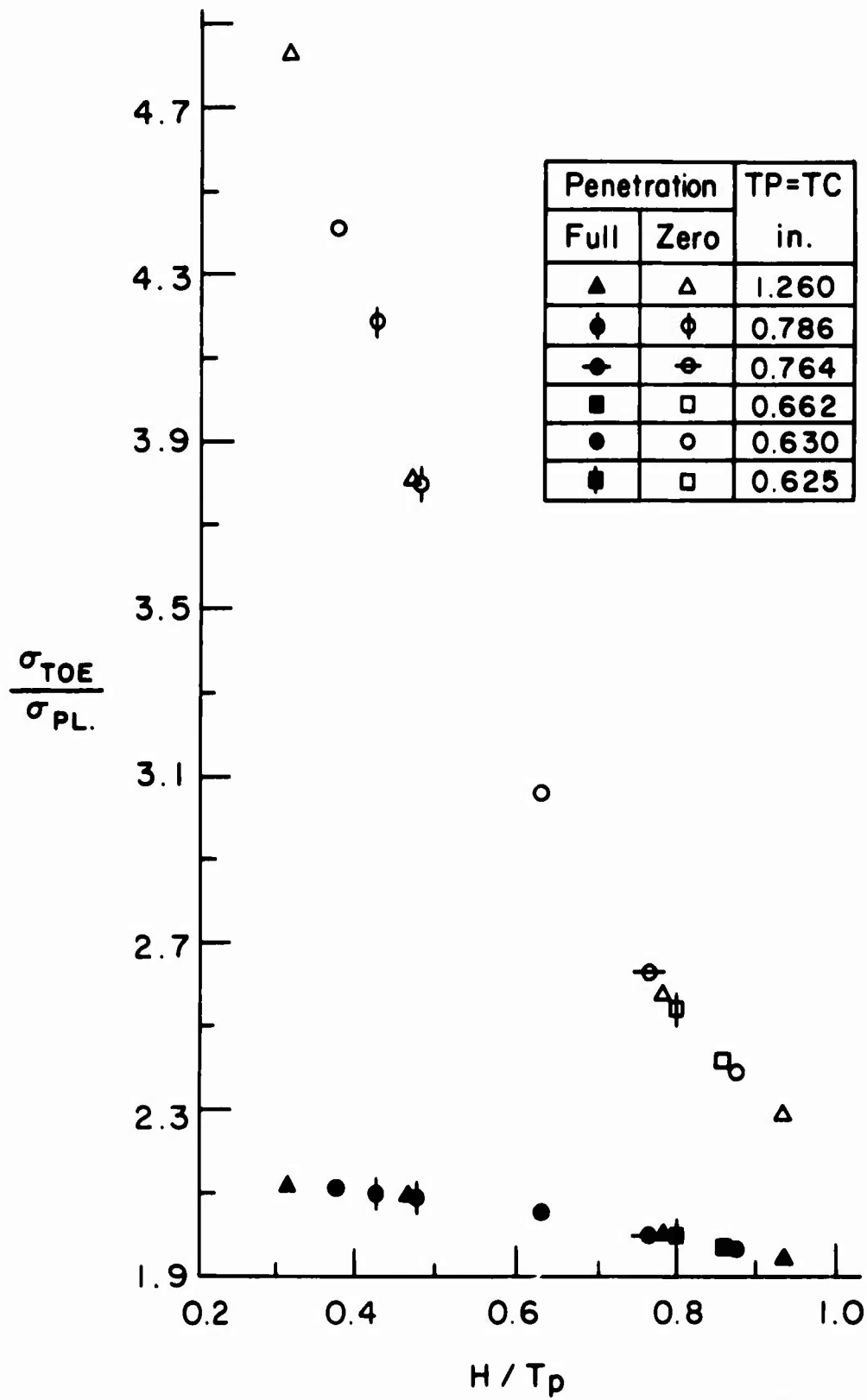$$\frac{\sigma_{TOE}}{\sigma_{PL.}}$$

$H / T_p$

Fig. 44   Variation of Stress Concentration at Weld Toe with
$H/T_p$ for Joints with Full and Zero Root Penetration
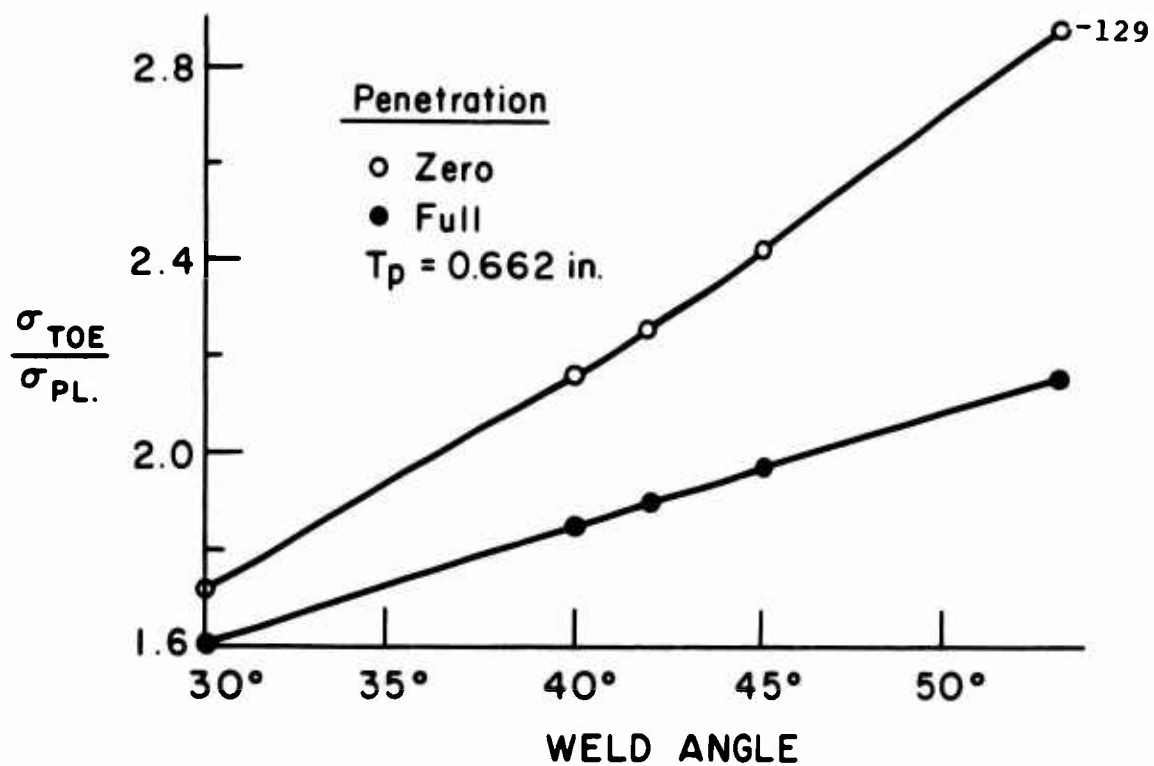
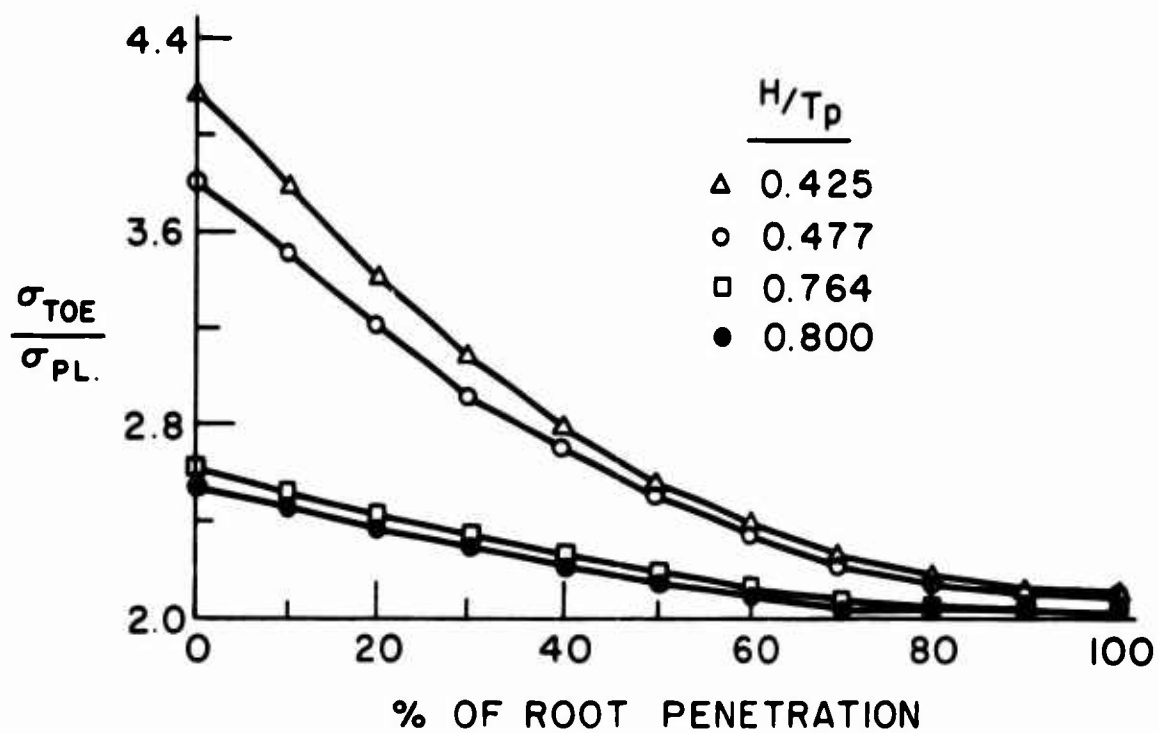Fig. 45    Change in Stress Concentration at Weld Toe With
           Weld Angle



Fig. 46    Change in Stress Concentration at Weld Toe With
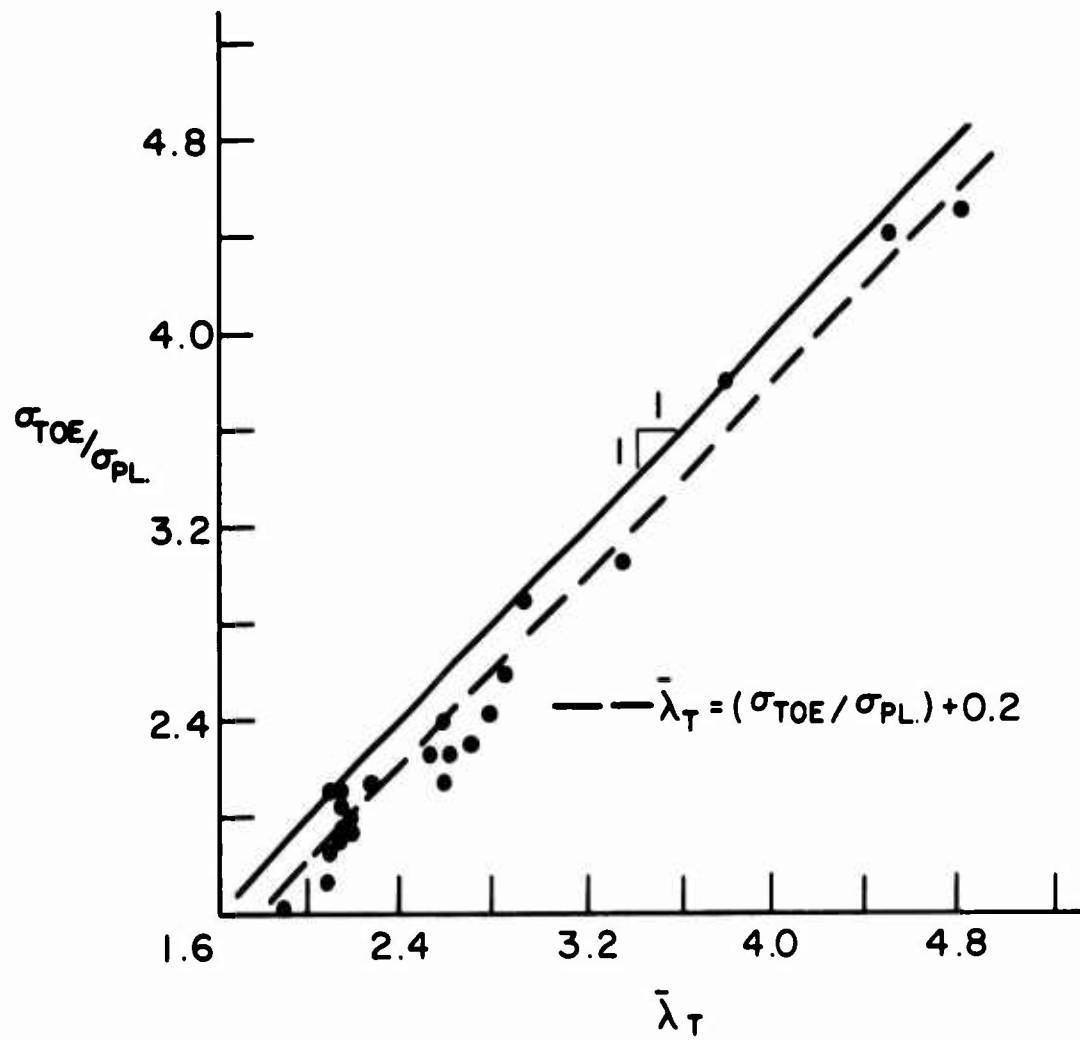           Root Penetration

Fig. 47 Correlation of $\bar{\lambda}_T$ With Stress Concentration at Weld Toe
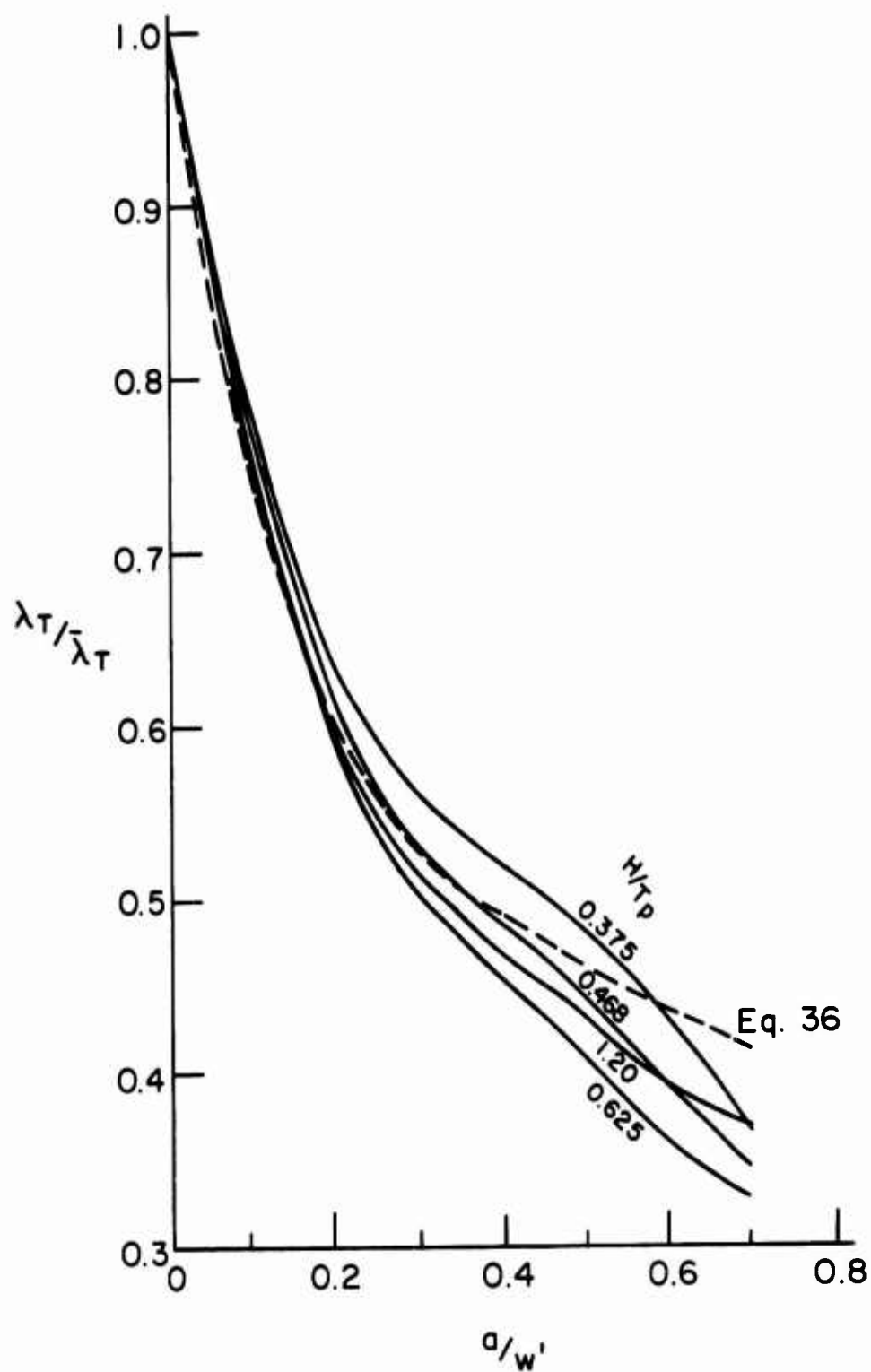
Fig. 48  Variation of $\lambda_T/\overline{\lambda}_T$ With Crack Length - Small Penetration Welds
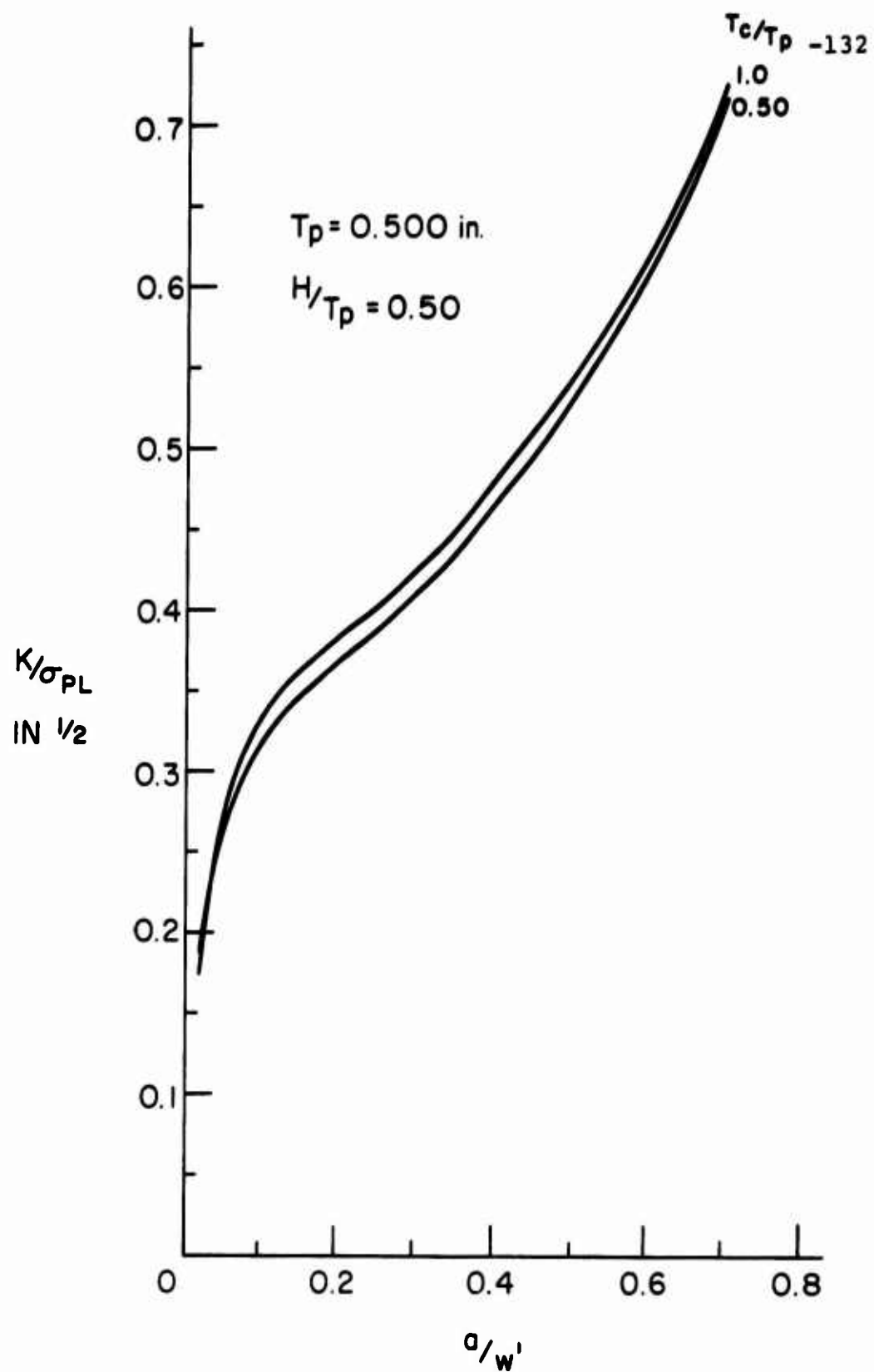
Fig. 49   Variation of $K/\sigma_{pl}$ With a/w' for Non-Load Carrying Weld Joints
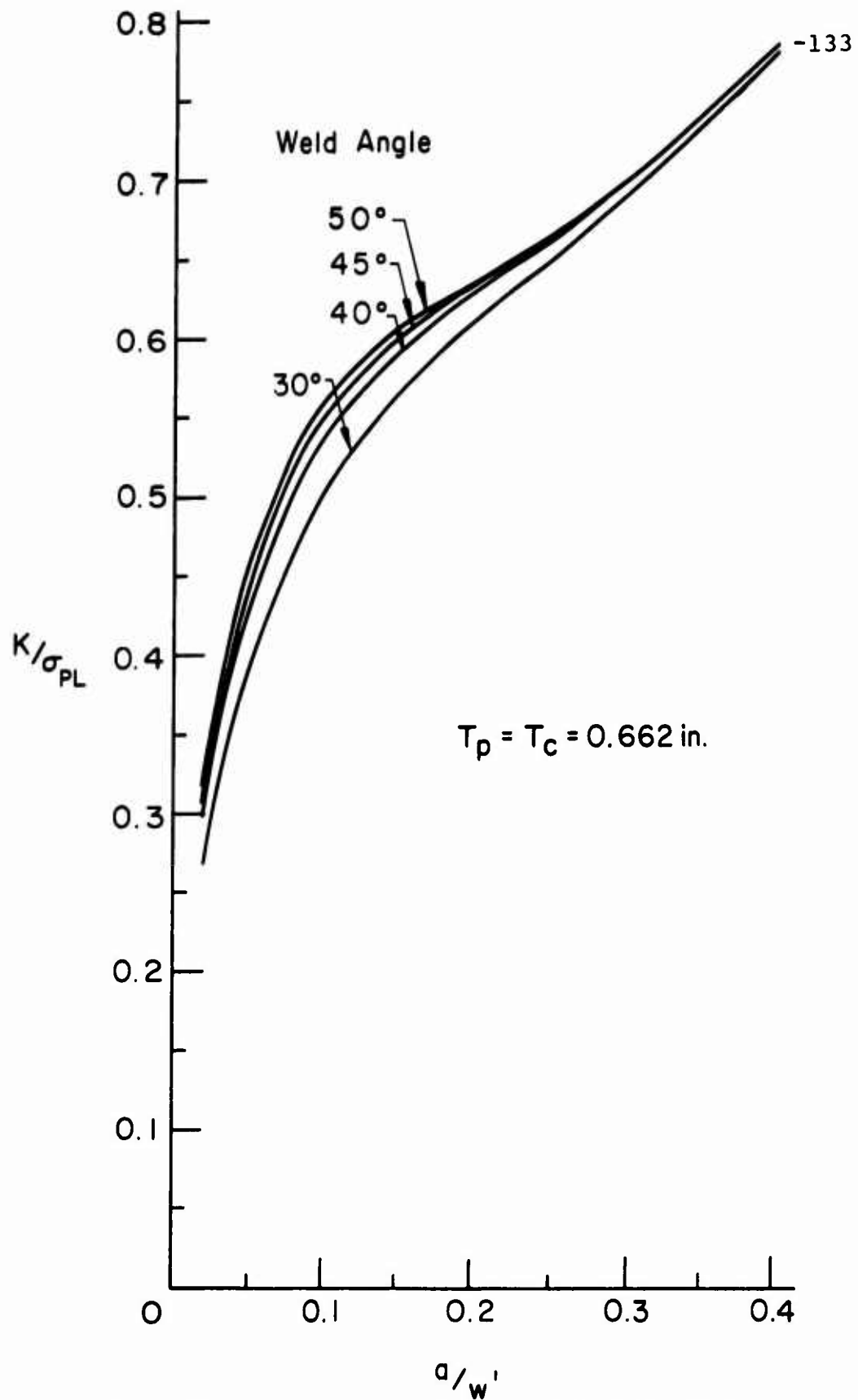
Fig. 50   Variation of $K/\sigma_{pl}$ With Weld Angle
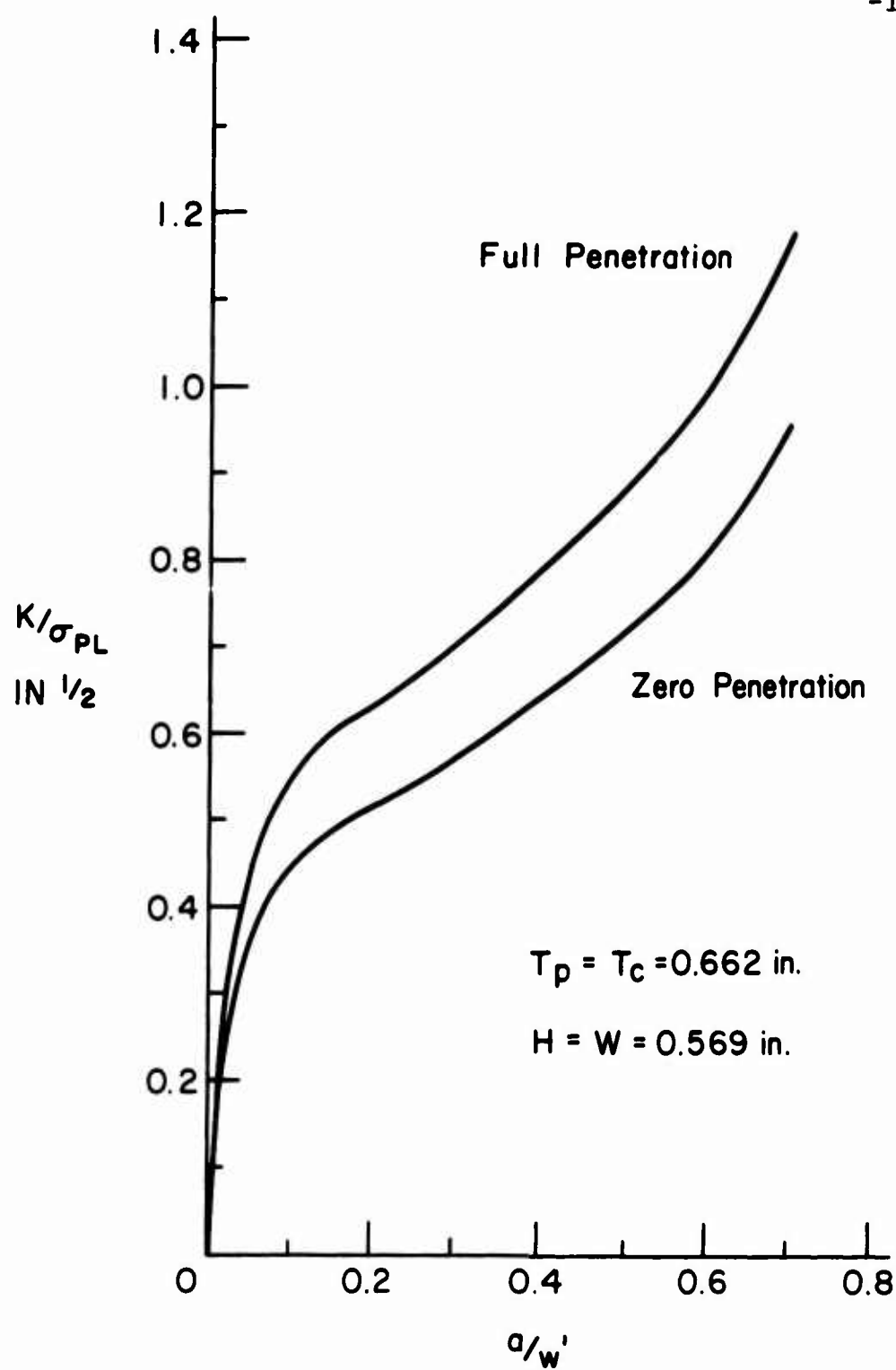
Fig. 51  Variation of $K/\sigma_{pl}$ With Weld Penetration
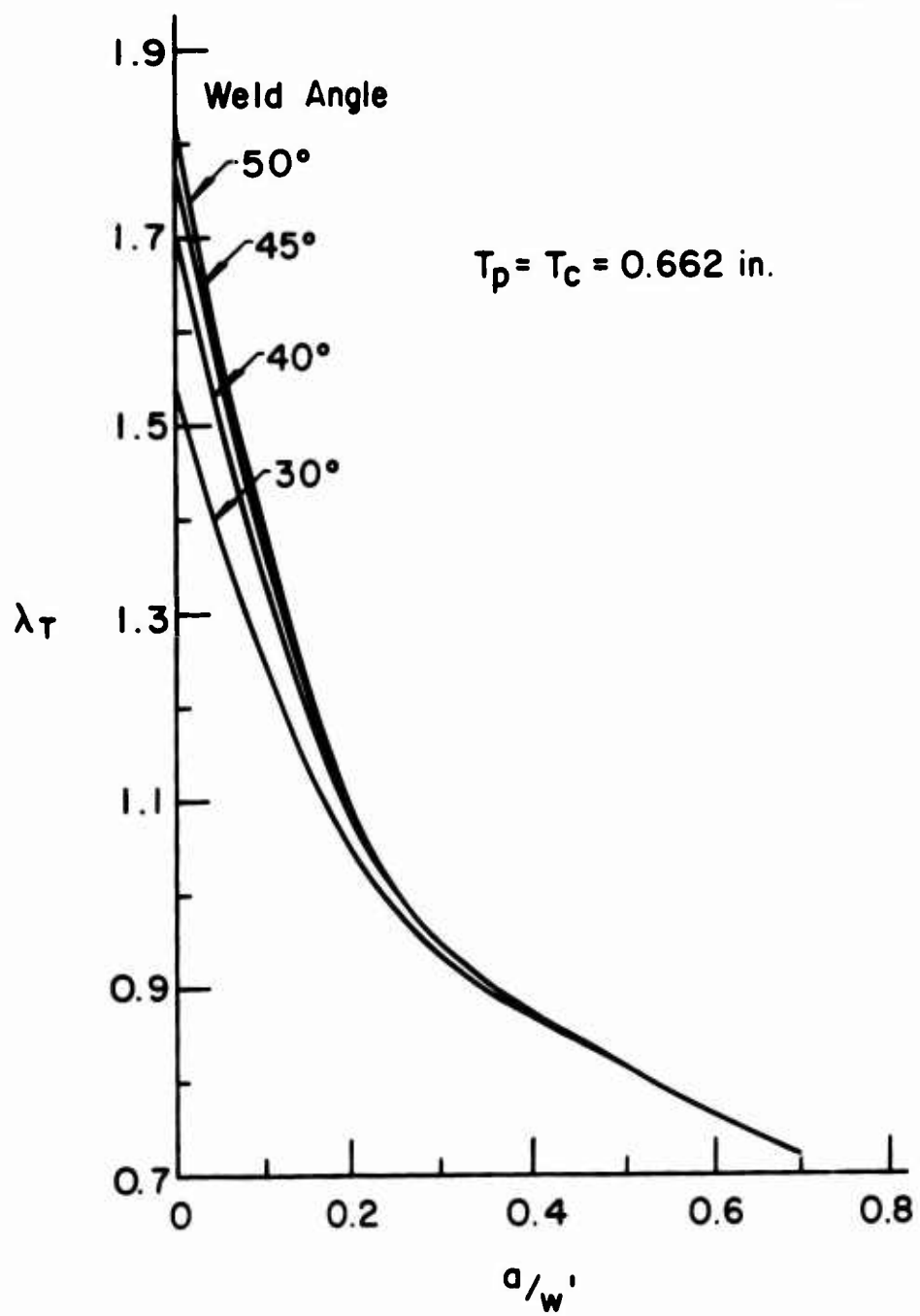
Fig. 52   Change in $\lambda_T$ With Weld Angle
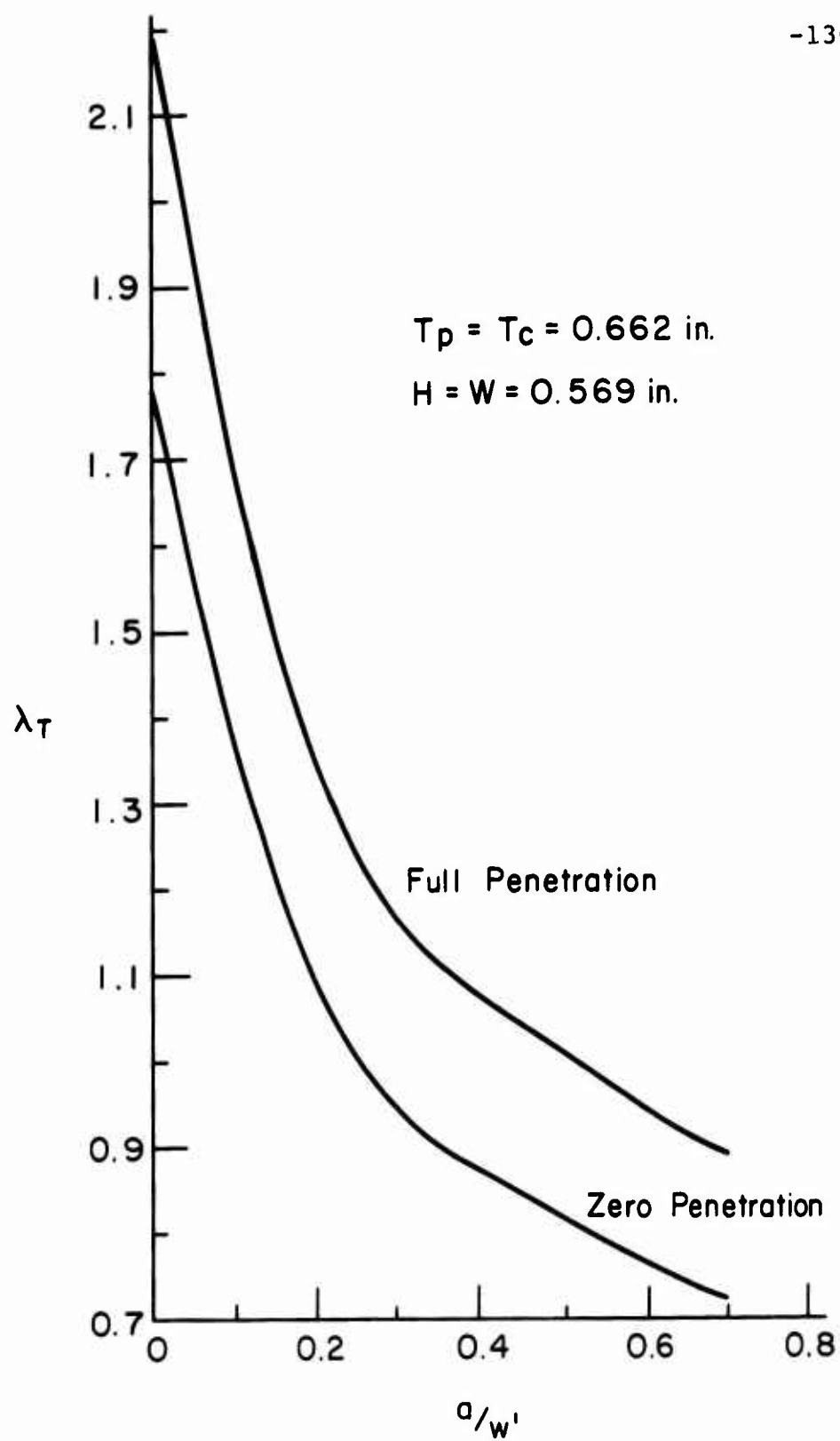
Fig. 53  Change in $\lambda_T$ With Weld Penetration
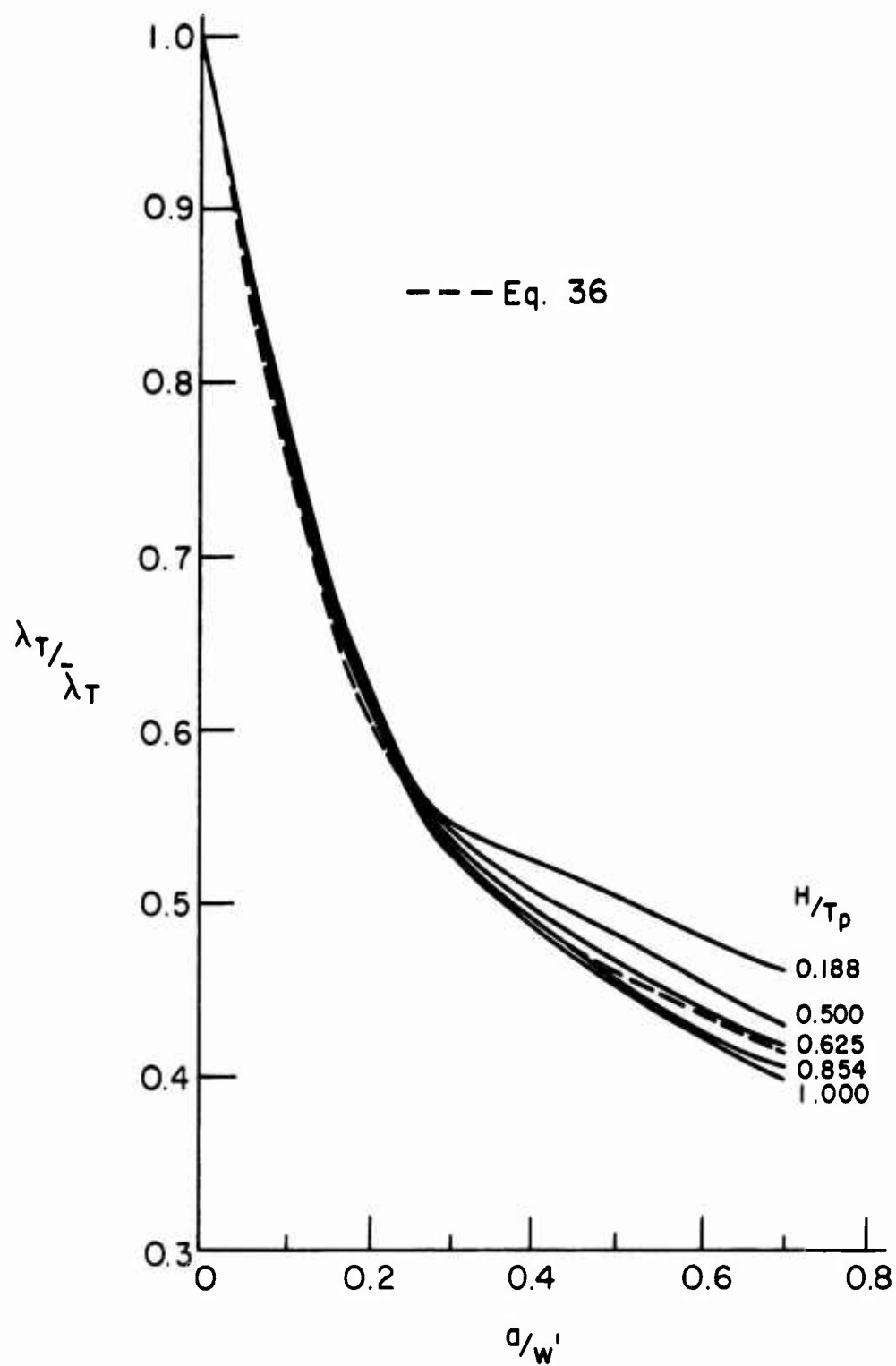
Fig. 54  Variation of $\lambda_T/\bar{\lambda}_T$ With a/w' Non-Load Carrying
Weld Joints
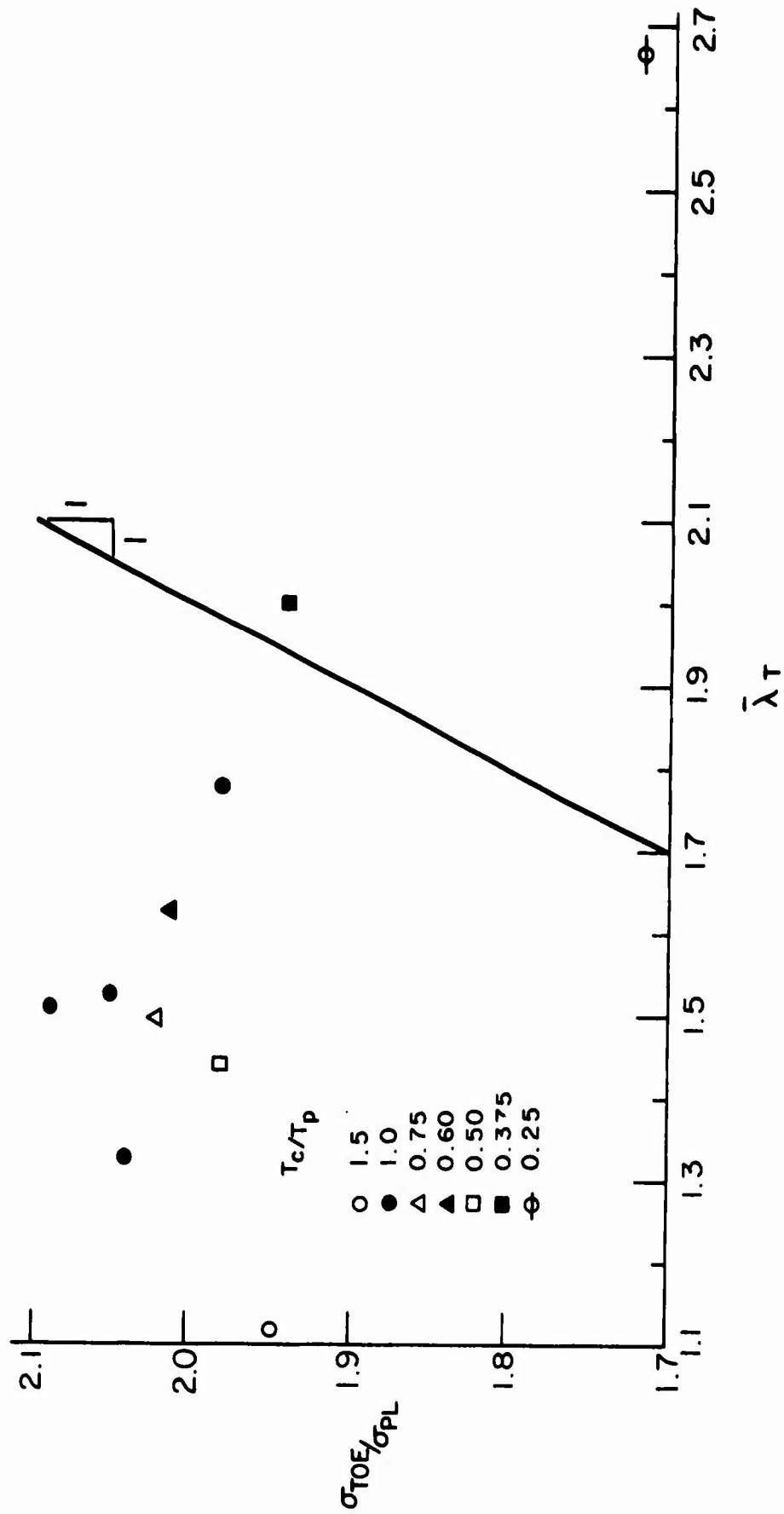
Fig. 55 $\bar{\lambda}_T$ versus Stress Concentration at Weld Toe for Non-Load Carrying Welds

-138
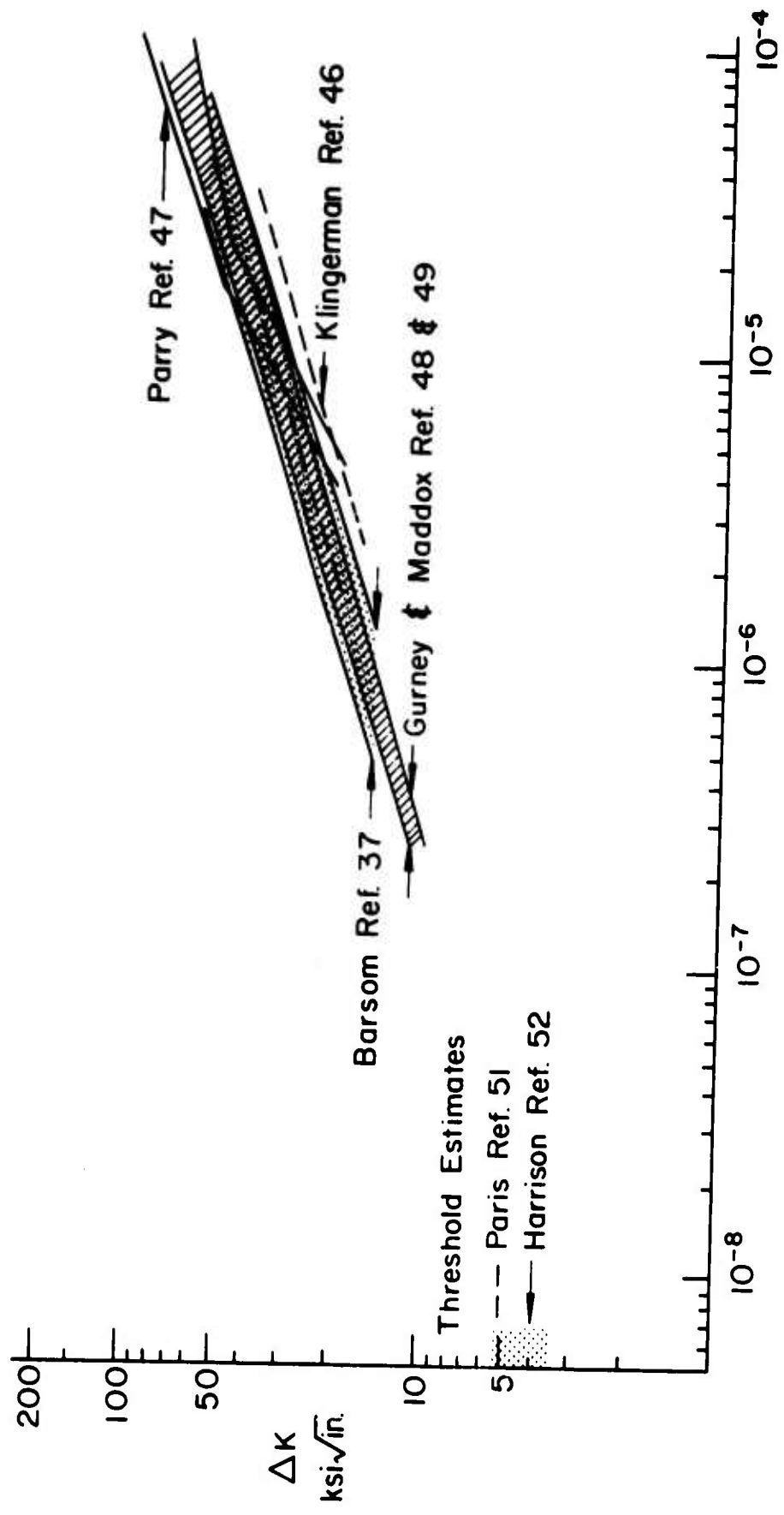
Fig. 56   Crack Growth Rate Behavior of Structural Steels
and Weldments

-139
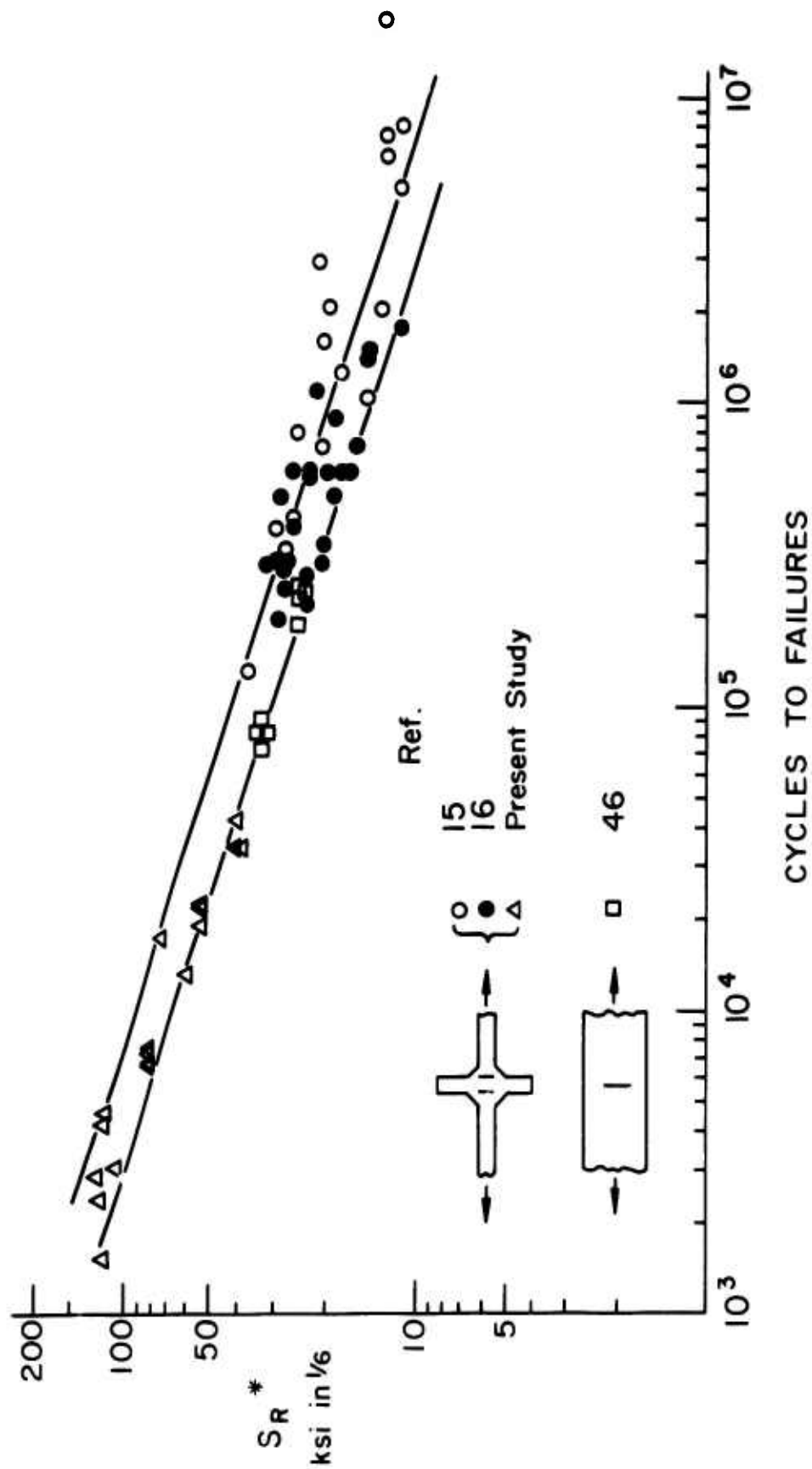
Fig. 57  Modified Stress Range versus Cycles to Failur for
Root Crack Failures
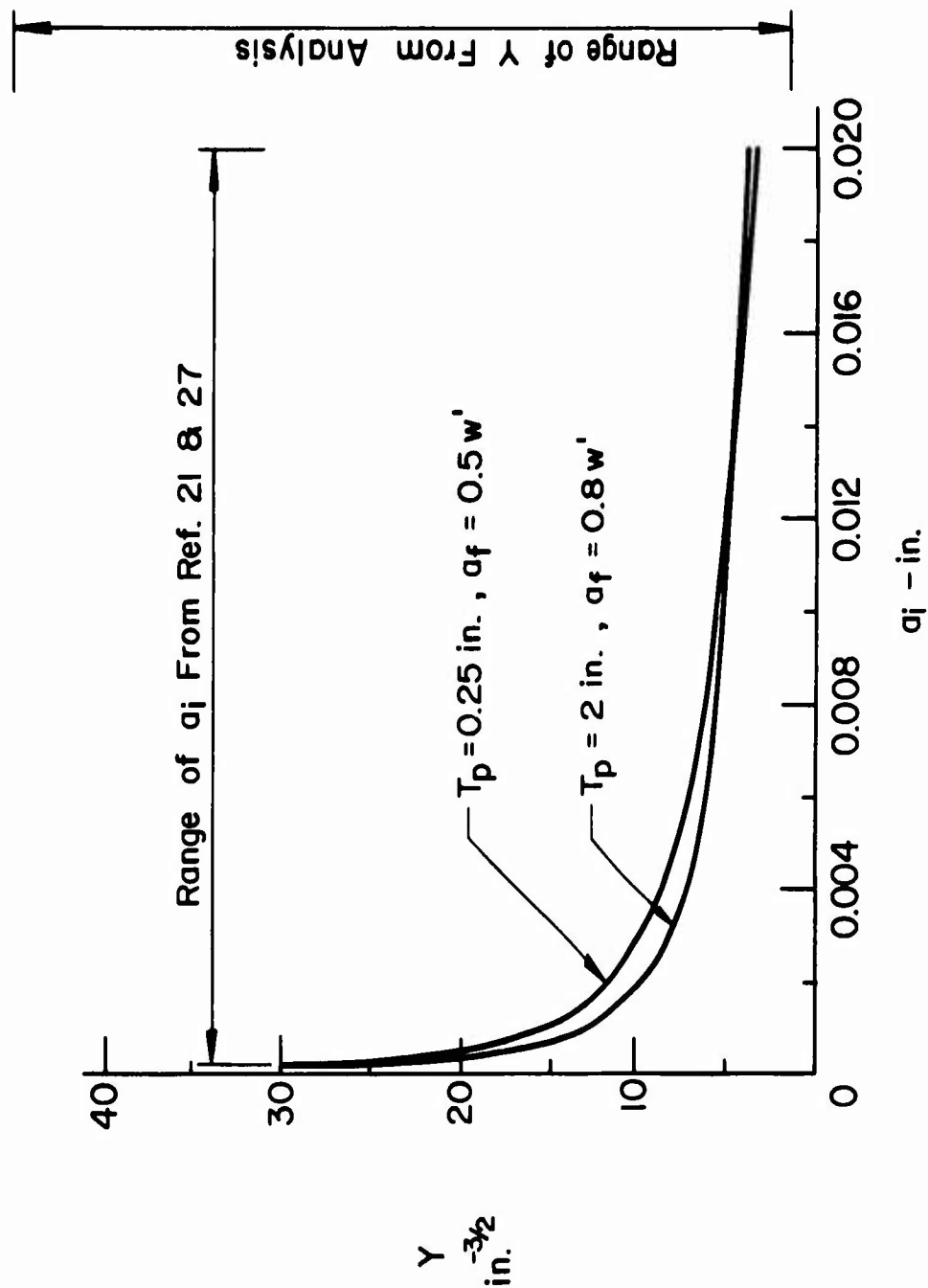
Fig. 58   Change in the Value of the Integral with Initial
Crack Size ($a_i$)
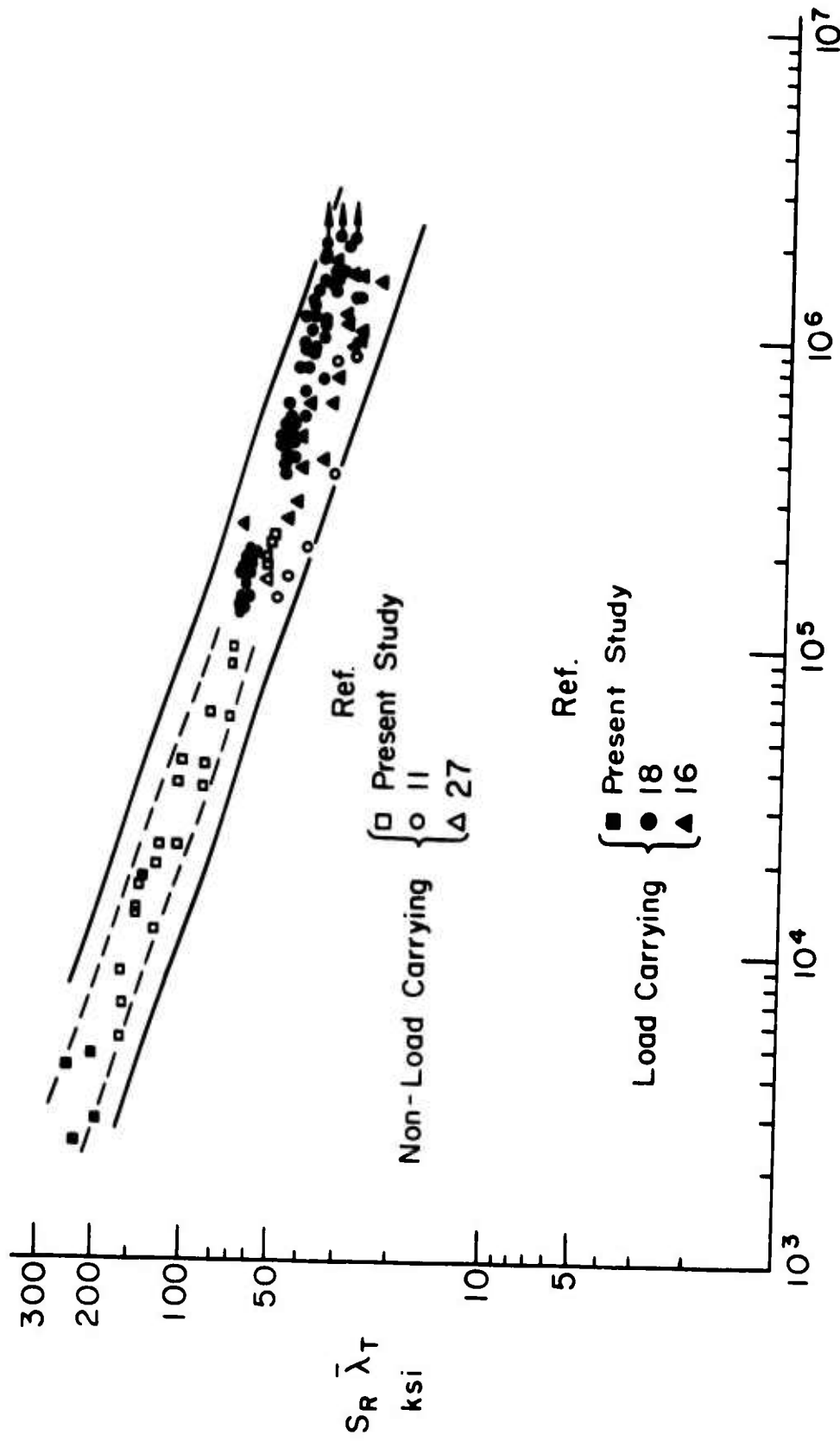
Fig. 59  Stress Range in Main Plate Times $\bar{\lambda}_T$ versus Cycles to Failure for Toe Crack Failures

-142

-143

## APPENDIX

## Methods of Solution of Finite Element Equations

The method of solution used to solve the set of equations resulting from a finite element analysis becomes important when the size of the system of equations is large. The mesh used to determine the stress distribution in the joint had approximately four-hundred nodal points. This resulted in an 800 x 800 stiffness matrix. The solution for this mesh was found using the Gauss-Seidel procedure with over relaxation. The form of the program and its logic was based on the program in Ref. 53. This method was used since only the non-zero terms of the stiffness matrix need to be stored. The displacement of all nodal points are solved and can be used to determine element stresses. The solution was assumed to have converged when the percent change in the displacement at the loaded nodes at the end of the main plate was less than one-tenth of a percent.

The mesh used to determine the compliance of the joints was considerably more refined. Fifteen-hundred nodal points were used and resulted in a global stiffness matrix of 3000 x 3000. The finite element mesh away from the crack itself does not change with crack length and therefore the

stiffness matrices of these areas are constant. The method of solution made use of the constant stiffness of these areas and minimized the non-zero terms in the global stiffness matrix.

The procedure used to solve the load carrying weld geometry is summarized here. The solution of other crack geometries was similar. The first step was to divide the structure into sub-structures. A total of 19 substructures were used. The stiffness matrix [A] for a substructure can be expressed as

$$
\begin{array}{c} F_\alpha \\ F_\beta \end{array} = \begin{bmatrix} A_{\alpha\alpha} & A_{\alpha\beta} \\ A_{\beta\alpha} & A_{\beta\beta} \end{bmatrix} \begin{array}{c} \delta_\alpha \\ \delta_\beta \end{array} \tag{A1}
$$

where subscript $\alpha$ refers to the exterior connected nodes of the substructure and $\beta$ the interior nodes. If no loads are applied to the interior nodes, this reduces to

$$
F_\beta = 0 = A_{\beta\alpha}\, \delta_\alpha + A_{\beta\beta}\, \delta_\beta \tag{A2}
$$

The displacement of the interior nodes can be determined as

$$
\delta_\beta = A_{\beta\beta}^{-1}\, A_{\beta\alpha}\, \delta_\alpha \tag{A3}
$$

Substituting Eq. A3 into Eq. A1 results in the reduced fully populated stiffness matrix of the substructure. Equation A4 relates the exterior nodal forces and displacements.

$$F_\alpha = [A_{\alpha\alpha} - A_{\alpha\beta} \ A_{\beta\beta}^{-1} \ A_{\beta\alpha}] \ \delta_\alpha \qquad (A4)$$

Symmetry of the stiffness matrix requires that

$$A_{\beta\alpha} = A_{\alpha\beta}^{t} \qquad (A5)$$

Hence, Eq. A4 can be expressed as:

$$F_\alpha = [A_{\alpha\alpha} - A_{\alpha\beta} \ A_{\beta\beta}^{-1} \ A_{\alpha\beta}^{t}] \ \delta_\alpha \qquad (A6)$$

Only $A_{\alpha\alpha}$, $A_{\alpha\beta}$, and $A_{\beta\beta}$ need be generated in the program.

The displacement boundary conditions along the planes of symmetry were accounted for by multiplying the diagonal terms associated with these displacements by one million. This is analogous to considering the displacement boundary conditions to be enforced by stiff one way connections or having a stiffness of

$$A_{ROLLER} = A_{ii} \ [10^6 - 1]$$

where $A_{ii}$ is the value of the diagonal terms associated with the displacement boundary condition. The consequence of this modification to the stiffness matrix is that the boundary node becomes an interior node connected to the stiff roller. Therefore the nodes along the lines of symmetry can be treated as interior nodes and included in the $\beta$ listing.

After the reduced stiffness matrix for each sub-structure is found they were combined. For example, consider two substructures i and j with reduced stiffness matrice $A_i$ and $A_j$ and connected at nodes $\gamma$. The other unconnected nodes are $\alpha$ for substructure i and $\beta$ for substructure j. Equilibrium of the nodes $\gamma$ requires that

$$F_{\gamma_i} + F_{\gamma_j} = 0 \tag{A7}$$

and compatibility of the displacements requires that

$$\delta_{\gamma_i} = \delta_{\gamma_j} \tag{A8}$$

Partioning the reduced substructures stiffness matrices yields the stiffness matrix for the combined substructures as

$$\begin{Bmatrix} F_\alpha \\ F_\gamma \end{Bmatrix}_i = \begin{bmatrix} A_{\alpha\alpha} & A_{\alpha\gamma} \\ A_{\gamma\alpha} & A_{\gamma\gamma} \end{bmatrix}_i \begin{Bmatrix} \delta_\alpha \\ \delta_\gamma \end{Bmatrix}_i \tag{A9}$$

and

$$\begin{Bmatrix} F_\gamma \\ F_\beta \end{Bmatrix}_j = \begin{bmatrix} A_{\gamma\gamma} & A_{\gamma\beta} \\ A_{\beta\gamma} & A_{\beta\beta} \end{bmatrix}_j \begin{Bmatrix} \delta_\gamma \\ \delta_\beta \end{Bmatrix}_j \tag{A10}$$

The solution of Eq. A7-A10 yields

$$\begin{Bmatrix} F_\alpha \\ F_\beta \end{Bmatrix} = \begin{bmatrix} A_{\alpha\alpha} - A_{\alpha\gamma} F A_{\gamma\alpha} & -A_{\alpha\gamma} F A_{\gamma\beta} \\ -A_{\beta\gamma} F A_{\gamma\alpha} & A_{\beta\beta} - A_{\beta\gamma} F A_{\gamma\beta} \end{bmatrix} \begin{Bmatrix} \delta_\alpha \\ \delta_\beta \end{Bmatrix} \tag{A11}$$

where

$$F = [A_{\gamma\gamma_i} + A_{\gamma\gamma_j}]^{-1} \tag{A12}$$

The substructures to the left of the crack were combined using Eq. A11. This yielded the stiffness matrix for this part of the structure. This was repeated to the right of the crack. These stiffness matrices are independent of crack length and consequently are only determined once for each joint geometry analyzed.

The stiffness matrices of the substructures near the crack were determined for each crack length. They were then combined with the stiffness matrices for the areas to the right and left to yield the stiffness matrix relating the displacement at the loaded nodes to their nodal forces. This 12 x 12 matrix was inverted and multiplied by the known nodal loads to determine the nodal point displacements.

The size of the matrices to be inverted by this solution scheme are kept to a minimum. The inversions required are dependent on the number of interior nodes, matrix $A_{\beta\beta}$ in Eq. A4, and the number of connected nodes, matrix $F^{-1} = A_{\gamma\gamma_i} + A_{\gamma\gamma_j}$, in Eq. A11. The time required for the symmetric inversion routine used was proportional to the cube of the matrix size.[54] By dividing the structure into small substructures the time required for inversion was minimized. As the size of the matrix $A_{\beta\beta}$ decreased, fewer non-zero off diagonal terms were considered.

Another advantage of the method of substructures was that the stiffness matrix of the segment of the main plate from the toe of the weld to the loaded nodes did not have to be calculated for each joint geometry. This segment geometry is only a function of the main plate thickness, $t_p$. The stiffness matrix of this segment was independent of $t_p$. Therefore the stiffness matrix of this segment need only be developed once for all joint geometries. This allows a considerable reduction in solution time.

The programs used for both the compliance and stress analysis made use of mesh generation subroutines which determined the nodal point locations and element coordinates. This minimized the error associated with the generation of the element stiffness matrix. All calculations were performed on a CDC 6400 in single precision.

# REFERENCES

1. Wilson, W.M., Bruckner, W.H., Commbe, J.V. and Wilde, R.A., "Fatigue Tests of Welded Joints in Structural Steel Plates", University of Illinois Bulletin No. 27, February, 1941.

2. Wilson, W.M., Munse, W.H. and Bruckner, W.H. "Fatigue Strength of Fillet Weld, Plug Weld, and Slot-Weld Joints Connecting Steel Structural Members", University of Illinois Bulletin No. 68, May, 1949.

3. Soete, W. and Van Crombrugge, R. "Fatigue Strength of Welded Assemblies", Revue de la Soudre, Vol. 7, 1951.

4. de Lieris, H. and Puttillevl, H. "Fatigue Tests of Arc-Welded Joints", Welding Journal, Vol. 31, 1952, p. 104.

5. Lea, F.C. and Whitman, J.G. "The Failure of Girders Under Repeated Stresses", Journal of the Institute of Civil Engineers, Vol. 7, 1937-1938.

6. Chapman, E. "Welded Joints", Welding Journal, Vol. 13, 1934, pp. 10-14.

7. Wilson, W. M. "Flexural Fatigue Strength of Steel Beams", Bulletin No. 377, University of Illinois Engineering Experiment Station, 1948.

8. Solakian, A. G. "Stresses in Tranverse Fillet Welds by Photoelastic Methods", Welding Journal, Vol. 33 1954 , pp. 22-29.

9. Cherry, W. R., "Stress Concentration Factors in Main Members due to Welded Stiffeners", Welding Journal Vol. 20, No. 12, 1941.

10. Gurney, T. R., "Influence of Residual Stresses on Fatigue Strength of Plates with Fillet Welded Attachments", Welding Research Abroad, Vol. 7, 1961, pp. 46-62.

11. Gurney, T. R., "Fatigue Strength of Beams with Stiffeners Welded to the Tension Flange", British Welding Journal, September 1960, pp. 569-576.

12. Fisher, J. W. and Viest, I. M., "Fatigue Tests of Bridge Materials of the AASHO Road Test", Special Report 66, Highway Research Board, 1961.

13. Gurney, T. R., "Influence of Artificially Induced Residual Stresses on Fatigue Strength of Load-Carrying Fillet Welded Joints in Mild Steel", Welding Research Abroad, Vol. 8, 1962, pp. 2-14

14. Yen, B. T. and Cooper, P. B., "Fatigue Tests of Welded Plate Girders", Fritz Engineering Laboratory Report No. 251.26, Lehigh University, February, 1962.

15. Hoisveen, S. and Persson, H. A., "Intrangningens Inverkan pa Utmattningshallfastheten Vid Automatsvetsade Kalsvetsforland", Svetsen, Arg. 22, nr. 3, May, 1963, pp. 75-84.

16. Ouchida, H. and Nishioka, A. "A Study of Fatigue Strength of Fillet Welded Joints", Hitashi Review, April, 1964, pp. 3-14.

17. Yamaguchi, I. Yasuharu, T., and Nitta, A., "On The Fatigue Strength of Structural Steels for Ships", Trans. of the Society of Naval Architects of Japan, Vol. 115, May, 1964.

18. Nilsson, H., Larsson, B., and Westerlund, R., "Utmattningsundersokning Av Svetsado Provstavar", The Swedish Shipbuilding Research Foundation Report No. 46, 1965.

19. Maefarlane, P. S. and Harrison, J. D., "Some Fatigue Tests of Load Carrying Tranverse Fillet Welds", Welding Research Abroad, Vol. 12, 1966, pp. 53-63.

20. Gurney, T. R., "Some Fatigue Tests on Fillet Welded Mild and High Tensile Steel Specimens in the As-Welded and Normalized Condition", British Welding Journal, November, 1966, pp. 648-651.

21. Signes, E. G., Baker, R. G., Harrison, J. D., and Burdekin, F. M., "Factors Affecting the Fatigue Strength of Welded High Strength Steels", British Welding Journal, February, 1967, pp. 108-116.

22. Braithwaite, A. B. and Gurney, T. R., "Fatigue Tests on Cross Girder Connections", British Welding Journal, February, 1967, pp. 71-81.

23. Mueller, J. A. and Yen, B. T., "Girder Web Boundary Stresses and Fatigue", Fritz Engineering Laboratory Report No. 327.2, Lehigh University, July, 1967.

24. Harrison, J. D., "Further Techniques for Improving the Fatigue Strength of Welded Joints", British Welding Journal, November, 1966, pp. 642-647.

25. Fisher, J. W., Frank, K. H., Hirt, M. A., and McNamee, B. M., "Effect of Weldments on the Fatigue Strength of Welded Beams", NCHRP Report No. 102, Highway Research Board, National Academy of Sciences - National Academy of Engineering, 1970.

26. Gurney, T. R., Fatigue of Welded Structures, Cambridge Press, 1968.

27. Watkinson, F., Bodger, P. H., and Harrison. J. D., "The Fatigue Strength of Welded Joints in High Strength Steels and Methods for Its Improvement", Proceedings, Fatigue of Welded Structures Conference, The Welding Institute, Brighton, England, Paper No. 7, July, 1970.

28. Harrison, J. D., "An Analysis of the Fatigue Behavior of Cruciform Joints", Welding Institute Report No. E/21/12/68, 1968.

29. Gurney, T. R. and Maddox, S. J., "A Re-Analysis of Fatigue Data for Welded Joints in Steel", Welding Institute Members Report, The Welding Institute, 1970.

30. Maddox, S. J., "Calculating the Fatigue Strength of a Welded Joint Using Fracture Mechanics", Metal Construction, Vol. 2, No. 8, 1970, p. 327.

31. Heiser, F. A. and Hertzberg, R. W., "Anisotropy of Fatigue Crack Propagation", Transactions of ASME, Journal of Basic Engineering, Vol. 93, Series D, No. 2, 1971, p. 211.

32. "Fatigue Crack Propagation", American Society for Testing and Materials Special Technical Publication 415, 1967.

33. "Proceedings of the Air Force Conference on Fatigue and Fracture of Aircraft Structures and Materials", AFFDL TR 70-144, 1970.

34. Paris, P. C. and Sih, G. C., "Stress Analysis of Cracks", American Society for Testing and Materials, Special Technical Publication 381, 1964.

35. Paris, P. C., "The Fracture Mechanics Approach to Fatigue", Fatigue - An Interdisciplinary Approach, Syracuse University Press, 1964.

36. Paris, P. C., et al, "A Rational Analytic Theory of Fatigue", The Trend in Engineering, January, 1961.

37. Barsom, J. M., "Fatigue-Crack Propagation in Steels of Various Yield Strengths", U.S. Steel Corp., Applied Research Laboratory, Monroeville, Pa., 1971.

38. Paris, P. C. and Erdogan, R., "A Critical Analysis of Crack Propagation Laws", Transactions of ASME, Journal of Basic Engineering, December, 1963.

39. Pelloux, R. M., "Review of Theories and Laws of Fatigue Crack Propagation", Proceeding of the Air Force Conference on Fatigue and Fracture of Aircraft Structures and Materials, AFFDL TR 70-144, 1970, p. 409.

40. Chan, S. K., Tuba, I. S., and Wilson, W. K., "On the Finite Element Method in Linear Fracture Mechanics", Engineering Fracture Mechanics, Vol. 2, No. 1, 1970, p. 1.

41. Wilson, W. K., "On Combined Mode Fracture Mechanics", Research Report 69-1E7-FMECH-R1, Westinghouse Research Laboratories, Pittsburgh, Pa., June, 1969.

42. Hilton, P. D. and Hutchinson, J. W., "Plastic Intensity Factors For Cracked Plates", Report SN-34, Harvard University Division of Engineering and Applied Physics, Cambridge, Mass., May, 1969.

43. Mowbray, D. F., "A Note on the Finite Element Method in Linear Fracture Mechanics", Engineering Fracture Mechanics, Vol. 2, No. 2, 1970, p. 173.

44. Byskov, Esben, "The Calculation of Stress Intensity Factors Using the Finite Element Method with Cracked Elements", _International Journal of Fracture Mechanics_, Vol. 6, No. 2, 1970, p. 159.

45. Shrawley, J. E., Jones, M. H., and Gross, B., "Experimental Determination of the Dependence of Crack Extension Force on Crack Length for a Single-Edge-Notch Tension Specimen", _NASA Technical Note TN D-2396_, August, 1964.

46. Klingerman, D. J., Frank, K. H., and Fisher, J. W., "Fatigue Crack Growth In A36 Steel", _Fritz Engineering Laboratory Report No. 358.31_, Lehigh University, May, 1971.

47. Parry, M., Nordberg, H., and Hertzberg, R. W., "Fatigue Crack Propagation In A514 Base Plate and Welded Joints", _Fritz Engineering Laboratory Report No. 358.33_, Lehigh University, September, 1971.

48. Gurney, T. R., "An Investigation of the Rate of Propagation of Fatigue Cracks in a Range of Steels", _Members' Report No. E18/12/68_, The Welding Institute, December, 1968.

49. Maddox, S. J., "Fatigue Crack Propagation In Weld Metal and Heat Affected Zone Material", _Members' Report No. E/29/69_, The Welding Institute, December, 1969.

50. Hirt, M. A., "Fatigue Behavior of Rolled and Welded Beams", Ph.D. Thesis, Lehigh University, Department of Civil Engineering, October, 1971.

51. Paris, P. C., "Testing for Very Slow Growth of Fatigue Cracks", Closed Loop, MTS System Corp., Vol. 2, No. 5, 1970 pp. 11-14.

52. Harrison, J. D., "An Analysis of Data on Non-Propagating Fatigue Cracks on a Fracture Mechanics Basis", _Metal Construction and British Welding Journal_, Vol. 2, No. 3, 1970, p. 93.

53. Schultchen, E. G. and Kostem, C. N., "User's Manual For CSTES Finite Element Program", _Fritz Engineering Laboratory Report No. 237.58_, Lehigh University, June, 1969.

54. Iyengar, S. N. S. and Kostem, C. N., "FLMXPK - A Matrix Package", <u>Fritz Engineering Laboratory Report No. 400.4</u>, Lehigh University, September, 1971.